NASA CONTRACTOR REPORT 195449

HIGH PRESSURE EARTH STORABLE ROCKET TECHNOLOGY PROGRAM HIPES - BASIC PROGRAM FINAL REPORT

M. L. Chazen, D. Sicher, D. Huang, T. Mueller
TRW Space & Technology Division
Redondo Beach, California 90278

MARCH 1995

Prepared for:
NASA-LeRC
Cleveland, Ohio 44135
Contract: NAS3-27002

National Aeronautics and
Space Administration

NASA CONTRACTOR REPORT 195449

HIGH PRESSURE EARTH STORABLE ROCKET TECHNOLOGY PROGRAM HIPES - BASIC PROGRAM FINAL REPORT

M. L. Chazen, D. Sicher, D. Huang, T. Mueller
TRW Space & Technology Division
Redondo Beach, California 90278

MARCH 1995

Prepared for:
NASA-LeRC
Cleveland, Ohio 44135
Contract: NAS3-27002

TABLE OF CONTENTS

LIST OF FIGURES

LIST OF TABLES

1.0 SUMMARY

The High Pressure Earth Storable Rocket Technology (HIPES) Basic Program was initiated in mid August 1993 and was completed on schedule in early November 1994. The program was very successful in meeting its overall objectives.

The systems studies (Task 1) reviewed potential applications of NASA, DOD and commercial spacecraft to assess uses for the HIPES engine. Studies of pressure-fed and pump-fed systems for these applications were studied using both N_2O_4-N_2H_4 and N_2O_4-MMH. The N_2O_4-N_2H_4 system indicated it provides the maximum payload for large, medium and lightsat satellites. The major benefits of the HIPES engine are high performance within a confined length resulting in maximization of payload for lightsats which are volume and length constrained. The nominal engine design based on preliminary system/engine requirements is presented as follows:

Propellants	N_2O_4-N_2H_4
Thrust (F_∞)	50 lbf
Chamber Pressure (Pc)	500 psia
Specific Impulse (Isp_∞)	330 lbf-sec/lbm
Nozzle Expansion (ε)	150

A preliminary and detailed design was developed for the HIPES engine consisting of workhorse copper heatsink, water-cooled and rhenium thrust chambers with the flexible TRW pintle injector. An integrated performance and thermal model developed by TRW was used to define the attributes of the design.

The engine hardware was fabricated and tested to establish engine performance and thermal characteristics at various chamber pressures at constant thrust. Very high performance was achieved with thermal characteristics compatible with rhenium engine operation. Combustion efficiency of 98.5% (ODE C*) was achieved and based on TDK Cf (including boundary layer losses) indicated a vacuum specific impulse of ~337 lbf-sec/lbm (ε=150). The rhenium engine (bolt-on configuration) was demonstrated substantiating the high performance and compatible thermal characteristics.

2.0 INTRODUCTION

During the past three decades, earth storable propellants, principally hydrazine(N_2H_4) as a monopropellant and nitrogen tetroxide(N_2O_4) - amine fuels as bipropellants, have been used extensively in liquid propulsion systems for spacecraft applications. The technology level for these propellants and their associated systems have been continually upgraded as spacecraft mission demands have grown. The introduction of the dual mode (N_2O_4-N_2H_4) system concept represented one of the last significant earth storable propulsion system improvements available. The dual mode system utilized a bipropellant liquid apogee engine for apogee circularization and insertion and various forms of hydrazine thrusters for attitude control stationkeeping. The attitude control thrusters used catalytic, electrothermally heated monopropellant hydrazine thrusters (EHT) or higher performance arcjets (when higher power is available) wherein the hydrazine for both the main engine and control system (ACS) were integrated into the same tank or tanks. TRW has qualified and flown on satellites (ANIK and Intelsat) 100 lbf thrust (100 psia) apogee engines using N_2O_4-N_2H_4 propellants demonstrating a specific impulse of 314.6 lbf-sec/lbm. Presently, TRW is developing an advanced dual mode liquid apogee engine operating at a specific impulse of 328 lbf-sec/lbm at a chamber pressure of 125 psia and a thrust of 125 lbf. It is clear that little further improvements can be attained as the theoretical limit is approached. As 98% C*(ODE) is approached and we look for other improvements, higher pressures have been considered good candidates because of the potential for higher thrust coefficients and C*, the enabling use of higher temperature materials, the reduced length and volume of the engine envelope, and the potential weight savings. It has also become clear that the use of the higher pressure engine is the only method of using the high performance engine due to volume and length constraints on certain spacecraft applications (i.e. small lightweight spacecraft).

The scope of the HIPES program includes four phases - basic program and three options.

The specific tasks of the basic program have been:

Task 1. System Parameter Selection

- o Reviewed applications of NASA, DOD and commercial spacecraft for assessing potential applications for the HIPES engine.
- o Conducted studies of pressure-fed and pump-fed systems for these applications and defined an operating envelope to be used for HIPES engine development.
- o Recommended a program to develop the HIPES engine for use in the candidate high pressure earth storable propulsion system.
- o Submitted an informal report on the results of Task 1.

Task 2. Rocket Testbed Design

- o Developed a detailed design of the HIPES engine including detailed drawings and associated analyses after approval of the Task 1 report.
- o Prepared a test plan that investigated the various performance and thermal effects on the HIPES engine for various configurations. This plan included the testing to accomplished for each configuration and test parameters and associated instrumentation.
- o Submitted a list of long lead items.
- o Presented the design including detailed drawings and analyses at an oral design review presentation at NASA-LeRC.

Task 3. Rocket Testbed Fabrication

- o Fabricated the testbed engine after approval of the design review presentation.

Task 4. Rocket Testbed Tests

- o Conducted the test program in accordance with the approved test plan.
- o Incorporated minor hardware modifications as required and tested until the test plan was completed.
- o Analyzed and evaluated the test data to assess performance and thermal characteristics.

The final report presents the results of the four tasks of the basic program.

3.0 SYSTEM STUDIES

The use of high pressure earth storable propellants offered the advantage of providing higher performance to achieve greater payload weight into orbit. This was due to the potential for higher thrust coefficients, the enabling use of higher temperature materials, the reduced length and volume of the engine and the potential weight savings. It was also clear that the use of the higher pressure engine was the only method of using the higher performance engine due to volume and length constraints on certain spacecraft applications (in particular, small lightweight satellites). The evaluation studied the following areas:

- o Mission evaluation usage of the HIPES engine technology
- o Evaluation of high pressure earth storable propellants
- o Propulsion systems evaluation to maximize payload to orbit
- o Preliminary system and engine requirements
- o Conclusions

3.1 Missions

Investigations were conducted based on inputs from various sources and analyses to determine the most likely missions to utilize advanced spacecraft technology. The results of these inputs indicated three prime mission categories:

- o Apogee earth orbit missions to place satellites of various sizes into geosynchronous earth orbit (GEO) using expendable launch vehicles (Delta, Atlas, Titan, Ariane, Long March or Shuttle). These missions include NASA, military and commercial applications for communications, surveillance, tracking, earth observation and meteorology.
- o Delta-V for earth orbit missions was considered another candidate mission. This included such operations as altitude raising, circularizing and inclination changing and orbit maintenance. The light satellite usage has become a more significant part of the total missions for cheaper, better, faster spacecraft and the philosophy to reduce risk of spacecraft (utilization of several small spacecraft to achieve mission objective over one very large expensive spacecraft).
- o Planetary orbit capture and soft landing missions

The best assessment of missions for 1994-2000 based on the evaluation conducted during the last third of 1993 is presented in Table 3-1. The average number of missions was defined as 27 per year for this seven year period although 37 per year was the average for

TABLE 3-1 MISSION PLANNING

VEHICLE CLASS	1994	1995	1996	1997	1998	1999	2000
SMALL	TOMS FAST AFRISTAR GMS-5 SAX	HETE/SAC-B SWAS AMOS COMET	ETS	SMEX-4	SMEX-5 UNEX	SMEX-6 UNEX	SMEX-7 AERO-1 UNEX ETS
MEDIUM	WIND POLAR RADARSAT NOAA-J SEDS-2 SCOT APSTAR ASIASAT BRAZILSAT(2) BS-3N DOMINION ERS-2 HELIOS ITALSAT MEASAT NAHUEL SFU THAICOM UNICOM	XTE ORSTED ARABSAT UNICOM CEROS IRIDIUM KOREASAT(2) MEASAT PACSTAR PALAPA-C THAICOM	NEAR SCOUT-1 MESUR NOAA-K ARABSAT IRIDIUM(7) SPOT DOMINION SFU	SCOUT-2 ACE LAGEOUS III NOAA-L HELIOS IRIDIUM(6) SFU SKYNET	LANDSAT-7 ASIASAT SKYNET SPOT	AXAF-S NOAA-M MESUR(2) HESP TIMED-L TIMED-H DFS-3 HELIOS SFU PALAPA-C	GPB FUSE NOAA-N EOS/SAR INIDEX IMI ARABSAT DFS-3 SFU SATCOM

TABLE 3-1 MISSION PLANNING

	1994	1995	1996	1997	1998	1999	2000
INTERMEDIATE	GOES-I ASTRA DIRECTTV INMARSAT INSAT-2CE ISO ORION PAS SAJAC(2) SOLIDARIDAD TELSTAR TURKSAT	GOES-J SOHO ADEOS INMARSAT INSAT-2CE MOBILESAT MSG NSTAR ORION PAS SPACENET ZOHREH TELECOM TURKSAT ASTRA	BS-4 DRS(2) INMARSAT INSAT-2CE TRMM ZOHREH PAS(2) ORION	EPOP-M EUTELSAT-3 INMARSAT MSG SPACENET	EOS-AMI TDRSS F-8 EUTELSAT(2) JC-SAT	GOES-K TDRSS F-9 EPOP-N JC-SAT SUPERBIRD	GOES-L EOS-PM TDRSS F-10 AURORA MSG
LARGE	I-VII F1 I-VII F2 MIL SURV MIL SURV	I-VII F3 I-VIIA F6 I-VIII F1 TDRSS-G MIL SURV MIL COM	I-VII F4 I-VIIA F7 I-VIIA F8 I-VIII F2 I-VIII F3 MIL SURV MIL COM	I-VIIA F9 I-VIII F4 MIL SURV MIL SURV	AXAF-I AXAF-II MIL SURV MIL COM MIL COM SURV SURV	PLUTO FLYBY	PLUTO FLYBY

the first three years (1994-1997). The lower number for the outer years was due to less certainty. The requirements have been constantly evolving and changing in response to market conditions associated with the world economy and political environment in addition to technological improvements.

3.2 Applications - Light and Heavy Satellites/Spacecraft

Preliminary investigations were conducted based on inputs from various sources and analyses were conducted to determine several likely missions which would utilize the HIPES engine. Many of the selected candidates were considered as a result of direct experience with them by TRW. Three representative general mission categories have been selected which will be discussed.

In all of these applications, high-pressure engines presented an advantage over low-pressure engines by providing higher performance (Isp) with less propellant, and smaller/lighter engines for a given thrust level and expansion ratio. However, in pressure-fed systems, propellant and pressurant tankage weight and pressurant weight may increase which was the basic trade. The increased performance required less propellant and smaller tankage while the higher pressure resulted in heavier tankage and more pressurant. However, the heavier tankage and increased pressurant may be mitigated by the use of composite, overwrapped tanks and pressure augmentation to decrease the pressurant. In this trade, there was a minimum value in the weight function curve which defined the optimum operating pressure for that particular mission/system. In addition to the weight trade, propulsion system volume (engines, tanks, lines, etc.) was reduced as operating pressures increased. In some applications minimum weight was considered most important while in others minimum volume dominated.

3.2.1 Perigee/Apogee Earth Orbit Missions

Many space missions started with the spacecraft placed in a nominal 100 nm circular low earth orbit (LEO) by the launch vehicle. Through one or more thrust applications, the orbit was altered to its required operational conditions.

One important and popular operational orbit has been GEO, which is 19,323 nm circular at zero degrees inclination. Most communication satellites have used this orbit because it allowed ground users to employ simple nontracking antennae.

Two typical GEO missions were selected, which will have the maximum usage in the next ten years. These included a lightsat earth science mission and a typical commercial communications satellite. The lightsat mission selected was a proposed NASA-MSFC Lightning Mapper satellite, utilizing GEO as a desirable orbit. The program goal was established as placement of 1400 lbm of wet satellite weight into GTO, resulting in about 800 lbm of dry weight in GEO to measure lightning events to provide storm warnings and improve the understanding of lightning phenomenology. The typical commercial communications satellite began with 5000 lbm of wet satellite weight in GTO which

resulted in about 2900 lbm of weight in GEO. A spacecraft delta-V of 5875 fps, which represented the apogee circularization and plane change maneuver, was assumed for the study.

3.2.2 Delta-V for Earth Orbit Missions

Earth orbit missions referred to relatively low earth orbits of various altitudes, eccentricities and inclinations. These missions may or may not be placed into their required operational orbits by the launch vehicle. If they are not, the spacecraft propulsion system is required to perform the required delta-V to transfer from the launch-vehicle-delivered initial orbit to the operational orbit. Once in an operational orbit, some missions required that some orbit parameters be maintained by the spacecraft propulsion system throughout the satellite lifetime. This orbit maintenance requirement included many different types of delta-V maneuvers. The light satellite usage was considered second only to the communication satellites.

For this study, the Total Ozone Mapping Spectrometer-Earth Probe (TOMS-EP) mission was selected for analysis as representative of a current, typical LEO mission. The launch vehicle placed the spacecraft into an initial near-polar orbit of 275nm x 350 nm and 99.3 degrees inclination. The spacecraft integral propulsion system then performed perigee and apogee burns to place itself into the final operational sun-synchronous circular orbit of 955 nm altitude. The TOMS-EP spacecraft weighed 636 lbm wet at launch vehicle separation with the required mission delta-V of 1681 fps.

3.2.3 Planetary Orbit Capture and Soft Landing Missions

Planetary orbit capture (including lunar) has a unique minimum thrust requirement. These missions usually are flown on a hyperbolic approach trajectory whereby the vehicle flys-by-the body unless a retro-thrust has been applied to remove some of its velocity. The orbit can be changed by retrofirings of the low thrust engine at perigee/apogee for efficiency. This has been a major advantage of liquid rocket engines as opposed to solid rocket motors which must burn to depletion and cannot be restarted.

Planetary soft-landing has another unique set of requirements. For these missions, a minimum thrust level is required to overcome gravity and allow a near zero impact velocity. These missions often begin with the vehicle in planetary or lunar orbit where the landing site can be accurately targeted and/or changed. Constant retro-thrust is applied to break out of orbit and start the descent. The thrust is then varied as the descent continued to touchdown, following a predetermined acceleration profile.

MESUR was selected due to the fact it is a NASA science mission involving the soft-landing of 16 vehicles, named Network, on the surface of Mars in 1999-2003. As part of this mission, a separate data-relay spacecraft will be launched to orbit Mars for providing a communication link between the surface craft and earth. The wet spacecraft weight of 4000 lbm at launch vehicle separation requires a total mission delta-V of 11,800 fps.

3.3 Missions Summary

The results of the mission investigation indicated the predominance of spacecraft missions fall into two categories: apogee earth orbit missions to place satellites of various sizes into GEO and delta-V for earth orbit missions. In addition there is a small number of planetary missions. The largest number of missions are considered in the medium to intermediate payload range with a significant number in the small (lightsat) payload range. The trend selected by the agencies is to use small, better, cheaper satellites to perform missions over the very large and and expensive satellites to reduce assets at risk. Therefore, the missions analyzed in the system studies evaluated the following:

- o Commercial satellites into GEO (medium to intermediate class)
- o MESUR which included a Mars data-relay spacecraft to provide a communication link between the surface craft and earth (medium class)
- o Lightning Mapper (small to medium class)
- o TOMS-EP earth orbit mission (small class)

3.4 Propellant Selection

Over the last three decades, flight-qualified space engines utilizing earth-storable propellants have been limited almost exclusively to N_2O_4-MMH for bipropellant systems and N_2H_4 for monopropellant systems. As a consequence, the demand for these propellants have resulted in their ready availability and relatively low cost. Both test and launch facilities have routinely stored and used these propellants, and ground crews have developed well-established handling procedures to minimize the health risks associated with exposure. In addition, material compatibility issues have been clearly defined and as a result, the design of propulsion system components utilizing these propellants have become rather straightforward.

TRW achieved a significant milestone in the development of bipropellant engine technology by qualifying the Dual Mode Liquid Apogee Engine (DM-LAE). This engine used N_2H_4 instead of MMH as the fuel and offered significant spacecraft weight savings by virtue of its higher performance (Isp) over N_2O_4-MMH. TRW has recently demonstrated Isp=328 lbf-sec/lbm on an Advanced Dual Mode Liquid Apogee Engine (ADM-LAE).

The combination of already demonstrated high performance and mature status of production, handling and component/material compatibility has led TRW to baseline N_2O_4-N_2H_4 as the preferred propellant combination for the HIPES program.

3.5 System Analyses

Systems analyses to determine the effect of varying engine thrust and chamber pressure on total propulsion system weight were conducted for the four missions discussed - commercial satellites into GEO, MESUR data-relay spacecraft, Lightning Mapper and TOMS-EP. The analyses compared the use of both pressure-fed and pump-fed dual mode propulsion systems using N_2O_4-N_2H_4 and bipropellant systems using N_2O_4-MMH. Since the engine performance (effects propellant load), pressurant weight, engine weight, pump weight, and propellant and pressurant tank weights have been the principle factors that change as the engine chamber pressure was varied, only these factors were examined in the trade study; it was assumed that variations in the weights of the remaining propulsion feed system components for different operating pressures were negligible compared to the principal factors.

The engine performance used in the analyses for both N_2O_4-N_2H_4 (O/F=1.0) and N_2O_4-MMH (O/F=1.65) at varying thrust levels (50-100 lbf) and chamber pressures (100-1000 psia) is presented in Figure 3.5-1. These values of specific impulse were obtained by analysis using two-zone two dimensional kinetic (TDK) with boundary layer losses.These values of specific impulse were based upon the use of rhenium radiation cooled engines with a nozzle expansion ratio (ε) of 150 (typical for the length constraint of a lightweight satellite). The assumptions for the systems analyses are summarized as follows:

Propellant Residuals			Ullage Volume
N_2O_4-N_2H_4	Ox=1%	Fuel=3%	1%
N_2O_4-MMH	Ox=3%	Fuel=3%	1%

Propellant Tanks - Graphite fiber epoxy overwrapped tanks with aluminum liner

Pressurant Tank - Graphite fiber epoxy overwrapped tank with aluminum liner

The results of the systems analyses are presented in Figures 3.5-2 through 3.5-5 for the four types of missions. Figure 3.5-2 (Communication Satellite-COMSAT) showed the pump-fed system payload weight for a length constrained nozzle was fairly flat from Pc=500-1000 psia while the pressure-fed system payload weight for a length constrained nozzle maximized at Pc=300-500 psia. Figure 3.5-3 (MESUR) showed the pump-fed system payload weight for a length constrained nozzle was fairly flat from Pc=500-1000 psia while the pressure-fed system payload weight for a length constrained nozzle was relatively insensitive from Pc=100-500 psia. Figure 3.5-4 (Lightning Mapper-LM) showed the pump-fed system payload weight for a length constrained nozzle was fairly flat from Pc=500-1000 psia while the pressure-fed system payload weight for a length constrained nozzle maximized at Pc=500 psia. Figure 3.5-5 (TOMS) showed the pressure-fed system payload weight exceeded the pump-fed system payload and was fairly flat from Pc=500-1000 psia. A comparison of N_2O_4-N_2H_4 and N_2O_4-MMH propellant combinations for both pressure-fed and electric pump-fed systems is presented in Figure 3.5-6 and indicated the hydrazine fuel with its higher performance increased the spacecraft payload by 1-7% over the MMH fuel.

FIGURE 3.5-1 ENGINE PERFORMANCE

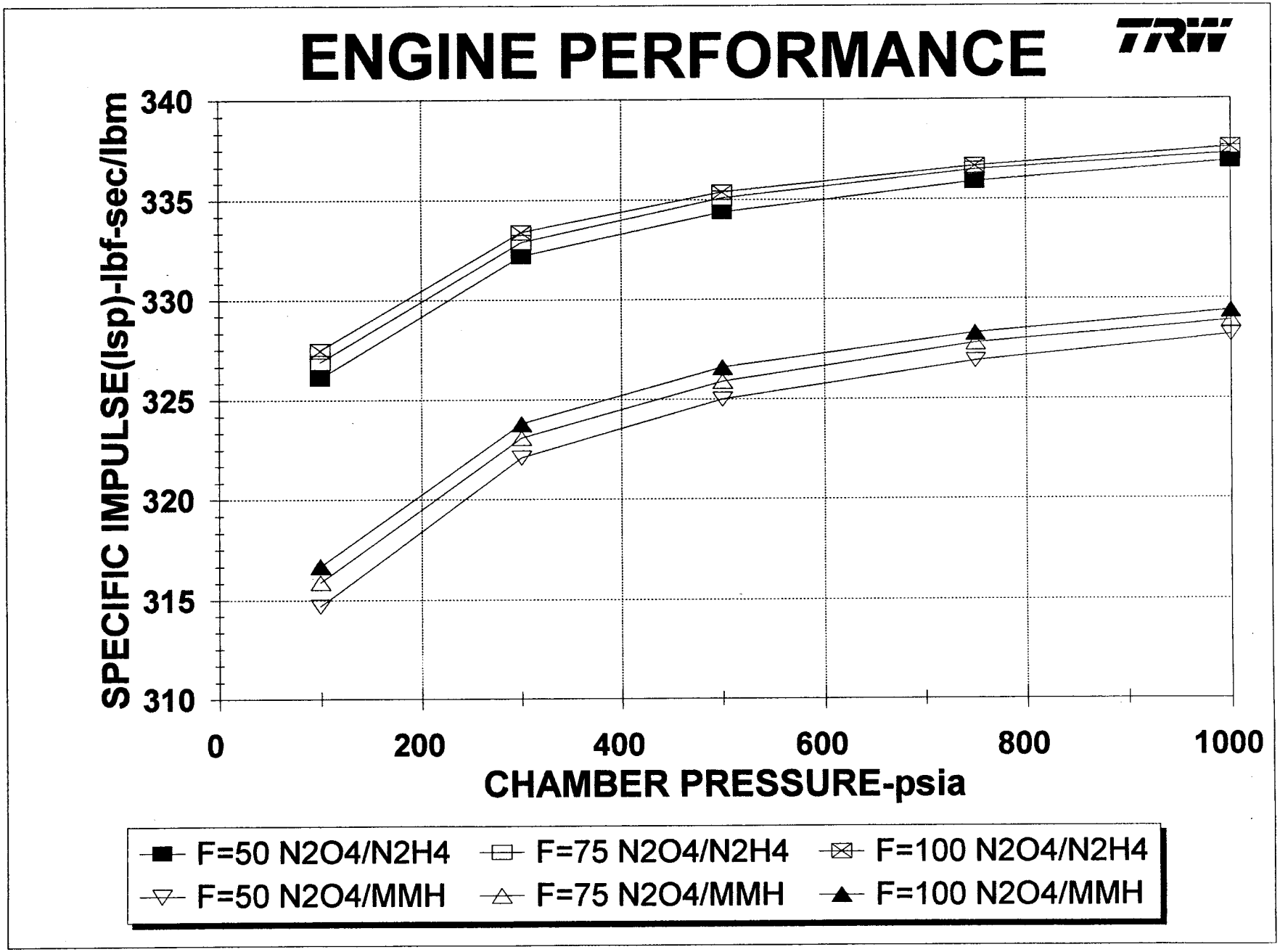

FIGURE 3.5-2 COMSAT PAYLOAD-N2O4-N2H4

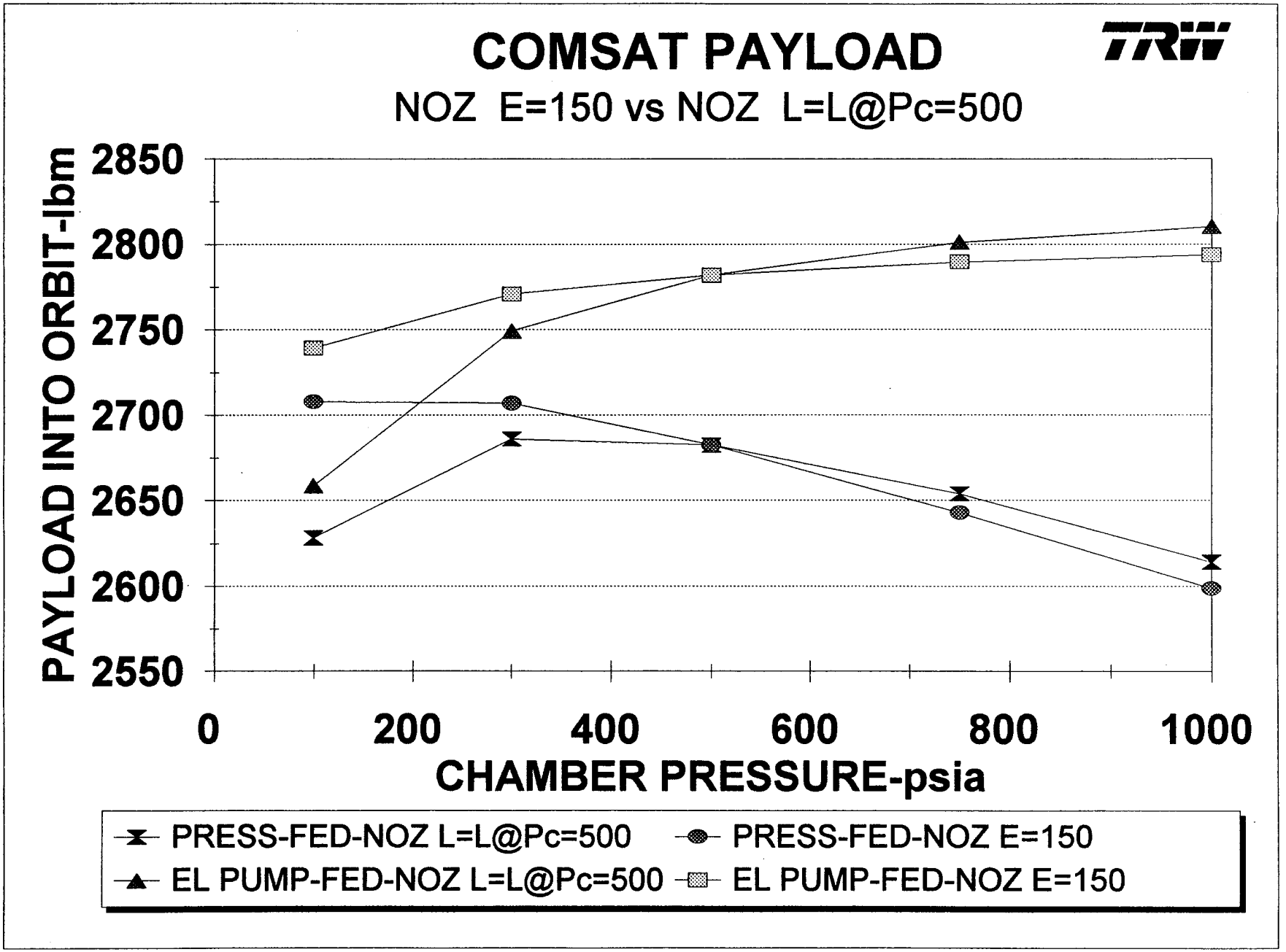

FIGURE 3.5-3 MESUR PAYLOAD-N2O4-N2H4

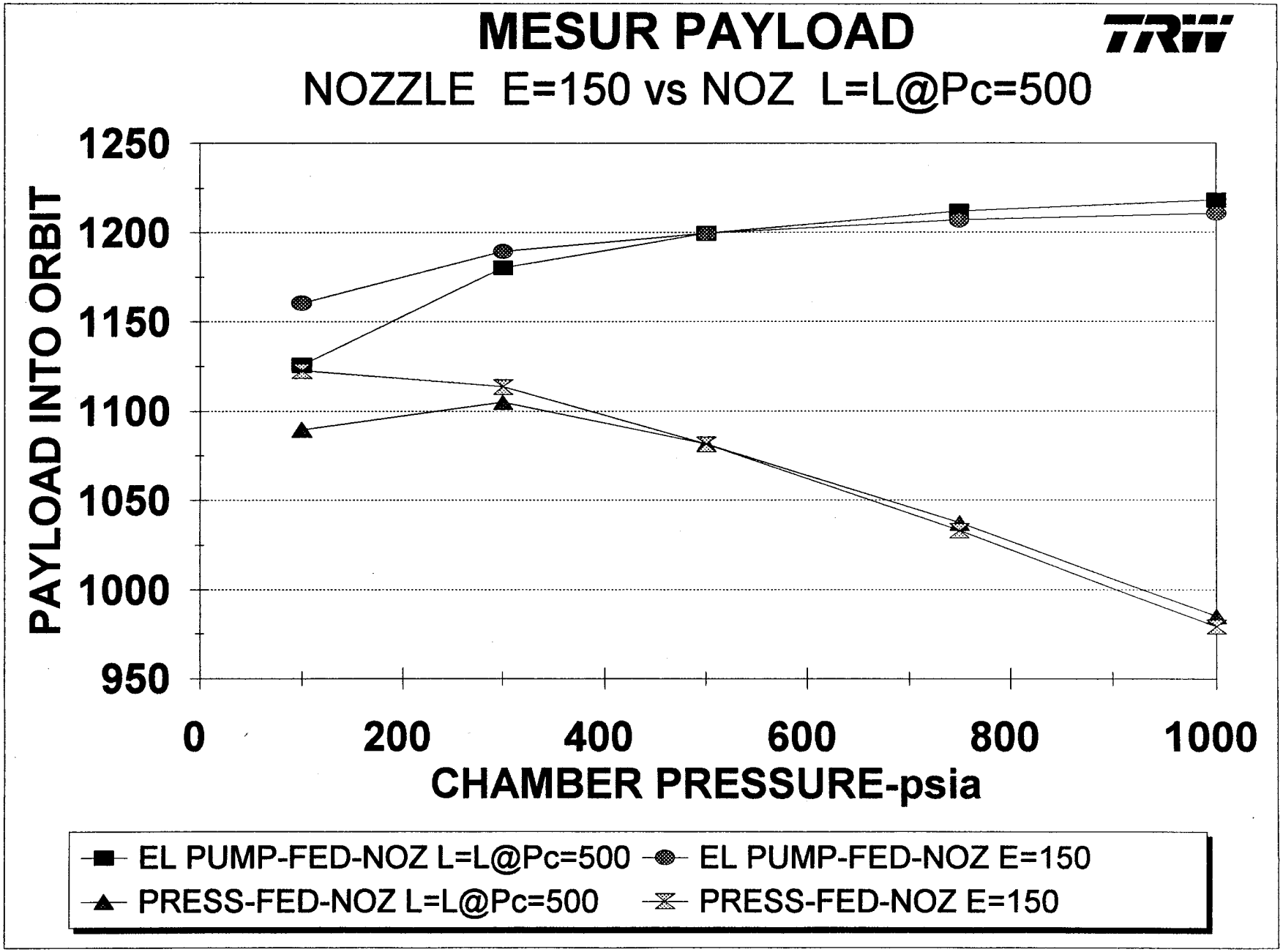

FIGURE 3.5-4 LM PAYLOAD-N2O4-N2H4

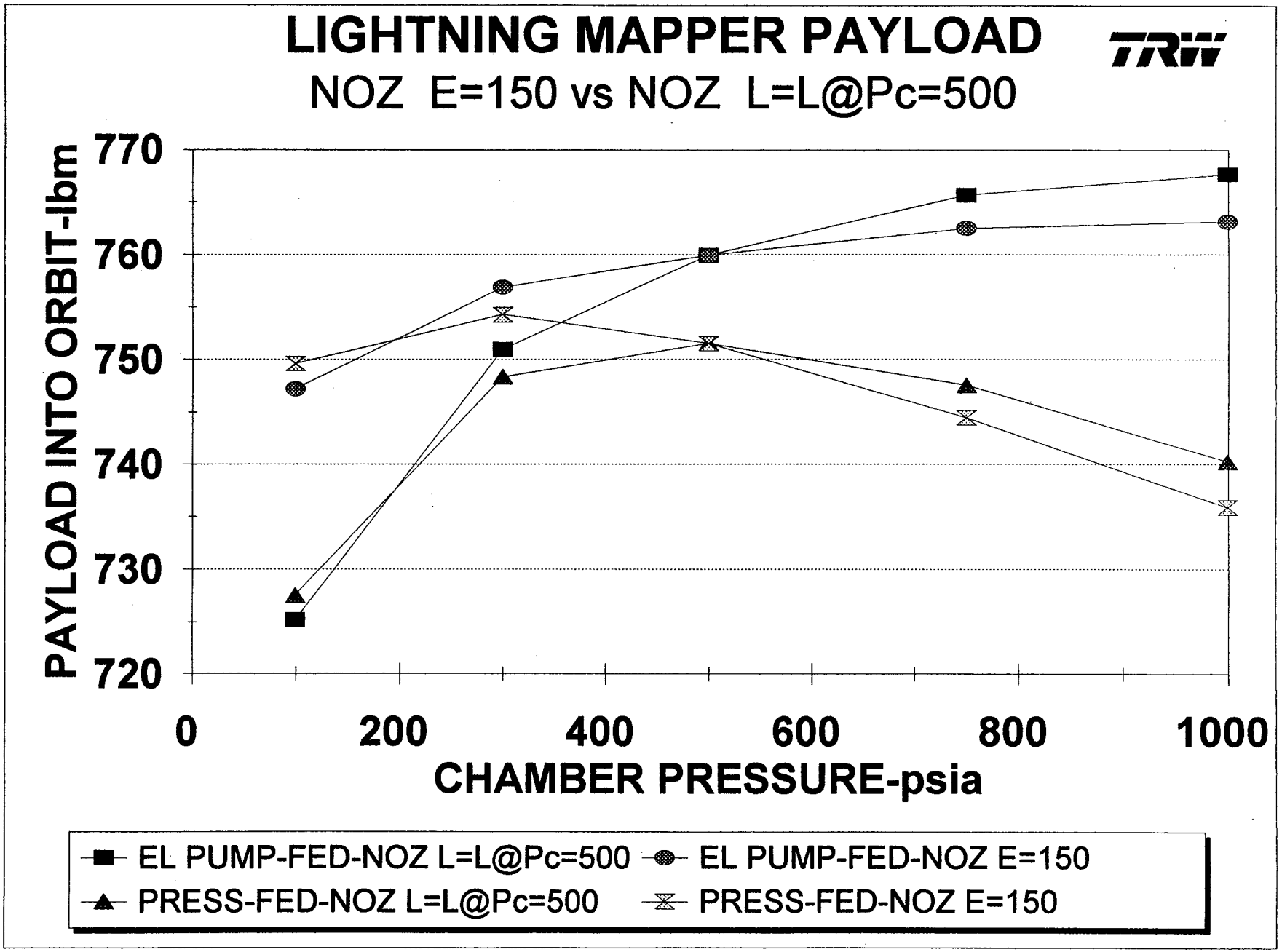

FIGURE 3.5-5 TOMS PAYLOAD-N2O4-N2H4

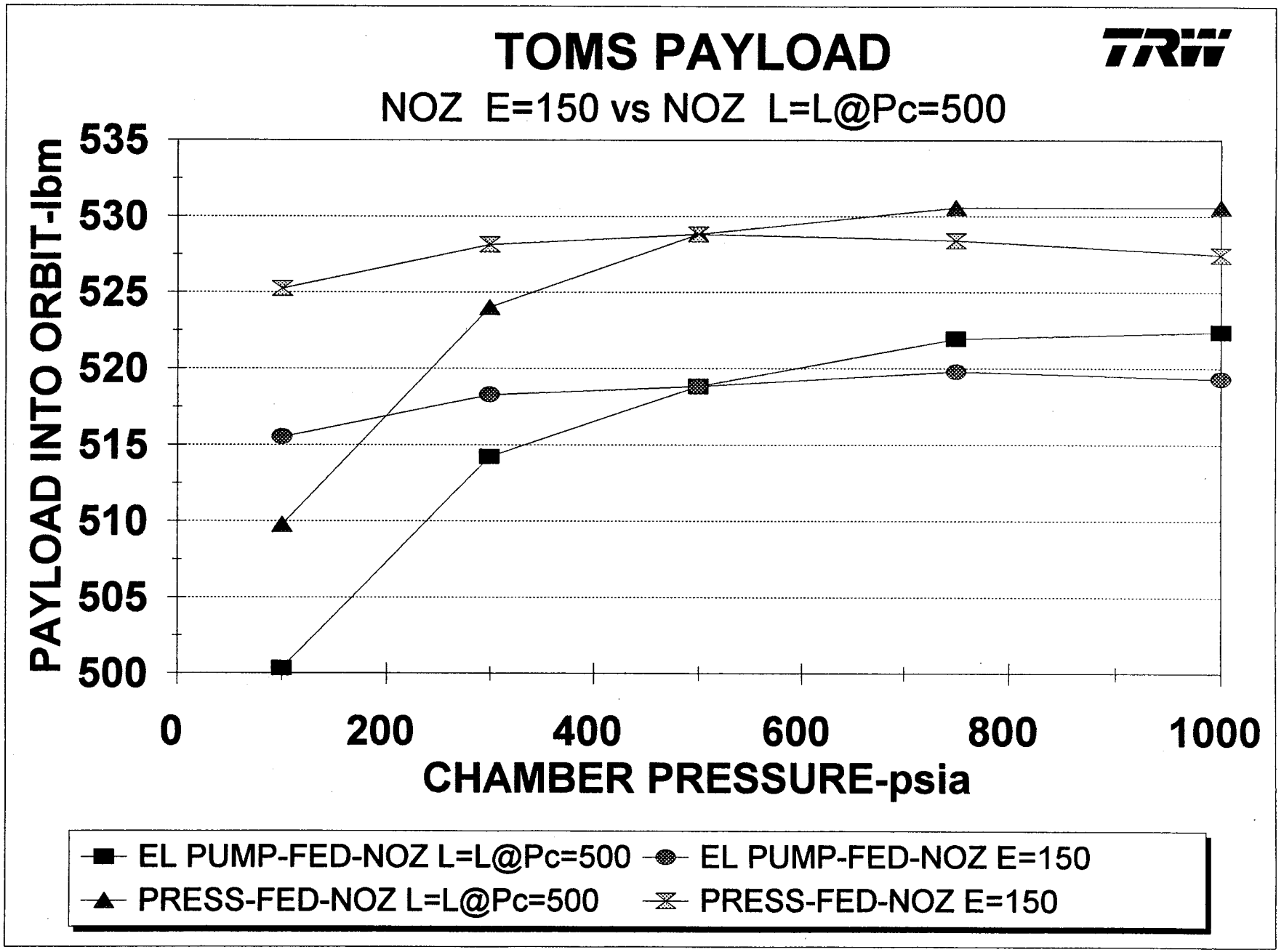

FIGURE 3.5-6 COMPARISON N2O4-N2H4 TO N2O4-MMH

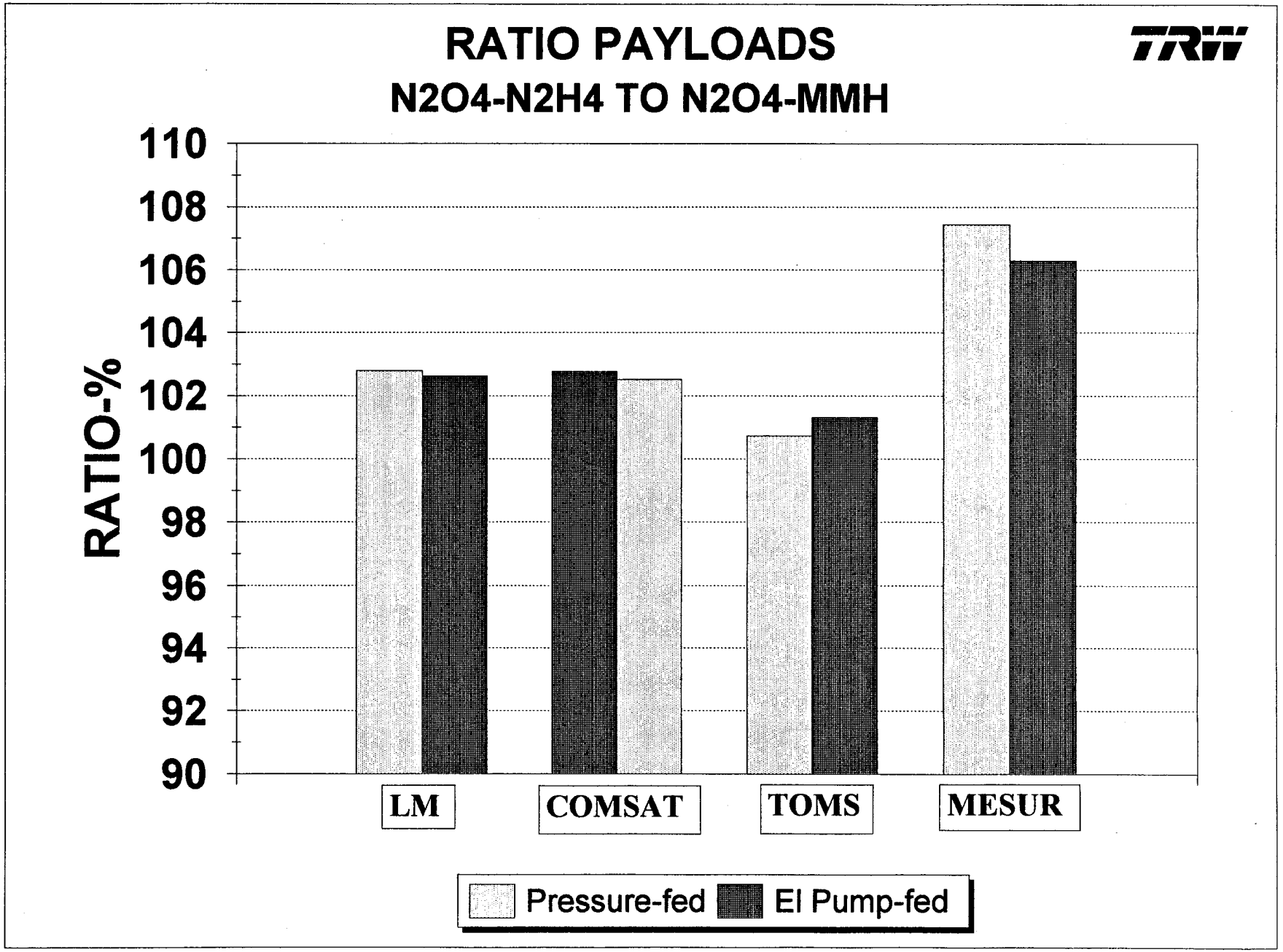

In summary Figure 3.5-7 showed that the payload at Pc=500 psia was within 1.5% of the maximum for both pressure and pump-fed systems except for Mesur(within 4%). The overall assessment was that the HIPES engine was most beneficial for lightsats with significant improvement in payload and fit within the spacecraft envelope due to its small envelope resulting from the high pressure (Pc=500 psia). For the large spacecraft, the 100 lbf class engines operating at Pc=100-125 psia were beneficial. TRW has been a leading producer of lightsats with such lightsats as TOMS, STEP, ROCSAT and SSTI. Figure 3.5-8 showed a comparison of the payload increases the HIPES engine would make on typical TOMS and Lightning Mapper spacecraft.

3.6 Propulsion System and Engine Requirements

As a result of the system analyses, preliminary system requirements were established for both a pressure-fed system and a pump-fed system. The preliminary requirements for both the pressure-fed and pump-fed systems is presented in Table 3.6-1.

Using the systems analyses and the preliminary systems requirements, a set of preliminary engine requirements was established. The engine requirements and operation are considered irrelevant as to pressure-fed or pump-fed systems as long as the engine inlet conditions are properly set. The preliminary engine requirements are presented in Table 3.6-2.

3.7 Conclusions

The greatest mission potential for the HIPES engine has been defined as apogee earth orbit missions to place satellites into GEO and delta-V for earth orbit missions. The trend selected by the various agencies has been to use smaller, better, cheaper satellites to perform these missions to reduce assets at risk.

As a result of the system studies which investigated pressure-fed, turbo-pump-fed and electric pump-fed systems, the electric pump-fed system maximized payload into orbit using N_2O_4-N_2H_4 at higher chamber pressures although operation required 1.3 -2.1 kw power for single or dual engine operation. The turbo-pump-fed system offered no advantage over the other systems. The pressure-fed system was determined to be better or the same for lightsats where power is usually limited.

Therefore, the HIPES engine development was focused on an engine operating at the following conditions:

Thrust (F_∞)	50 lbf
Mixture Ratio (O/F)	1.0
Propellants	N_2O_4-N_2H_4
Chamber Pressure (Pc)	500 psia
Specific Impulse (Isp_∞)	330 lbf-sec/lbm

FIGURE 3.5-7 PAYLOAD COMPARISON

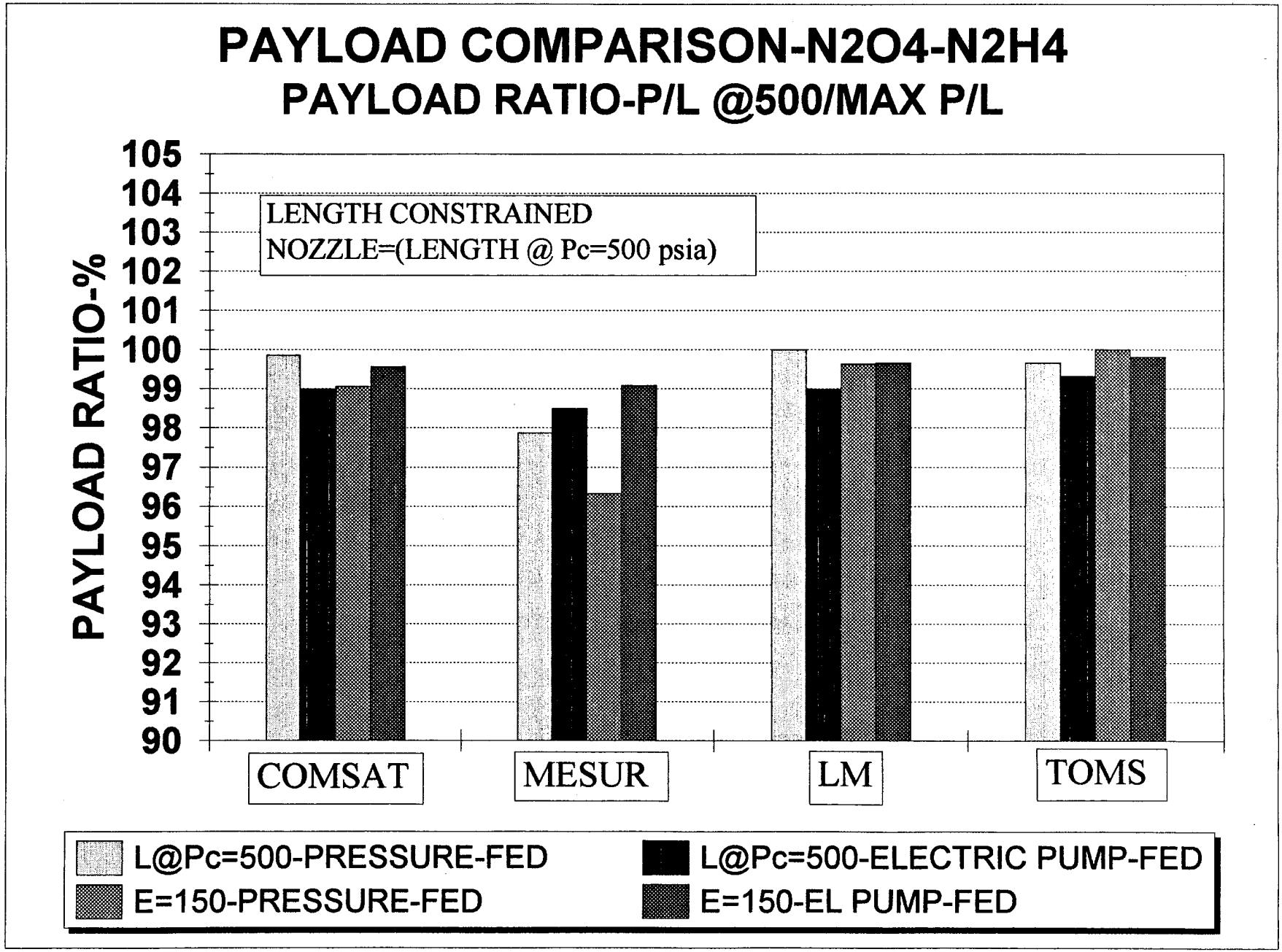

FIGURE 3.5-8 LIGHTSAT PAYLOADS

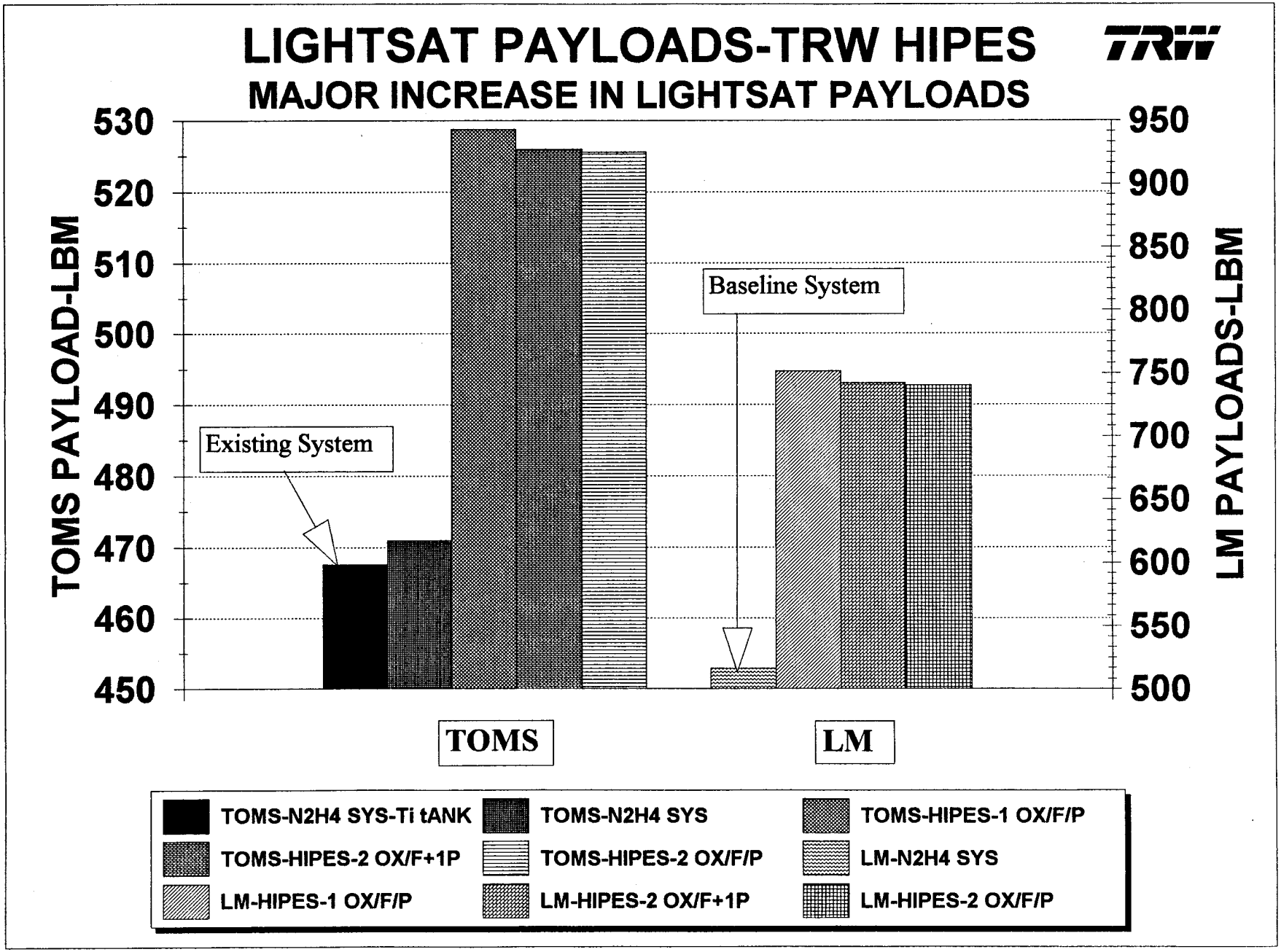

The HIPES engine development was based on these conditions during the Basic Program. This development allowed the engine to be used in either a pressure-fed or electric pump-fed system. The major challenge of development is demonstration of operation at 500 psia chamber pressure with a specific goal of 330 lbf-sec/lbm with thermal characteristics compatible with long duration firings and associated life.

The HIPES engine provides major benefits to lightsat applications where volume and/or length is constrained. Payload increases to these lightsats can be increased by 10-20% depending on the mission.

TABLE 3.6-1
PROPULSION SYSTEM REQUIREMENTS

System Definition:

Integral Propulsion System

Dual Mode Orbit Boost or Delta-V Subsystem - impulse to place satellite into GEO from parking orbit established by the expendable launch vehicle or provide Delta-V for an earth orbit satellite

Reaction Control Subsystem (N_2H_4) - necessary torques to control spacecraft attitude about all three axes and necessary impulse to accomplish 0.1 degree inclination limit for 10 years (N-S + E-W) for GEO satellite or necessary torques to control spacecraft attitude control for earth orbit satellite

Disposal - provide impulse to move the spacecraft into a disposal orbit at the end of its operational life

Configuration

Major Components

Pressurization: GHe - 7500 psia pressure regulated to tank pressure
Graphite/epoxy overwrapped tank with aluminum liner

Propellant Tanks: Oxidizer (N_2O_4) and Fuel (N_2H_4) - Cylindrical tanks with elliptical heads & graphite/epoxy overwrapped with a maximum pressure of 700 psia for pressure-fed system and 50 psia for pump-fed system

Engines:
Thrust (F_∞) - 50 lbf each - one or two per system using single seat valves
Operation - steady state with maximum firing duration of 1800 seconds
Mixture ratio (O/F) - 1.0
Life - 4000 seconds (Qualification - 6000 seconds)
Specific Impulse (Isp_∞) - 330 lbf-sec/lbm
Inlet pressure to engine - 650 psia
Engine weight - 3.5 lbm maximum
Engine length - 13.4 inches for inline valve configuration
10.0 inches for stacked valve configuration

Heaters required to prevent propellant freezing

System:

Delta-V - 5875 fps
RCS Delta-V - dependent on specific mission
Losses: Residuals - 1% oxidizer & 3% fuel Ullage - 1%
Cleanliness - Particulate matter below 50 microns
Electrical - 24-34 Vdc using electrical harness to components - pigtails used on all components
Mechanical interface - three point engine mount with tube stubs for welding to system manifold
Thermal environment
    Interior of spacecraft: 50-80F
    Exterior boundary conditions: Worst case solar inputs
        Worst case cold-exposure to deep space with no solar inputs
Random vibration:
    Qualification: 14.1 g-rms
    Acceptance: 10.0 g-rms
External leakage for system (exclusive of engine/valves) - 15 scc/hr GHe
External leakage for engine/valves - 5 scc/hr GHe per propellant side
Delta pressure between oxidizer and fuel tanks - ±5 psia
Engine alignment - 0.5 degree
Mixture ratio control: 1.0±0.08 over temperature and pressure tolerances
Operating life: 10 years + 4 years storage
Reliability: 0.995 with no single point failures of active components
System dry weight - TBD

TABLE 3.6-2
ENGINE REQUIREMENTS

Thrust (F_∞) - lbf	50±2.5
Propellants	N_2O_4-N_2H_4
Mixture Ratio (O/F)	1.0±0.03
Specific Impulse (Isp_∞) - lbf-sec/lbm	330
Inlet Pressure - psia	650+50,-10
Propellant Inlet Temperature - F	70±10 (excluding heat soakback)
System Mixture Ratio (O/F)	1.0±0.08(includes P & T variations)
Life - sec	4000 (Qual - 6000)
Maximum Continuous Firing - sec	1800
Operation	Steady state
Operating Voltage - Vdc	24-34
Engine Length - inches	10.0 - stacked valves 13.4 - inline valves
Engine Diameter - inches	7 maximum
Heaters	Required to prevent propellant freezing
Valve Seat Leakage (scc/hr Ghe)	5 per valve seat
Random Vibration	Qual - 14.1 g-rms Acceptance - 10.0 g-rms
Oxidizer - Fuel Inlet Pressure Variation	Fuel = ±5 psia of oxidizer pressure
Alignment	±0.5 degree
Engine Weight - lbm	3.5 maximum
Contamination Control	Particulate matter below 50 microns Valve inlet filter-25 microns
Valve Characteristics	
Pull - in Voltage - Vdc	19 maximum
Dropout Voltage - Vdc	≥2
Open Response - ms	≤30
Close Response - ms	≤30
Maximum Pressure - psia	700
Engine Cold Starts	25
Engine Roughness	±12%
Gas Ingestion	2 in^3
Oxidizer Depletion	Must have capability
Heat Shield	No impact on engine temperature

4.0 DESIGN and FABRICATION

4.1 Design

The design philosophy used on the HIPES engine was to design a testbed engine that incorporated the test results of other TRW programs applicable to HIPES, design hardware that met the NASA downselect criteria, incorporated flexibility into the design to facilitate parametric testing, incorporated interchangeability of parts to allow for assessments of various configurations and test flexibility to allow for expedious testing in a cost effective manner.

The guidelines used were to design an injector with replaceable elements for evaluation of injector slot geometry, utilized shimmable oxidizer and fuel elements to evaluate variations in velocity and momentum and incorporated a regenerative cooling passage near the chamber for assessment of the benefits/need. Different thrust chambers were utilized for different objectives. Workhorse copper heatsink thrust chambers were utilized to evaluate L* variability and Pc variability at constant thrust. A water-cooled thrust chamber was utilized to determine the heat absorbed to allow a prediction of the wall temperatures for the rhenium thrust chamber and allowed an assessment of the dome temperatures in long duration firings. A rhenium thrust chamber was also designed to evaluate performance and operation at high chamber pressure with a high performance injector.

A model, previously developed by TRW to assist in the design/analysis of TRW coaxial pintle injectors, was used to design the HIPES injectors. This model integrated the performance and thermal aspects of the engine. As a result, the model predicted atomization of the fuel from the injector design variables, calculated droplet trajectory, vaporization rate and penetration distance, predicted the fraction of fuel flow impinging on the injector splash plate as liquid, accounted for increasing wall zone mixture ratio along the chamber wall, calculated film coefficient as a function of chamber axial position and chamber wall temperature and finally predicted the C* based on the mixture ratio distribution of the wall and core zones at the throat. Correlation of this model with various TRW hot fire data from a number of programs has proven successful. The predicted performance of the HIPES engine was a specific impulse of 330 lbf-sec/lbm with a throat wall temperature of approximately 3500F.

The testbed engine consisted of a flexible injector and three types of thrust chambers. The injector consisted of a shimmable design to allow variations in injection velocity and momentum with ease in real time testing allowing for efficient cost effective testing. The injector incorporated replaceable elements to allow evaluation of slot geometries (number of slots, slot aspect ratio and open area between slots) for efficient effective wall control in real time cost effective testing. Three different types of thrust chambers were designed to demonstrate the overall objectives. Copper heatsink thrust chambers were designed to operate at 400, 500 and 600 psia chamber pressures at a constant 50 lbf thrust. Thermocouples were brazed into the inner wall of the thrust chamber to allow a determination of heat load and estimate of gas temperatures. Spool pieces were designed

to allow variation in L*. The copper heatsink chambers were designed for 5-sec tests. The HIPES heatsink engine is presented in Figure 4.1-1. In order to ascertain the overall engine capability, a water-cooled thrust chamber was designed to determine the heat absorbed to predict the rhenium engine wall temperatures and allow long duration testing to determine head end stabilized temperatures. The water-cooled HIPES engine is presented in Figure 4.1-2. A bolt-on rhenium engine was designed using a coated powder metallurgy rhenium thrust chamber to validate performance and demonstrate operation with high performance injector and associated high wall temperatures at high pressures. The HIPES rhenium engine is shown in Figure 4.1-3. As a result of the design and analyses of the testbed engine, a preliminary flight engine concept is shown in Figure 4.1-4.

FIGURE 4.1-1 HIPES TESTBED HEATSINK ENGINE

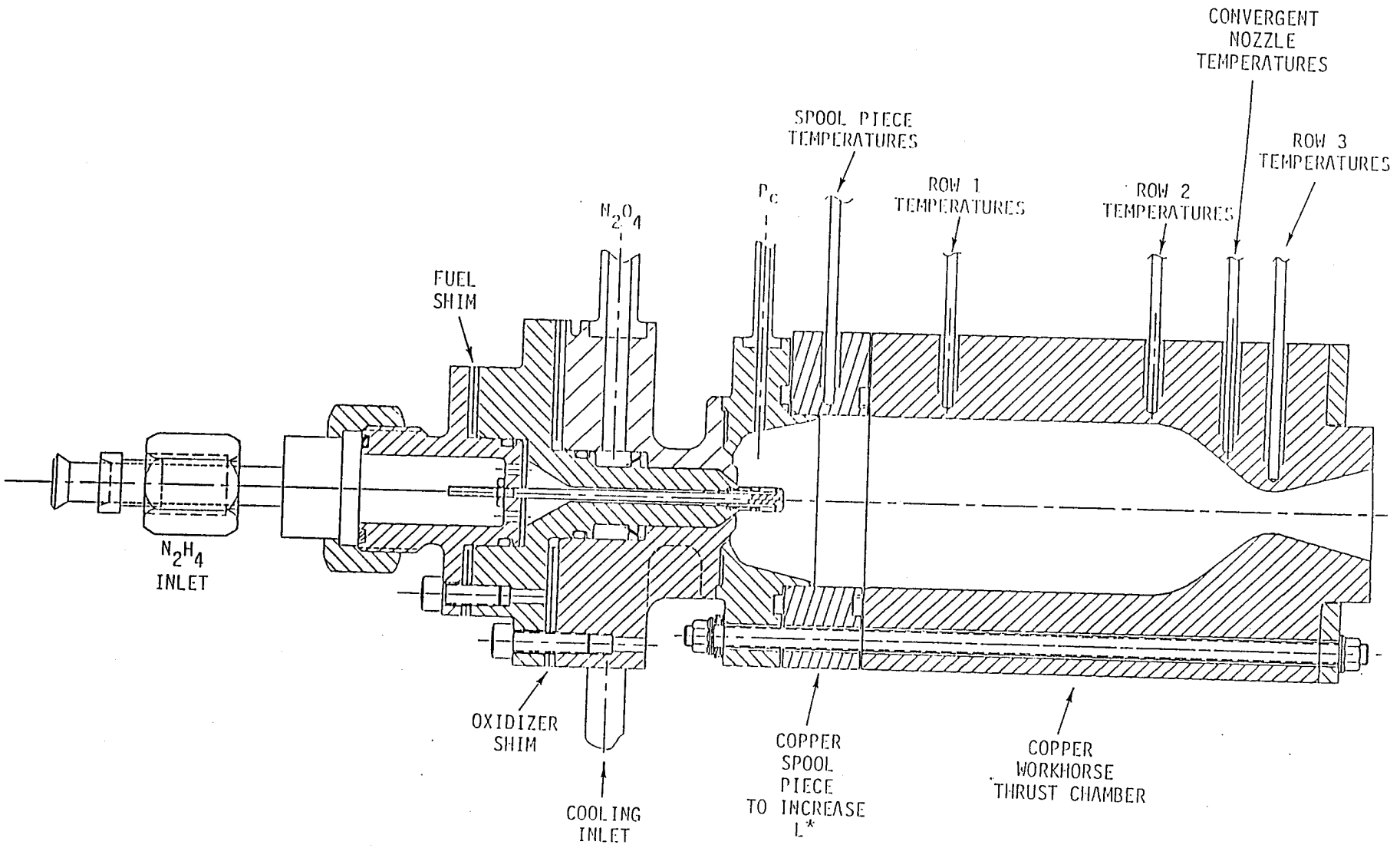

FIGURE 4.1-2 HIPES WATER-COOLED ENGINE

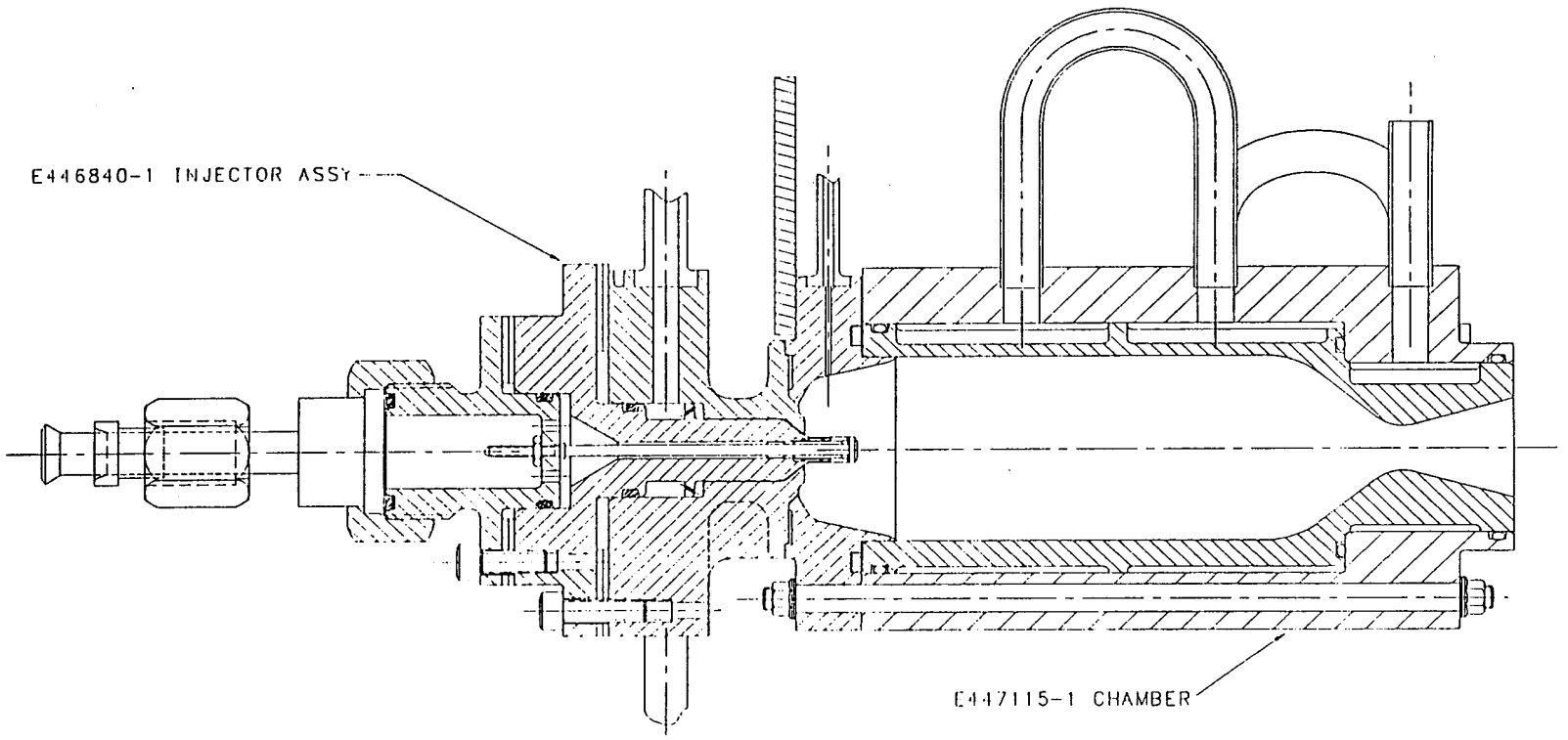

FIGURE 4.1-3 HIPES RHENIUM ENGINE

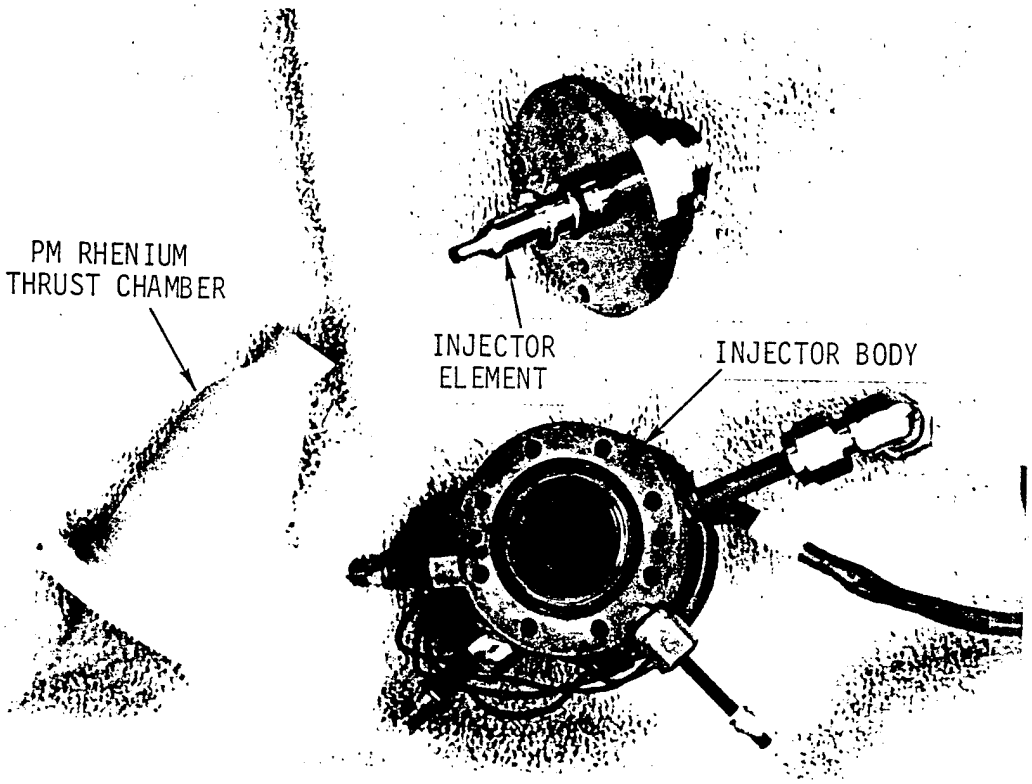

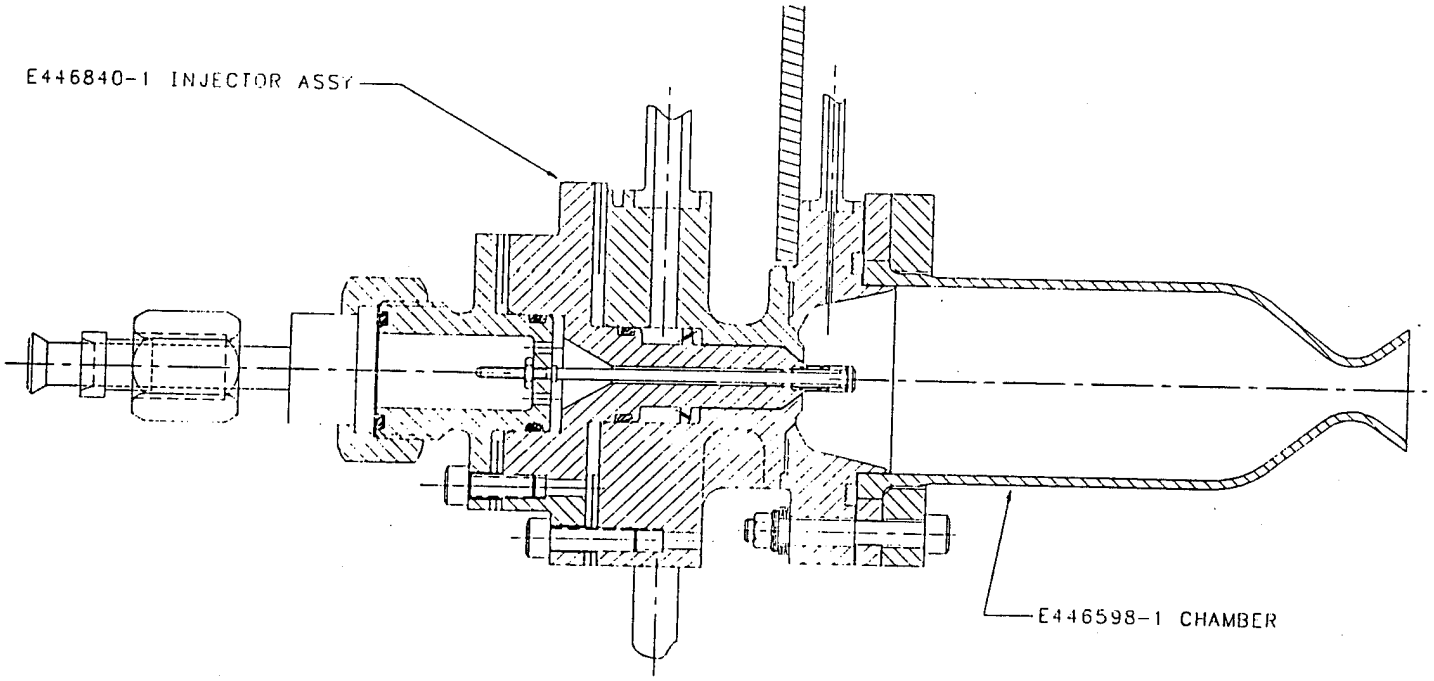

TRW

FIGURE 4.1-4 HIPES FLIGHT ENGINE CONCEPT

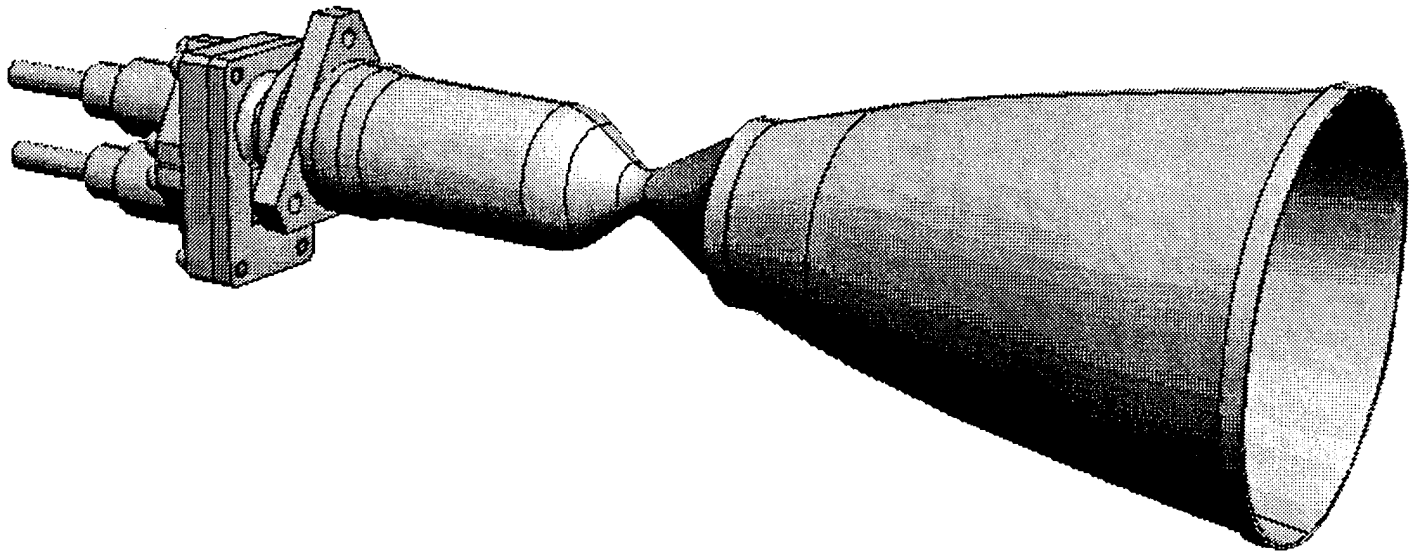

5.0 PERFORMANCE AND THERMAL DATA/ANALYSIS

A description of the test conduct and presentation of the data obtained from the hot-fire tests are discussed in this section. Any performance and thermal trends resulting from this test program will also be discussed.

An overview of the test conduct for the HIPES basic program is presented in Figure 5.0-1. Each block of testing will be discussed in detail in the corresponding subsections. The primary objectives of the test program were:

- o evaluated the performance characteristics for four different injectors
- o determined the effects of varying mixture ratio and total flowrate on the engine performance
- o investigated the performance and heat transfer at three different chamber pressures at constant thrust
- o ascertained the gas-side heat transfer rates into the injector dome
- o demonstrated the adequacy of coated PM rhenium engine operation to withstand the thermal environment at high performance and high chamber pressure
- o anchored thermal and performance analysis models with test data
- o predicted the operating characteristics of a flight-type engine

Engine performance was characterized through the measurement of characteristic velocity (C*). The observed C* was combined with the theoretical thrust coefficient (Cf) to yield projected specific impulse (Isp). Calculations of Cf were made using the standard NASA TDK program with a defined geometry of HIPES engine (100% bell nozzle) with an expansion ratio of 150:1. The predicted Cf as a function of both chamber pressure (Pc) and mixture ratio (O/F) is shown in Figure 5.0-2. These thrust coefficients consequently served as the basis for the Isp projections made throughout this report.

5.1 HEAT-SINK COPPER CHAMBER TESTING

The initial testing of the HIPES workhorse engine began with uncooled copper thrust chambers using N_2O_4-N_2H_4. These chambers had sufficient wall thicknesses to provide sufficient heatsink capability to allow test durations of at least 5 seconds, which was adequate to obtain comparative steady-state performance (C*) data.

5.1.1 INJECTOR EVALUATION

The first objective of the heatsink engine tests was to evaluate four different injector element candidates for selection of a baseline element to be used in subsequent testing. All of these tests were conducted at the nominal mixture ratio of 1.0, nominal flowrate of 0.152 lbm/sec, and nominal chamber pressure of 500 psia. Five to seven tests were performed on each injector to measure C* variation resulting from changing the oxidizer and/or fuel injector gaps (velocities). A test summary is provided in Table 5.1.1-1. Injector selection was based on a qualitative assessment of combustion efficiency, maximum injector dome temperature, and transient chamber throat temperature. The effect of varying injector

TEST LOGIC FOR BASIC PROGRAM

FIGURE 5.0-1

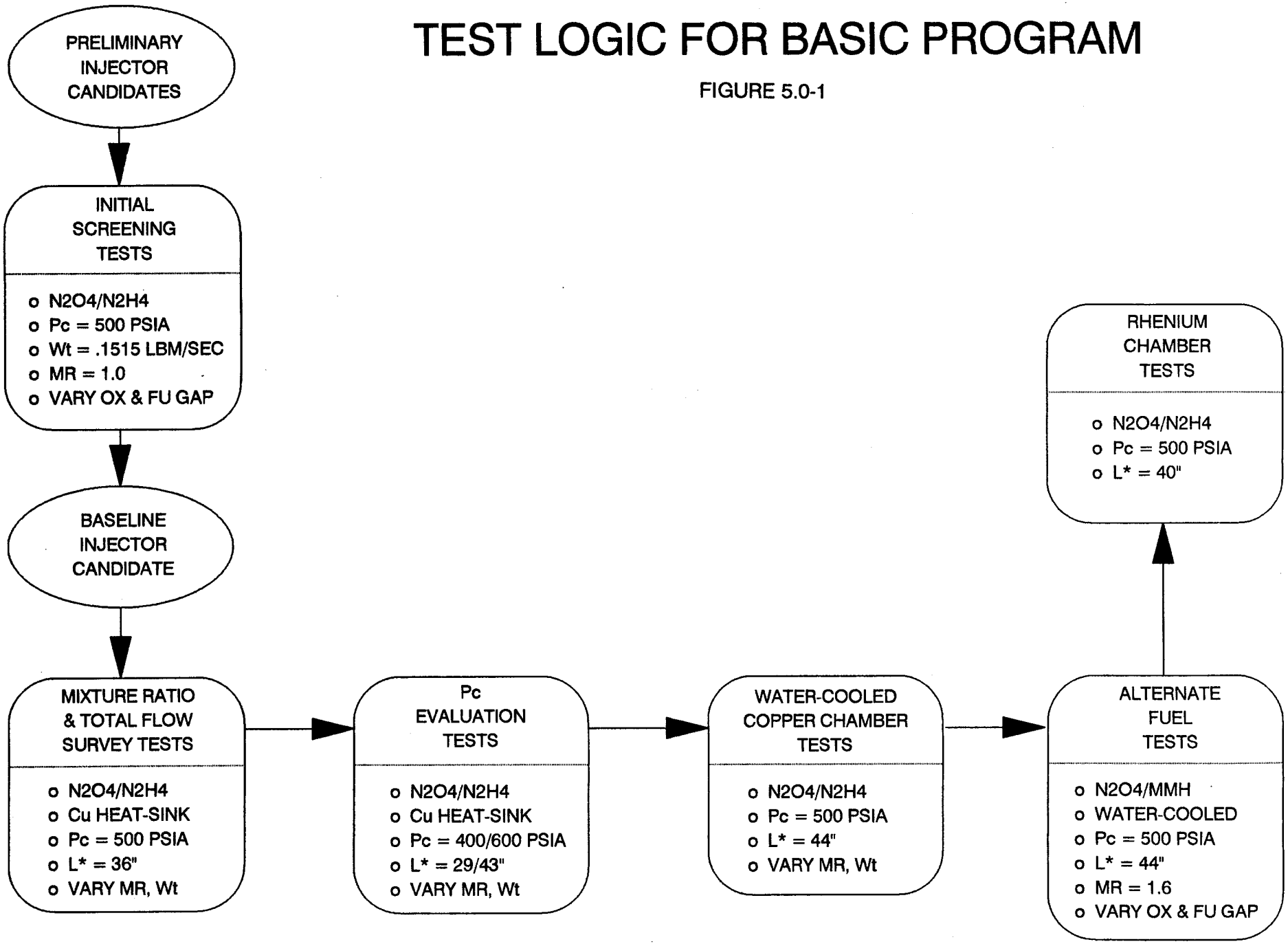

TDK THRUST COEFFICIENT

FIGURE 5.0-2

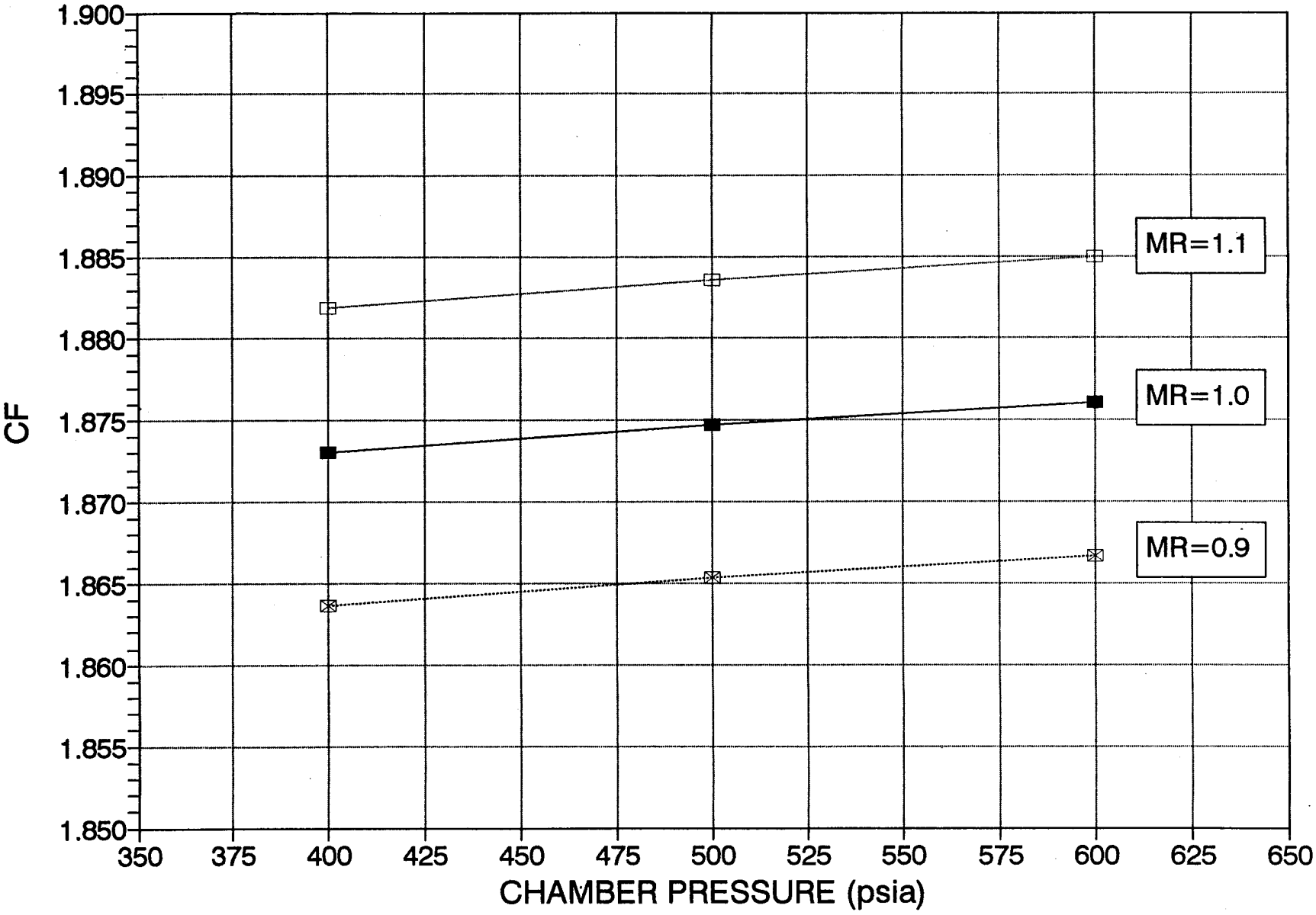

TABLE 5.1.1-1 HIPES INJECTOR EVALUATION TEST SUMMARY

TRW

TEST NO HA2A-	DUR SEC	INJ TYPE	Dox INCH	Df INCH	T/S SEC	MR O/F	Wt LBM/SEC	Pc PSIA	Tt(avg) F	Td(max) F	C* FPS	Isp(avg) SEC
4285	3	-1	0.006	0.002	2.9	0.998	0.1516	487	-	-		c/o
4286	5	-1	0.006	0.002	4.7	0.9999	0.151	487.2	666	315	5725	333.6
4287	5	-1	0.005	0.002	4.7	0.9975	0.1516	494.5	717	359	5777	336.6
4288	5	-1	0.0045	0.002	4.7	0.9983	0.1516	497.8	751	401	5805	338.3
4289	5	-1	0.006	0.0026	4.7	0.9978	0.1516	491.8	713	289	5743	334.6
4290	5	-1	0.006	0.003	4.7	0.9979	0.1516	486.8	715	239	5768	336.1
4291	5	-2	0.006	0.002	4.7	0.9958	0.1513	487.5	665	188	5685	331.3
4292	5	-2	0.005	0.002	4.7	0.9993	0.1514	488.8	677	247	5686	331.3
4293	5	-2	0.005	0.0026	4.7	0.9981	0.1513	496.2	705	285	5767	336.0
4294	5	-2	0.005	0.003	4.7	0.9975	0.1514	500	740	310	5802	338.1
4295	5	-2	0.005	0.0034	4.7	0.9964	0.1511	497	731	283	5778	336.7
4296	5	-2	0.006	0.0034	4.7	0.9996	0.1522	504.1	733	204	5804	338.2
4297	5	-2	0.006	0.0038	4.7	0.9988	0.1509	495.9	744	207	5753	335.2
4298	5	-3	0.006	0.0018	4.7	1.0001	0.1509	493.7	760	336	5725	333.6
4299	5	-3	0.006	0.0026	4.7	0.999	0.1522	500.5	784	341	5758	335.5
4300	5	-3	0.006	0.0034	4.7	0.9985	0.1519	505.1	861	201	5814	338.7
4301	5	-3	0.007	0.0034	4.7	0.9983	0.1516	508.7	866	182	5840	340.3
4302	5	-3	0.007	0.0026	4.7	0.9976	0.1515	502.1	844	280	5779	336.7
4303	5	-4	0.006	0.0019	4.7	0.9998	0.1519	511.4	857	189	5865	341.7
4304	5	-4	0.006	0.0027	4.7	1.0023	0.1519	504.4	826	213	5783	337.0
4305	5	-4	0.007	0.0027	4.7	1.0013	0.1517	502.8	766	193	5760	335.6
4306	5	-4	0.007	0.0019	4.7	1.0005	0.1514	506	811	202	5828	339.6
4307	5	-4	0.007	0.0013	4.7	1.001	0.1515	503.3	768	184	5772	336.3
4308	5	-4	0.006	0.0013	4.7	0.9996	0.1516	504.9	790	195	5787	337.2
4309	5	-4	0.005	0.0013	2.2*	1.0013	0.1517	502.8	731	213	5731	333.9

*Contamination in fuel slots

gaps on measured C* is presented in Figure 5.1.1-1. It was apparent that the combustion efficiency for most tests fell within a relatively narrow range of 98.0-99.5% (based on an ODE C* of 5860 ft/sec), and as a result of this finding each injector was judged suitable from a performance standpoint. Injector selection was therefore made based on thermal criteria, specifically the injector dome and chamber throat temperatures. A comparison of the average chamber throat temperatures observed for these tests at 4.7 sec into each test is presented in Figure 5.1.1-2. This data indicated that the -1 and -2 injectors yielded lower steady-state chamber temperatures than either the -3 or -4 injector. Finally, Figure 5.1.1-3 assessed the maximum injector dome temperatures and indicated that the thermal environment in the head-end region was more benign for the -2 injector than the -1 injector. As a result of a combination of high performance and relatively lower injector and chamber temperatures, the -2 injector was selected as the best candidate for proceeding into the remainder of the test program.

It should be noted that in addition to the aforementioned desirable characteristics, no evidence of "popping" was observed on the chosen injector. Popping is currently believed to be the result of the reaction of a small amount of hydrazine that, for some injectors at certain gaps under the right test conditions, can become trapped between the gap formed between the injector splash plate and the chamber wall. This popping was occasionally observed on other engine programs and has been known to deform the splash plate if the magnitude of the disturbance is sufficiently severe. In this group of tests, the last test on the -1 injector as well as every test on the -4 injector exhibited minor popping shortly after startup, as evidenced on the accelerometer and chamber pressure oscillograph traces. Post-test inspection revealed that this popping knocked off some of the outer layers of the disilicide coating near the tip of the splash plate, but did not result in any metal deformation.

A performance "map" of the -2 baseline injector is provided in Figure 5.1.1-4. The trends illustrated here are quite similar to those observed on previous engines. For instance, for a given oxidizer gap, as the fuel gap is increased, performance usually increased to a maximum and then decreased. Also, for a given fuel gap, a decrease in oxidizer gap usually resulted in higher injector dome temperatures. The lines of constant C* overlaid on the data can be considered somewhat speculative, but they provided a possible means of gaining insight into the response of a given injector to a change in either the oxidizer or fuel gaps (velocities).

5.1.2 CHAMBER PRESSURE EVALUATION

Having selected the baseline injector, the next objective was to expand the operating envelope by testing off-nominal mixture ratios and total propellant flowrates. The O/F and Wt envelope evaluated is shown in Figure 5.1.2-1. This matrix of tests was conducted on all three heatsink chambers (500, 600, and 400 psia, sequentially) for the establishment of the effect of chamber pressure on combustion performance and heat transfer. The test conditions and results from this phase of testing are summarized in Table 5.1.2-1.

HIPES INJECTOR GAP SURVEY TEST DATA

MR=1.0 Wt=.1516 lbm/sec Pc=500 psia

FIGURE 5.1.1-1

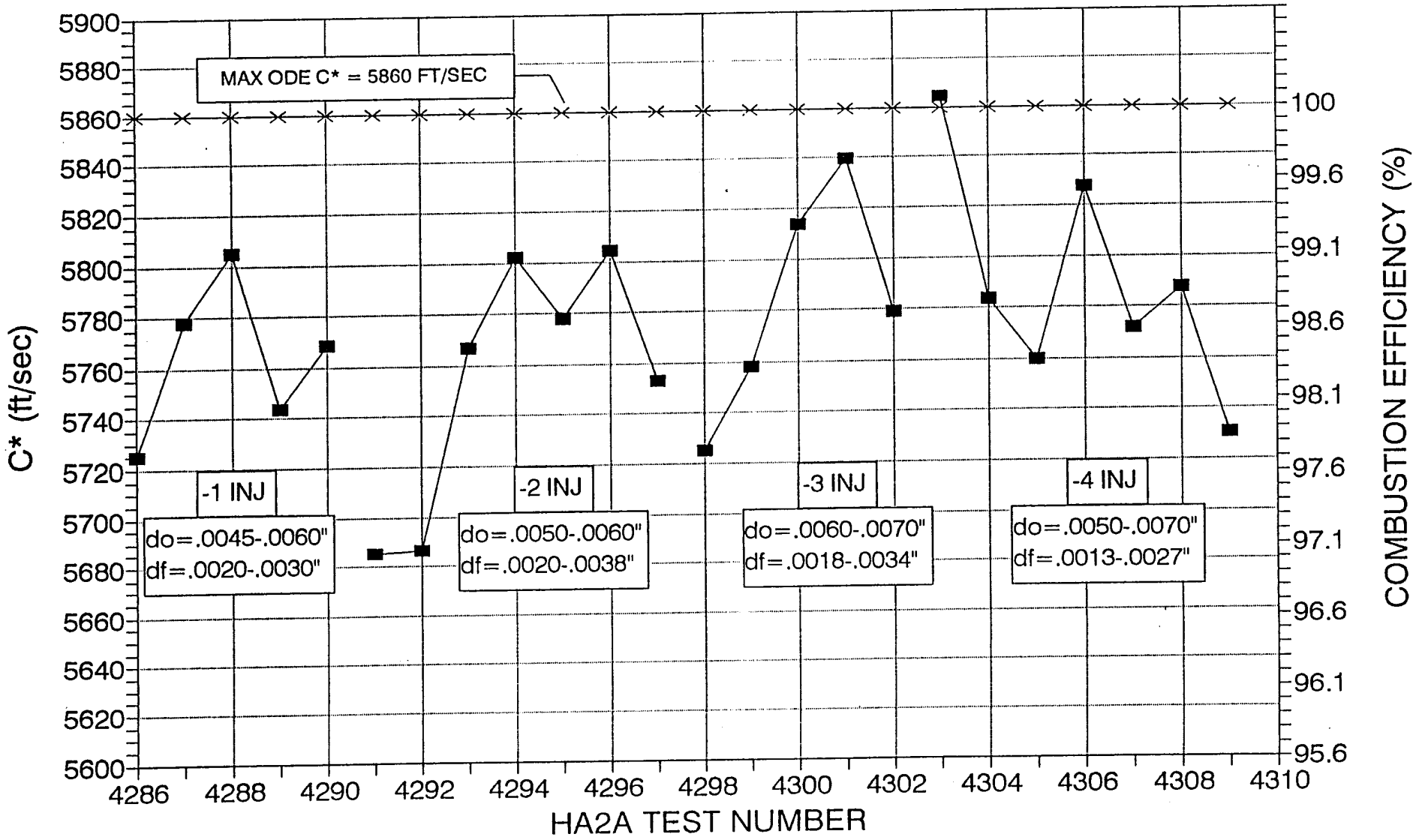

CHAMBER THERMAL CHARACTERISTICS

500 PSIA HEAT-SINK CHAMBER

FIGURE 5.1.1-2

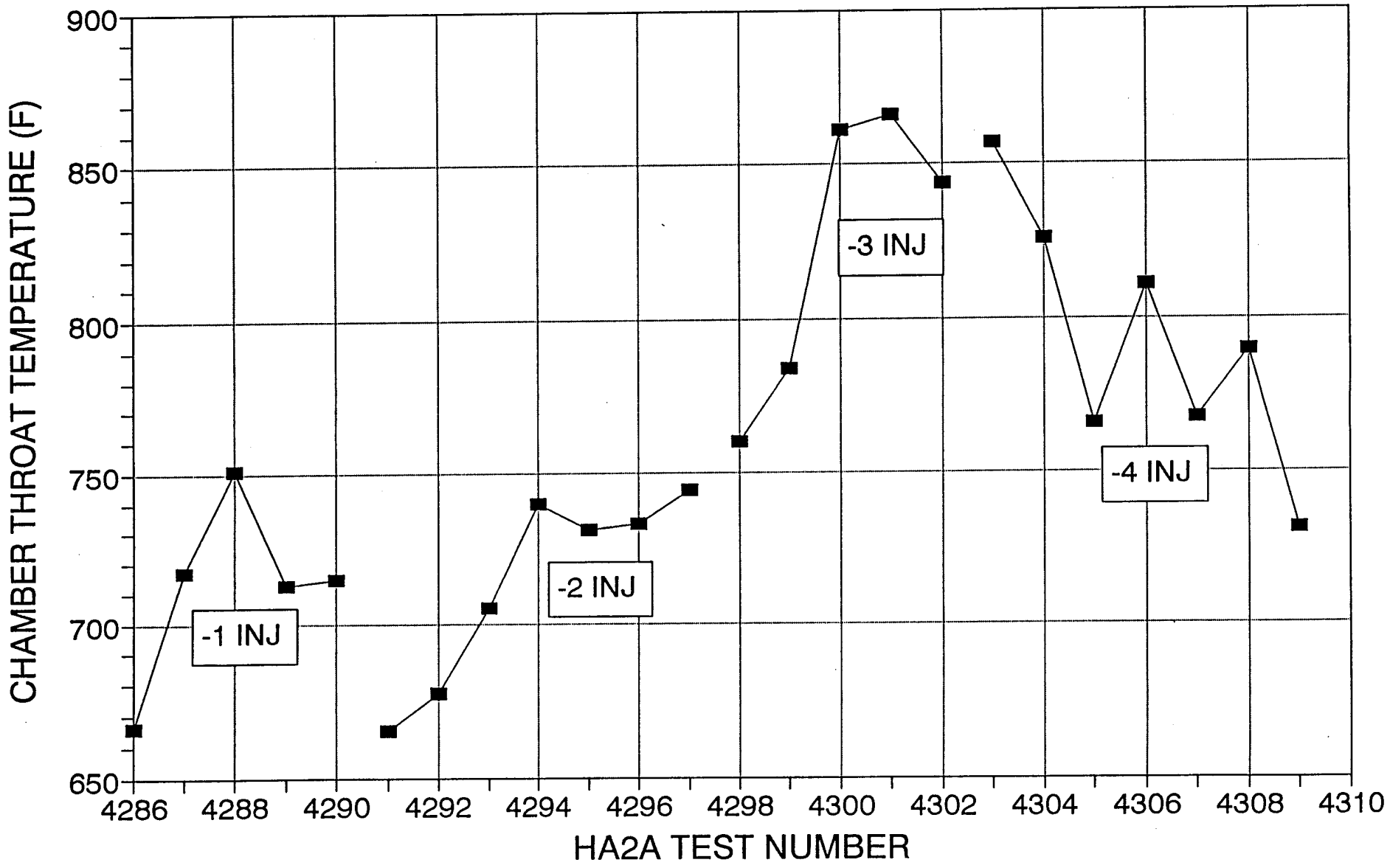

INJECTOR DOME THERMAL CHARACTERISTICS

500 PSIA HEAT-SINK CHAMBER

FIGURE 5.1.1-3

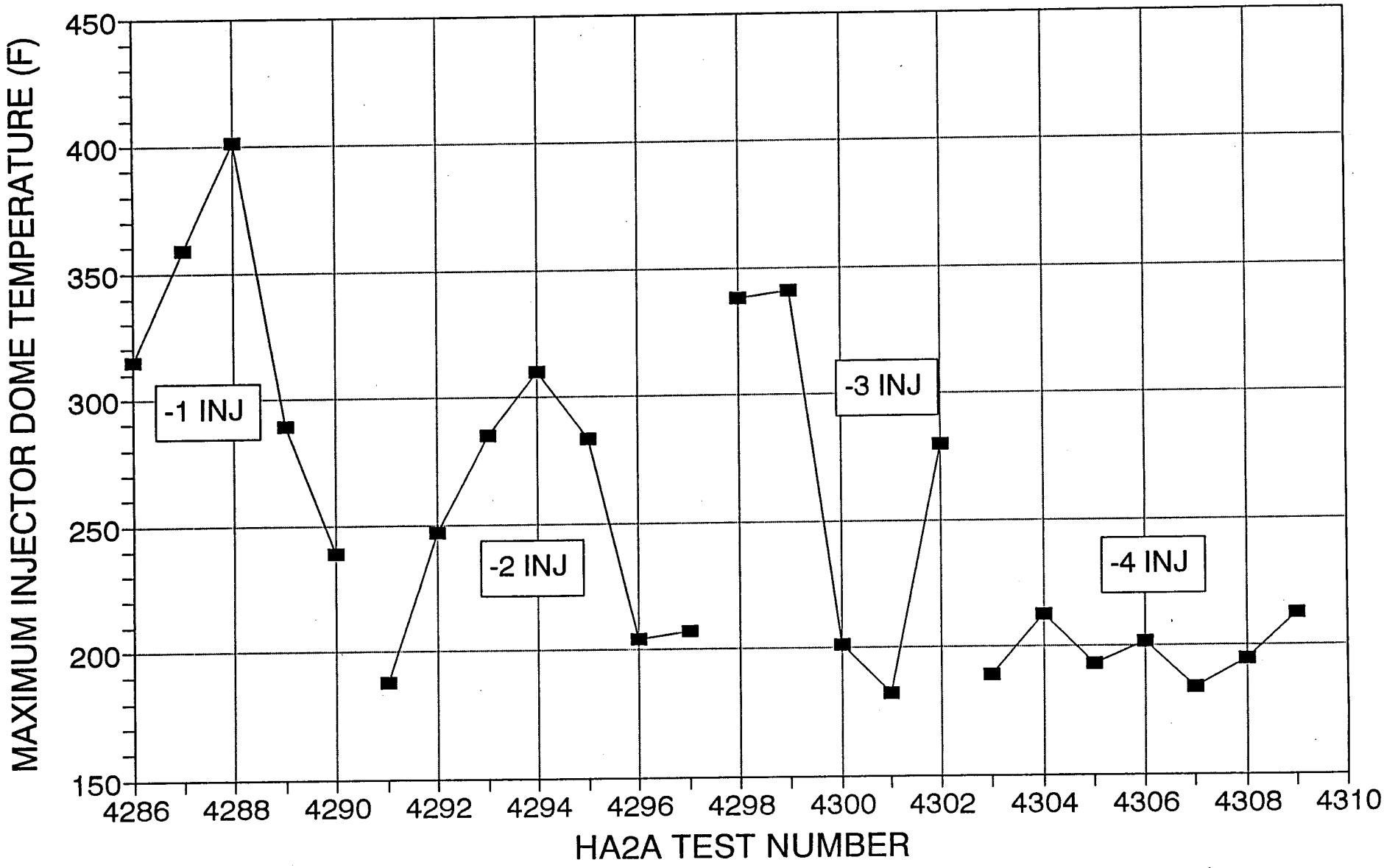

HIPES INJECTOR GAP SURVEY TEST DATA

MR=1.0 Wt=.1516 lbm/sec Pc=500 psia

FIGURE 5.1.1-4

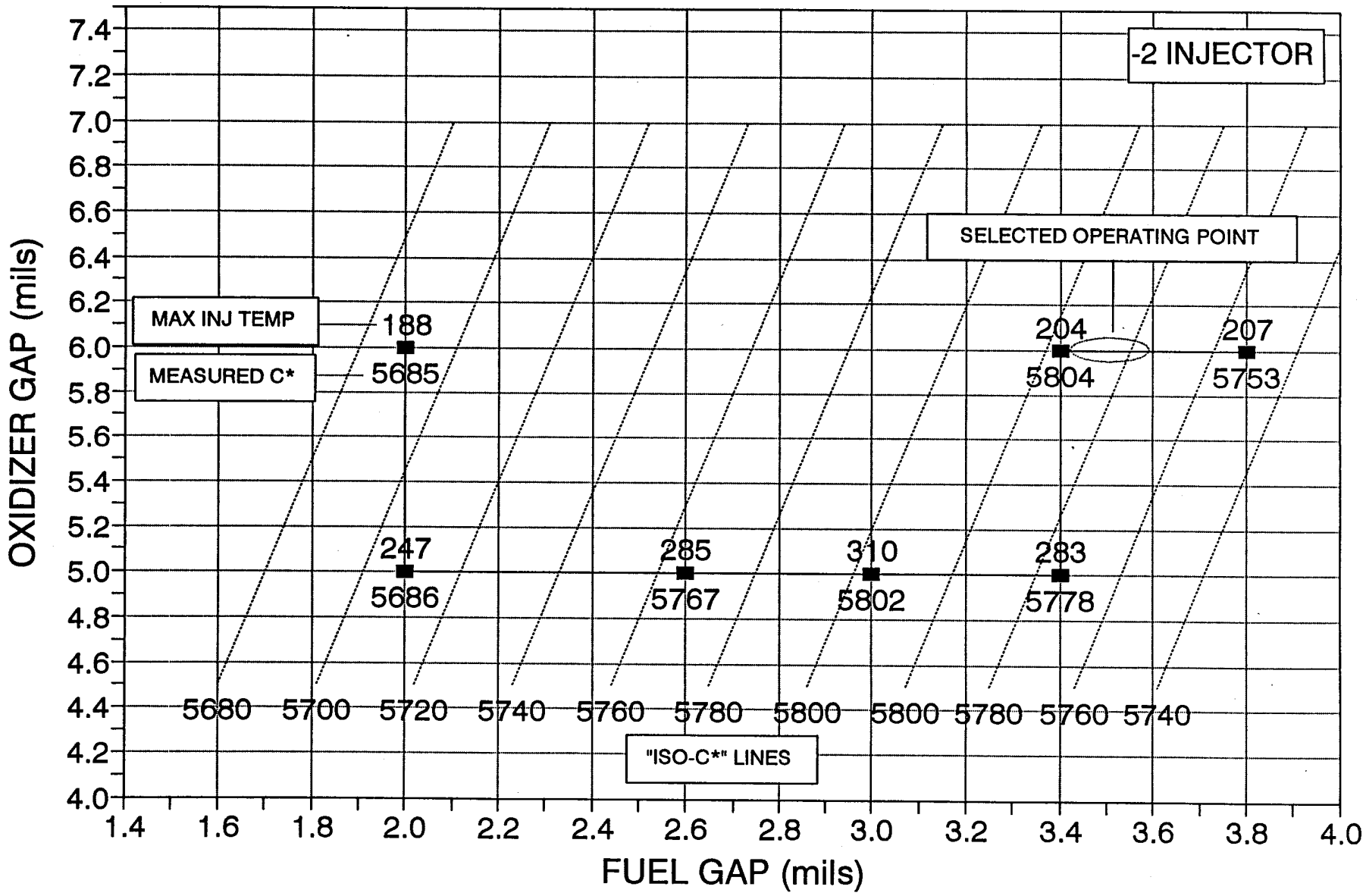

TABLE 5.1.2-1 HIPES CHAMBER PRESSURE EVALUATION TEST SUMMARY

TEST NO HA2A-	DUR SEC	INJ TYPE	Dox INCH	Df INCH	T/S SEC	MR O/F	Wt LBM/SEC	Pc PSIA	Tt(avg) F	Td(max) F	C*(avg) FPS	Isp(avg) SEC
4310	5	-2	0.006	0.0034	4.7	1.0045	0.1515	510.4	827	238	5790	337.4
4311	5	-2	0.006	0.0034	4.7	0.8933	0.1514	501.7	791	203	5698	332.0
4312	5	-2	0.006	0.0034	4.7	1.0943	0.1514	511.4	887	276	5802	338.1
4313	5	-2	0.006	0.0034	4.7	0.9982	0.1366	455.7	740	239	5732	334.0
4314	5	-2	0.006	0.0034	4.7	1.0981	0.1364	458.4	798	266	5769	336.1
4315	5	-2	0.006	0.0034	4.7	1.0014	0.1618	546	905	287	5801	338.0
4316	5	-2	0.006	0.0034	4.7	0.9985	0.1516	508.7	816	243	5760	335.6
4317	4#	-2	0.006	0.0034	3.7#	1.0051	0.1519	594.7	573	222	5730	333.9
4318	5	-2	0.006	0.0034	4.7	1.0075	0.1367	532.5	598	236	5702	332.2
4319	5	-2	0.006	0.0034	4.7	0.8988	0.1365	529.3	564	202	5658	329.7
4320	5	-2	0.006	0.0034	4.7	1.0909	0.1365	536.3	639	256	5728	333.8
4321	5	-2	0.006	0.0034	4.7	0.8969	0.1514	589.8	645	230	5680	331.0
4322	5	-2	0.006	0.0034	4.7	1.1003	0.1517	600	723	298	5748	334.9
4323	5	-2	0.006	0.0034	4.7	1.0005	0.1616	642.7	741	289	5774	336.4
4324	5	-2	0.006	0.0034	4.7	1.0032	0.1516	602.7	703	259	5766	336.0
4325	5	-2	0.006	0.0034	4.7	1.0014	0.1516	395	542	222	5636	328.4
4326	5	-2	0.006	0.0034	4.7	0.9982	0.1366	355	511	195	5607	326.7
4327	5	-2	0.006	0.0034	4.7	0.8992	0.1361	351.2	480	178	5575	324.8
4328	5	-2	0.006	0.0034	4.7	1.0913	0.1365	356.1	535	229	5628	327.9
4329	5	-2	0.006	0.0034	4.7	0.8984	0.1512	392.3	558	196	5599	326.2
4330	5	-2	0.006	0.0034	4.7	1.0959	0.1514	396.1	609	258	5642	328.7
4331	5	-2	0.006	0.0034	4.7	0.9935	0.1617	423.7	636	239	5644	328.9
4332	5	-2	0.006	0.0034	4.7	0.9981	0.1515	385.8	561	231	leak	leak

#Test duration reduced to 4 seconds due to high Pc

HIPES MIXTURE RATIO & TOTAL FLOW SURVEY

N_2O_4/N_2H_4

FIGURE 5.1.2-1

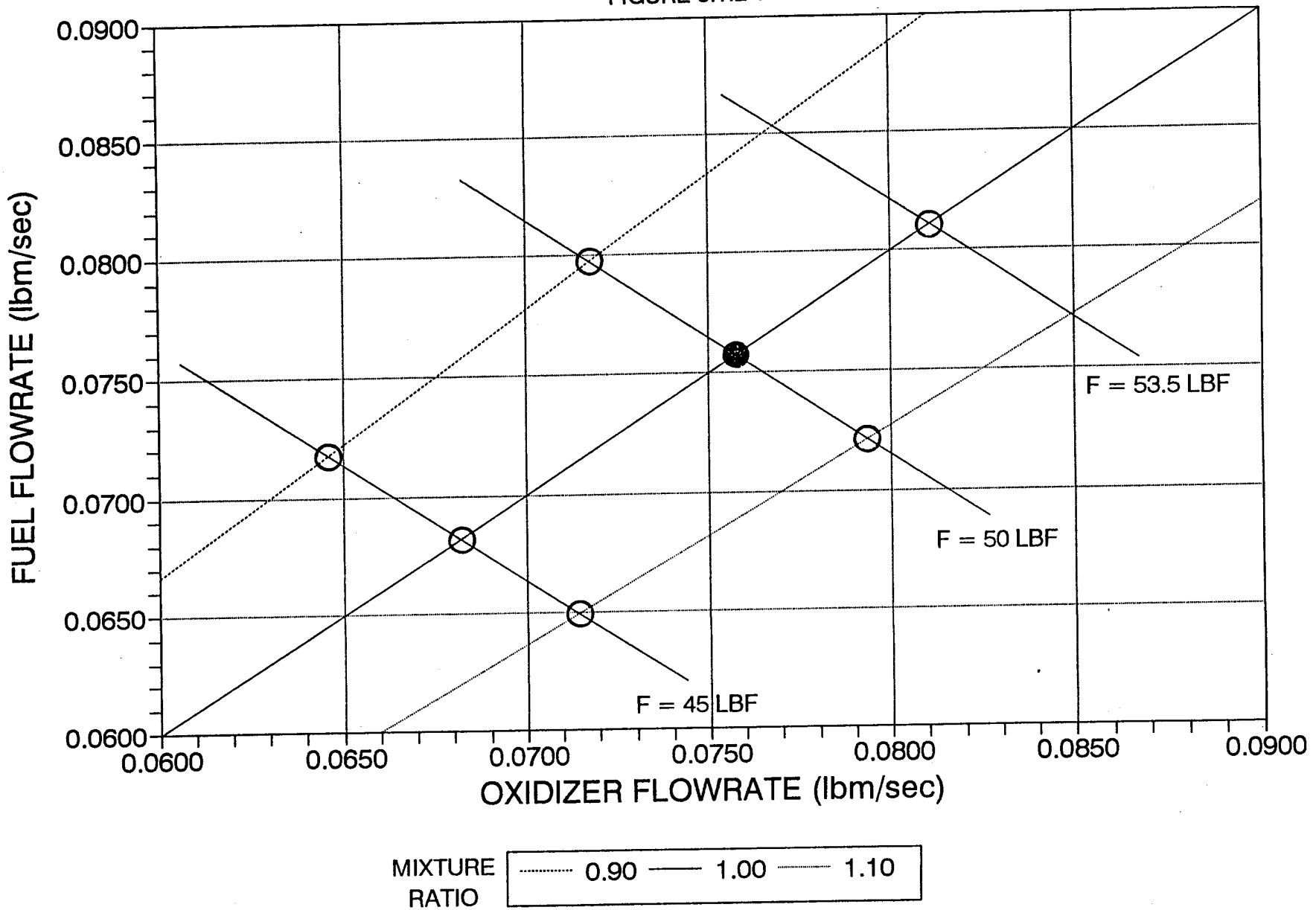

The performance results are presented in Figure 5.1.2-2. The preliminary data indicated that the performance was higher at a chamber pressure of 500 psia than at 600 or 400 psia. For reference, the predicted ODE C* as a function of chamber pressure is provided by Figure 5.1.2-3. Also shown is the predicted C* based on the film cooling model, which indicated that performance is expected to be monotonically increasing with chamber pressure. A summarization of the average throat temperature versus chamber pressure for the various test conditions is presented in Figure 5.1.2-4, and supported the conclusion that performance was indeed higher with the 500 psia heat-sink chamber than for the other two chambers. Post-test inspection of the three chambers indicated that the 500 psia chamber had some copper erosion in the head-end, unlike the 400 and 600 psia chambers. This erosion was probably caused by its greater usage (158 sec compared to only 40 sec on the other two). In addition, the 500 psia chamber was exposed to testing on all the injectors, and some of these tests were conducted with injector gap settings that further accelerated the erosion process. As a result, the 500 psia heatsink data cannot be accurately compared with the data from the 400 and 600 psia chambers. In essence, the chamber with a roughened headend promoted enhanced mixing of the fuel-rich wall zone boundary layer, which acted in increasing the wall zone mixture ratio at the throat. This served to increase both performance (due to the more uniform O/F distribution) as well as throat temperatures (due to the higher wall O/F at the throat). The resulting performance trend as a function of chamber pressure (after dropping the 500 psia heatsink data) is presented in Figure 5.1.2-5. The figure indicated an increase of about 50 ft/sec in C*(~1%) for a change (increase) in Pc of 100 psia for all test conditions (O/F and Pc). This increase cannot be attributed solely to Pc, however, since the L* differed between the 400 and 600 psia chambers. A discussion of this trend is presented in the next section- the results of the 500 psia water-cooled chamber tests. The average throat temperature and maximum observed injector dome temperature are presented in Figure 5.1.2-6 and 5.1.2-7 as a function of chamber pressure after deletion of the 500 psia data. The trends indicated that the slopes are practically equal for all the various test conditions, indicating that the effect of higher chamber pressure was roughly constant over the range of mixture ratios and total flowrates tested.

5.2 WATER-COOLED COPPER CHAMBER TESTING

Following the heatsink tests, a considerable amount of testing was conducted utilizing a water-cooled copper chamber. This permitted longer test durations (60-120 sec) so that steady-state injector dome and chamber heat transfer rates could be obtained. The majority of tests were performed with hydrazine; however, MMH was also evaluated as an alternate fuel.

5.2.1 WATER-COOLED CHAMBER TESTS WITH HYDRAZINE

All of these tests were conducted with the -2 baseline injector element set at an oxidizer gap of 0.0060" and a fuel gap of 0.0034. Since the 500 psia heatsink data was compromised due to the condition of the combustion chamber, these tests allowed the determination of performance data to be made so that a more valid comparison could be made with the 400 and 600 psia heatsink data. The same O/F and Wt excursion was performed on the water-

HIPES PERFORMANCE CHARACTERISTICS

HEAT-SINK CHAMBERS

FIGURE 5.1.2-2

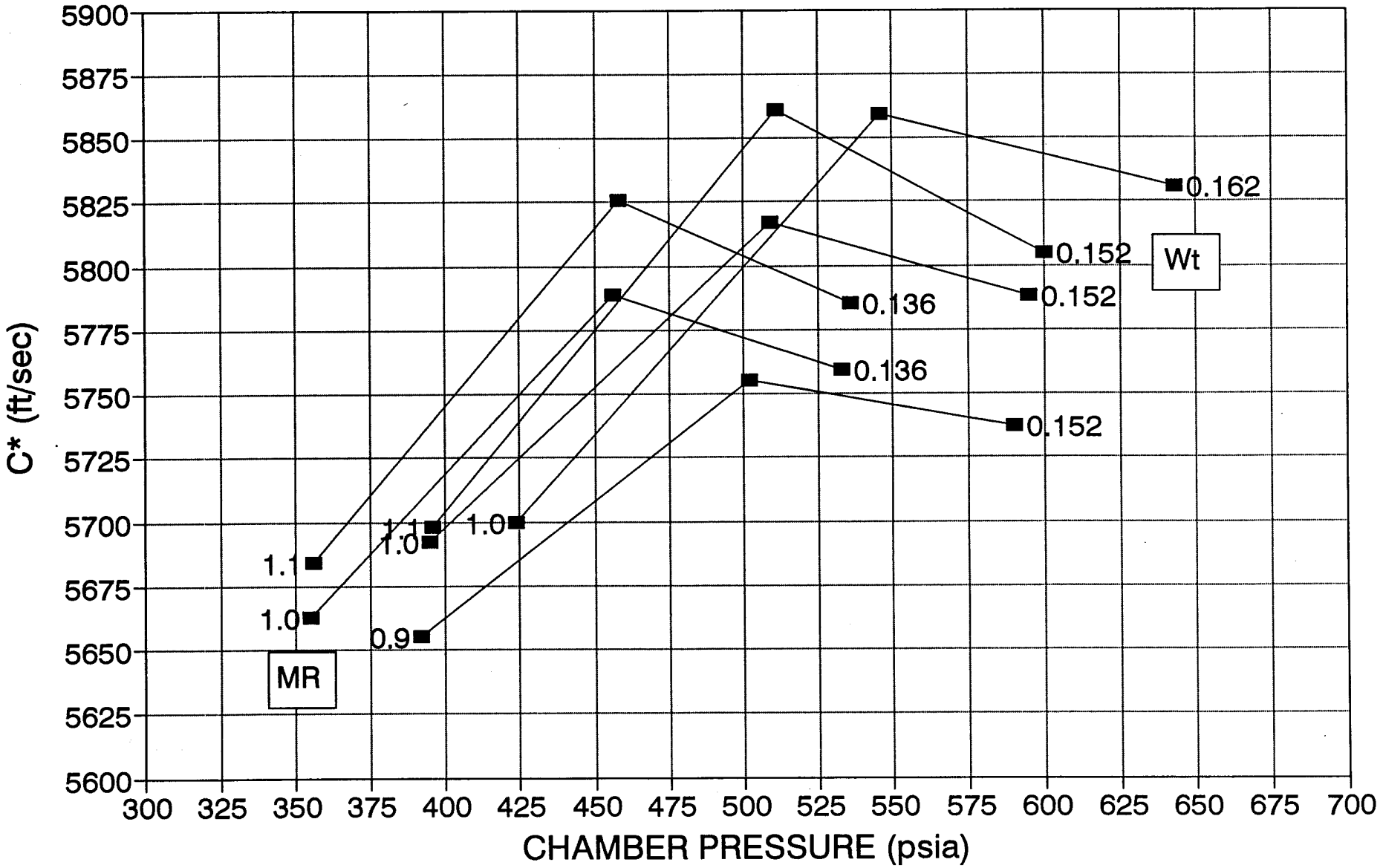

HIPES PERFORMANCE PREDICTIONS

HEAT-SINK CHAMBERS

FIGURE 5.1.2-3

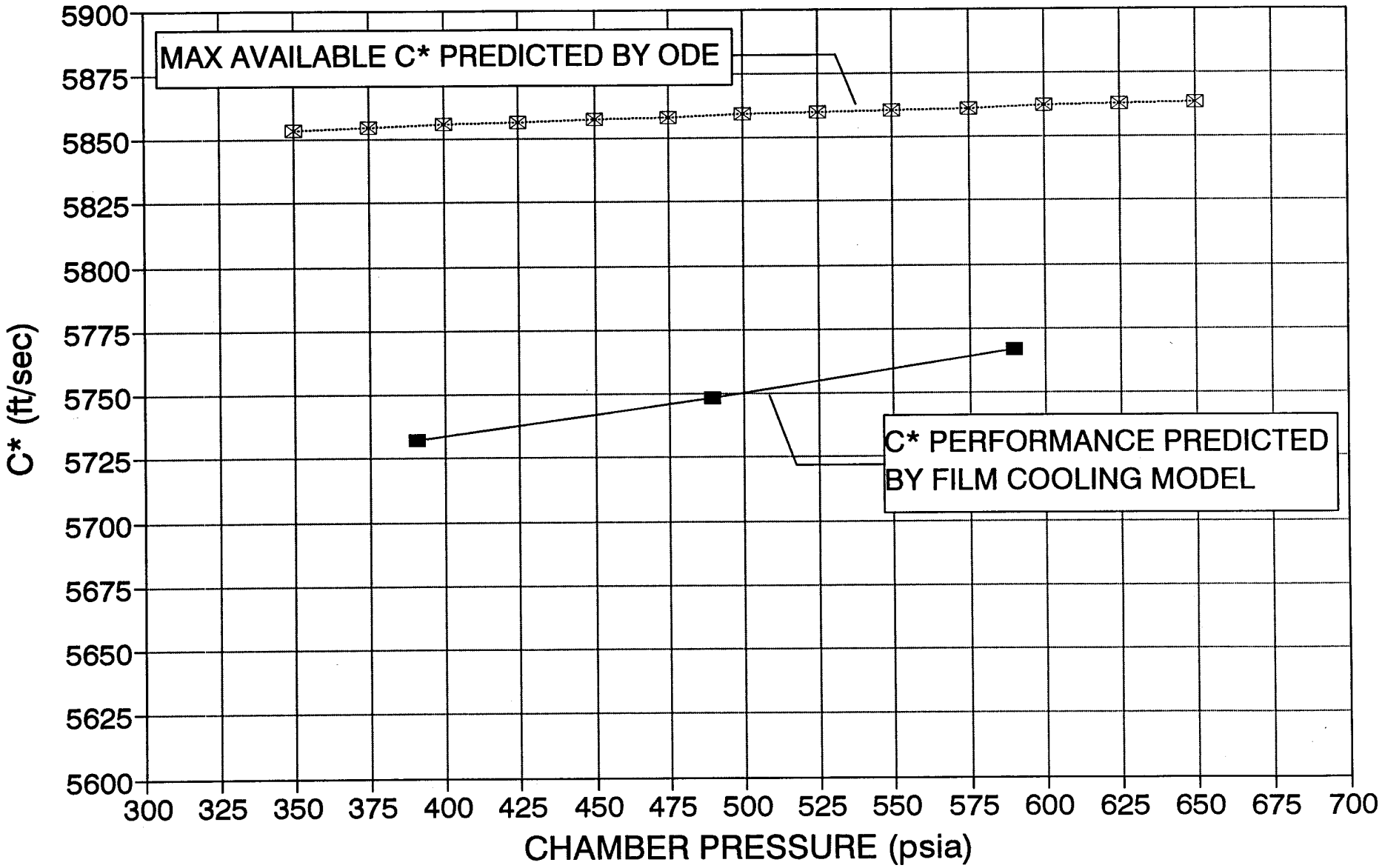

HIPES THERMAL CHARACTERISTICS

HEAT-SINK CHAMBERS

FIGURE 5.1.2-4

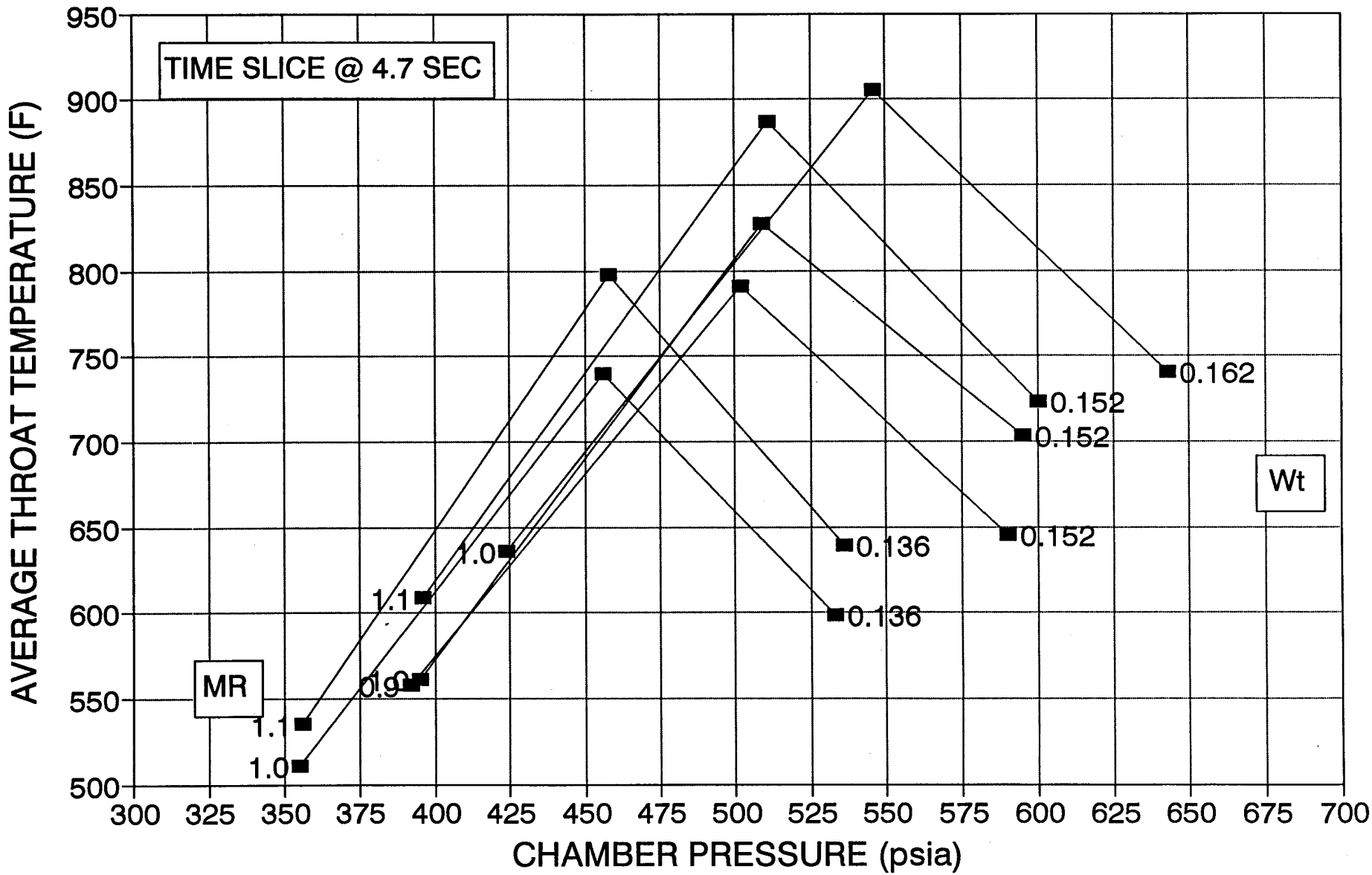

HIPES PERFORMANCE CHARACTERISTICS

HEAT-SINK CHAMBERS

FIGURE 5.1.2-5

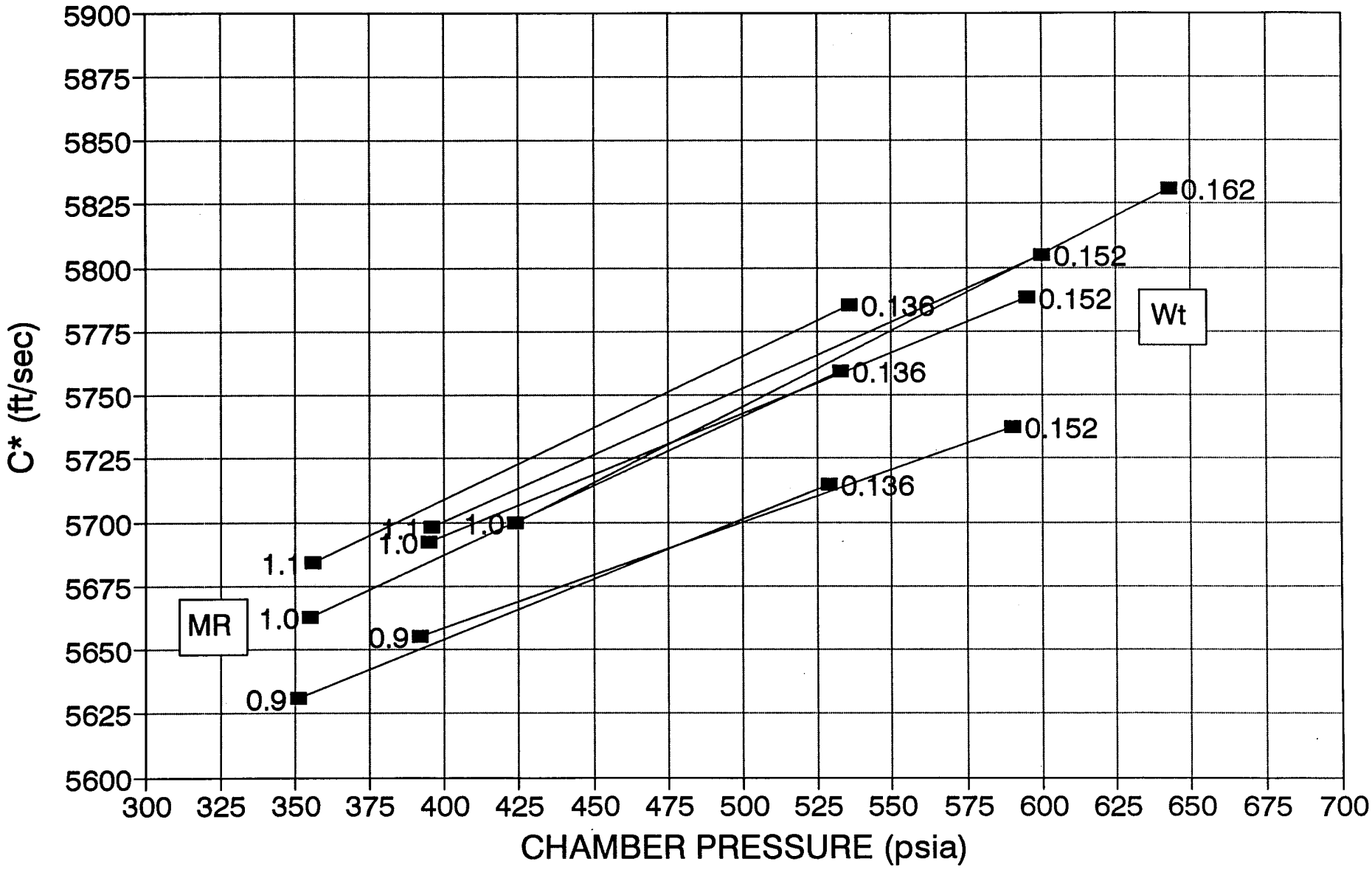

HIPES THERMAL CHARACTERISTICS

HEAT-SINK CHAMBERS

FIGURE 5.1.2-6

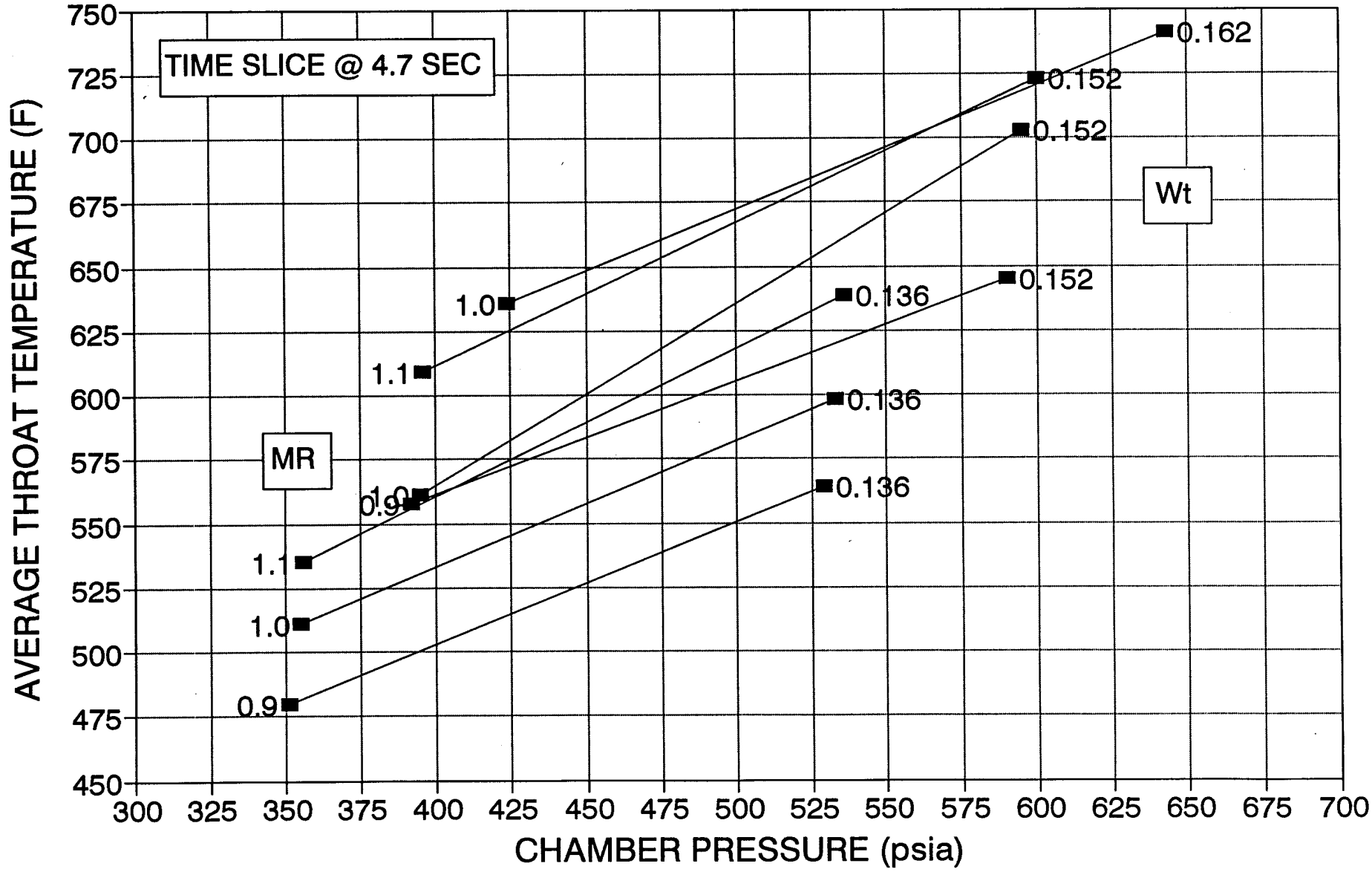

HIPES THERMAL CHARACTERISTICS

HEAT-SINK CHAMBERS

FIGURE 5.1.2-7

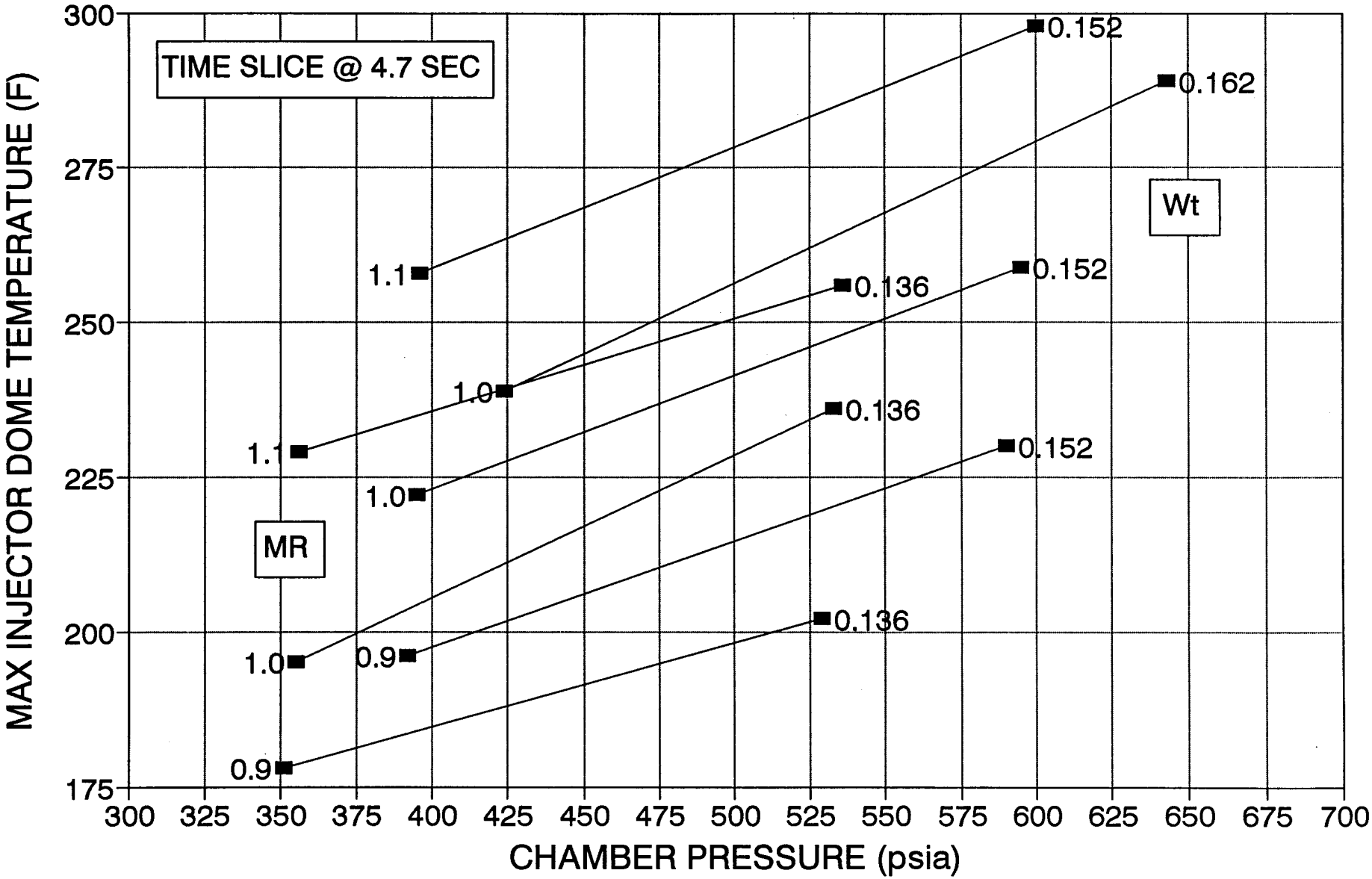

cooled chamber (reference Figure 5.1.2-1), and a summary of this test phase is presented in Table 5.2.1-1.

The first trend noticed during this series of tests was that the performance was significantly lower when compared to that of the 500 psia heat-sink chamber. The performance data for both the water-cooled and 500 psia heatsink chambers as a function of mixture ratio are presented in Figure 5.2.1-1. The water-cooled C* was on average 60 ft/sec lower than that observed for the corresponding heatsink tests. The surface condition of the water-cooled chamber was much smoother than the 500 psia heatsink chamber and was very similar to the 400 and 600 psia heatsink chambers. The observed drop in performance (as expected) lended credibility to the explanation that the uncharacteristically high performance for the 500 psia heatsink tests was in part due to the roughened surface of that chamber. Figures 5.2.1-2 through 5.2.1-4 included the following: heatsink data obtained at both 400 and 600 psia and water-cooled engine data obtained at 500 psia for measured C* versus chamber pressure for each of the three propellant flowrates evaluated. These figures illustrated the consistent trend of increasing C* with increasing Pc. Measured C* efficiency versus chamber pressure is presented in Figure 5.2.1-5 and clearly indicated an empirical trend of increasing efficiency at higher pressure. However, a portion of this increased performance was attributed to an increase in L*, and this effect will be discussed in more detail later. Finally, Figure 5.2.1-6 indicated that higher specific impulse could be expected as Pc and/or L* increased.

The location of the thermocouples for the water-cooled tests is shown in Figure 5.2.1-7, while the thermal data obtained from that instrumentation is summarized in Table 5.2.1-2. The variation in injector heat load as a function of mixture ratio for two different propellant flowrates is presented in Figure 5.2.1-8. For a given total flowrate, the heat transfer rate to the injector dome increased for higher mixture ratio. As the mixture ratio increased, the oxidizer momentum became greater relative to the fuel, causing the resultant spray cone angle to lessen. This exposed more of the injector dome to the recirculation zone in the headend region, thereby increasing the amount of surface area that the oxidizer droplets must cool. In addition, it appeared that at higher mixture ratio the amount of oxidizer droplets available to recirculate also decreased, which also resulted in increased injector dome temperatures. The heat loads likely increased for higher propellant flowrates at a given mixture ratio because greater chamber pressures result in larger heat transfer coefficients. Also, the increased momentum of the propellants caused by the higher flowrates resulted in less recirculated liquid oxidizer droplets available for film cooling of the injector headend.

The measured chamber heat loss as a function of mixture ratio for the three total propellant flowrates tested is presented in Figure 5.2.1-9. Total chamber heat loads increased with higher mixture ratio caused by the greater mixture ratio in the wall zone along the entire length of the chamber. Chamber heat loads increased with higher flowrates because of two reasons. First, the film cooling model predicted slightly greater mixing of the fuel-rich wall zone at higher chamber pressures, resulting in slightly higher gas temperatures along the

TABLE 5.2.1-1 HIPES WATER-COOLED ENGINE TEST SUMMARY

TEST NO HA2A-	DUR SEC	INJ	Dox INCH	Df INCH	T/S	O/F	Wt LBM/SEC	Pc PSIA	C* FT/SEC	Isp SEC	Tdome F
4333	5	-2	0.006	0.0034					C/O		
4334	20	-2	0.006	0.0034	19.6	1.01	0.1522	509.9	5773	336.4	172
4335	60	-2	0.006	0.0034	59.3	1	0.1516	514.2	5780	336.8	181
4336	120	-2	0.006	0.0034	117.9	1	0.1519	516	5770	336.2	179
4337	90	-2	0.006	0.0034	87.9	1	0.137	462.4	5728	333.8	168
4338	90	-2	0.006	0.0034	87.9	0.9	0.1364	458.2	5690	331.5	153
4339	90	-2	0.006	0.0034	87.9	1.1	0.1367	463.3	5754	336.9	173
4340	90	-2	0.006	0.0034	87.9	0.91	0.1523	515.5	5733	332.4	154
4341	90	-2	0.006	0.0034	87.9	1.11	0.1522	517.4	5768	337.7	169
4342	90	-2	0.006	0.0034	87.9	1	0.1618	553.4	5797	337.8	163
4343	73	-2	0.006	0.0034	71.9	1	0.152	517.8	5772	336.3	206
4345	20	-2	0.006	0.0034	19.9	1	0.1511	513.9	5773	336.4	182
4346	90	-2	0.006	0.0034	87.9	1	0.1514	515.9	5799	337.9	216
4347	90	-2	0.006	0.0034	87.9	1.11	0.1513	515.5	5858	343.0	232
4348	90	-2	0.006	0.0034	87.9	1	0.1515	519.6	5791	337.4	184
4349	90	-2	0.006	0.0034	87.9	1	0.1513	520	5801	338.0	183
4350	21	-2	0.006	0.0034	19.9	1	0.1515	519.7	5749	335.0	180

PERFORMANCE COMPARISON @ Pc=500 PSIA

HEAT-SINK vs WATER-COOLED CHAMBERS

FIGURE 5.2.1-1

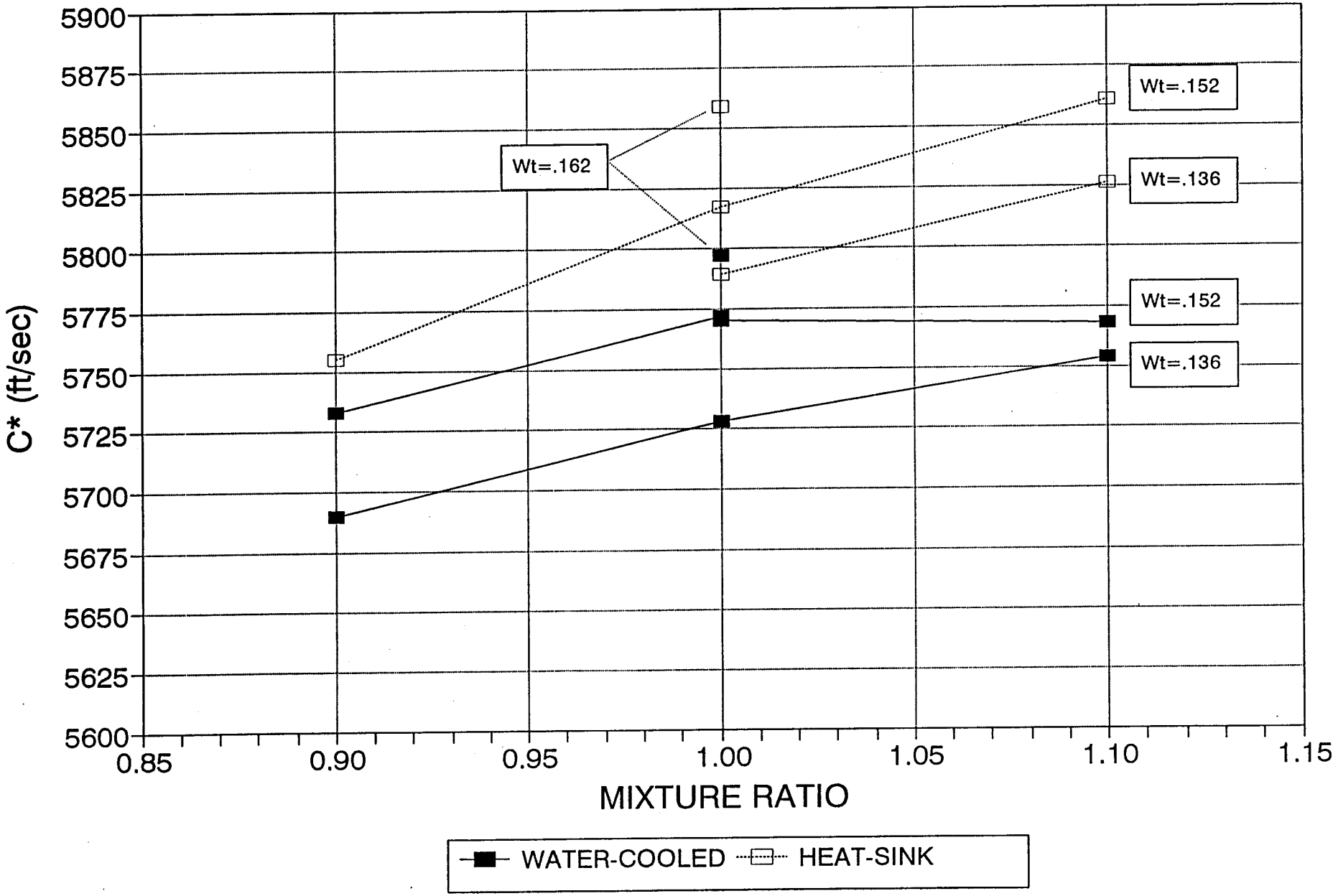

EFFECT OF PC ON PERFORMANCE

MEASURED C*

FIGURE 5.2.1-2

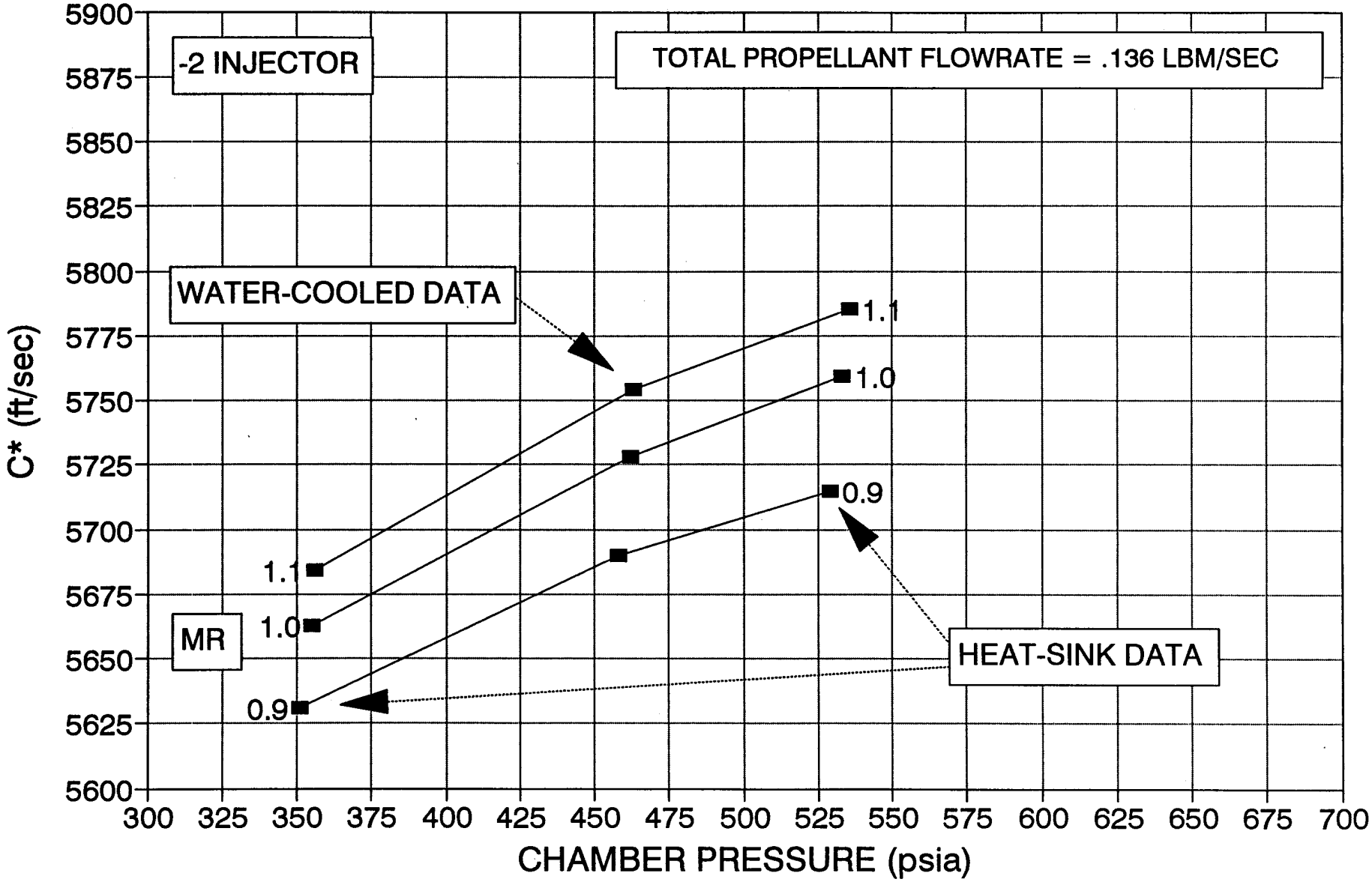

EFFECT OF PC ON PERFORMANCE

MEASURED C*

FIGURE 5.2.1-3

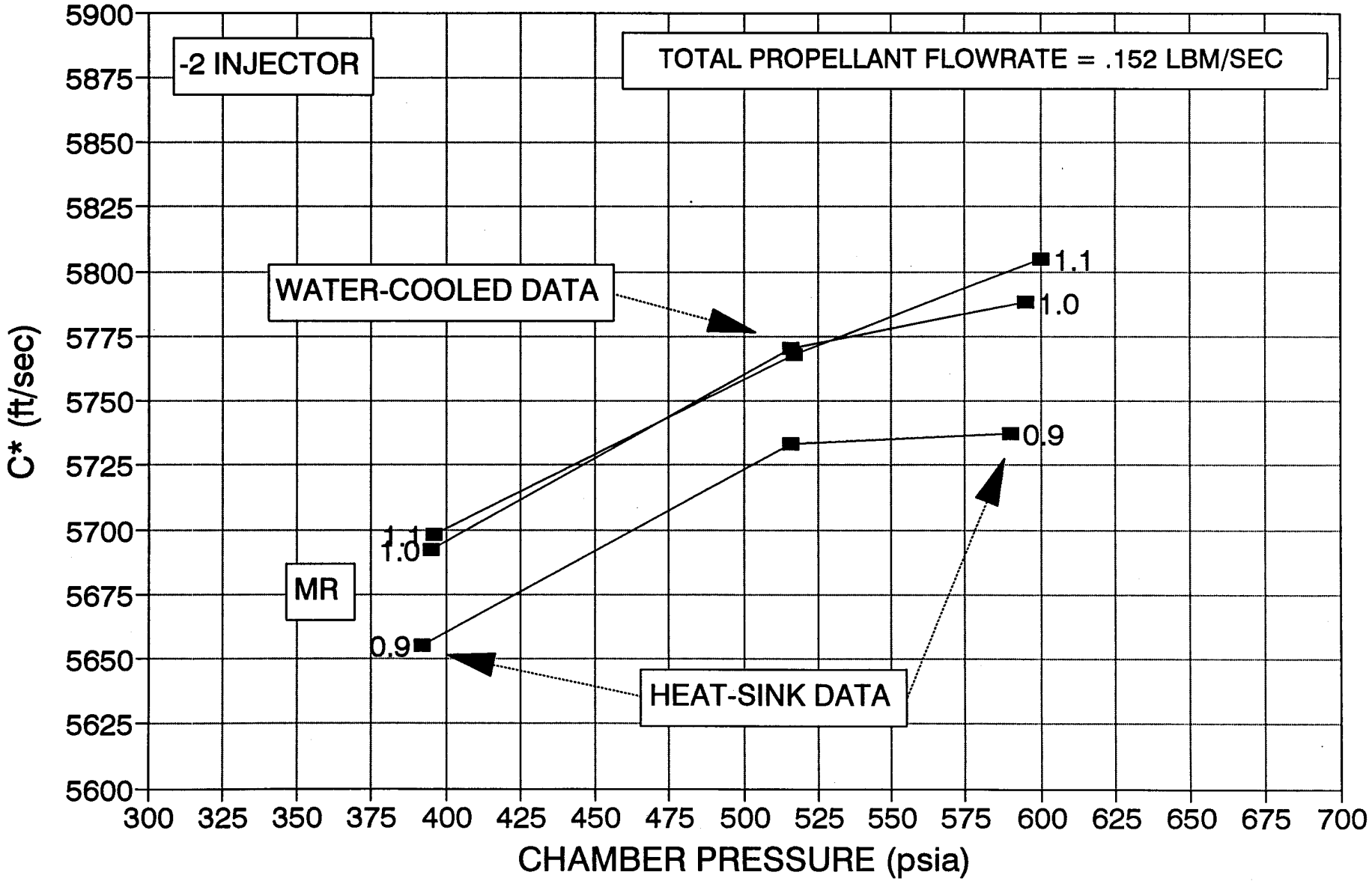

EFFECT OF PC ON PERFORMANCE

MEASURED C*

FIGURE 5.2.1-4

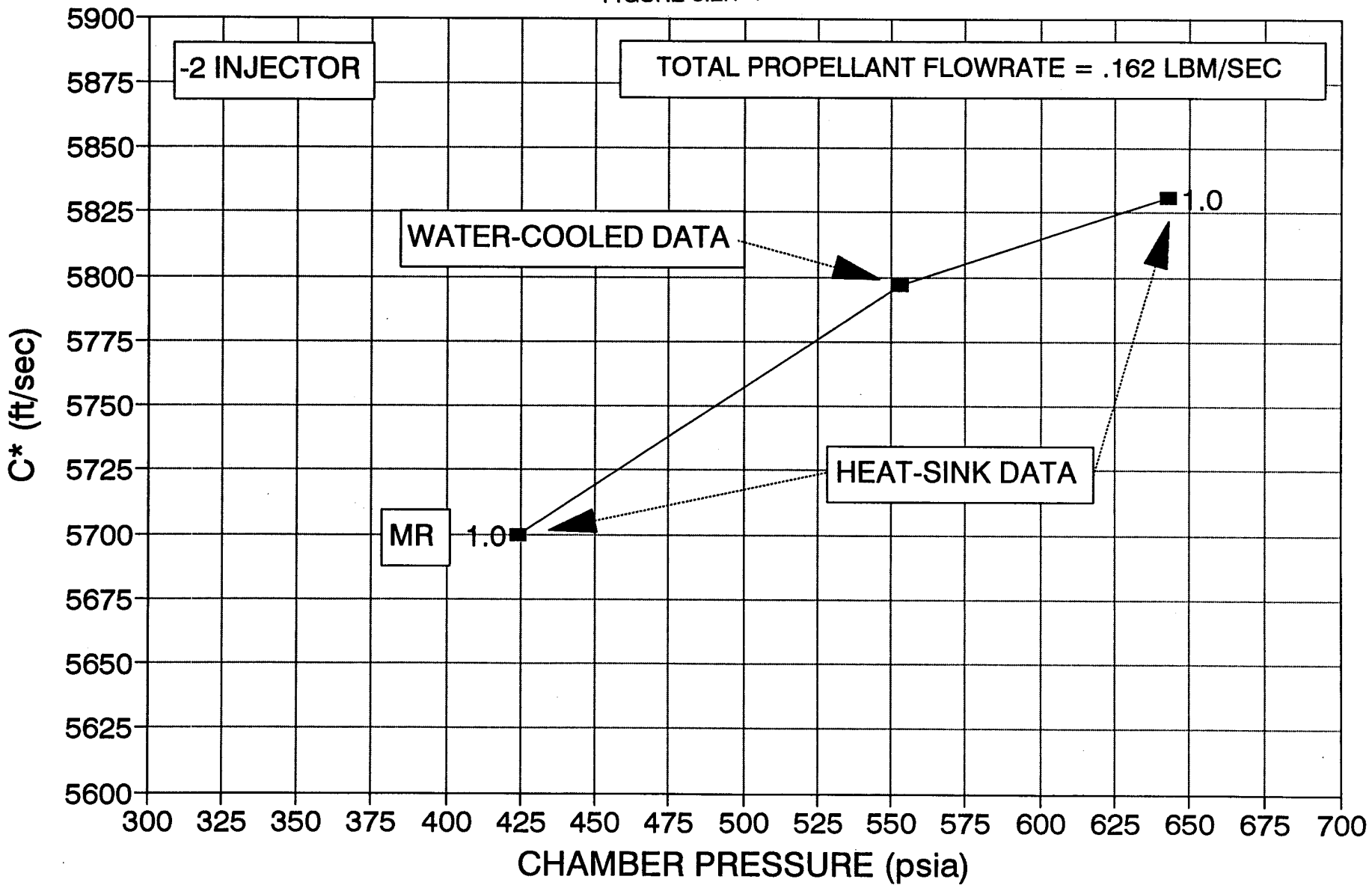

EFFECT OF PC ON PERFORMANCE
MEASURED COMBUSTION EFFICIENCY

FIGURE 5.2.1-5

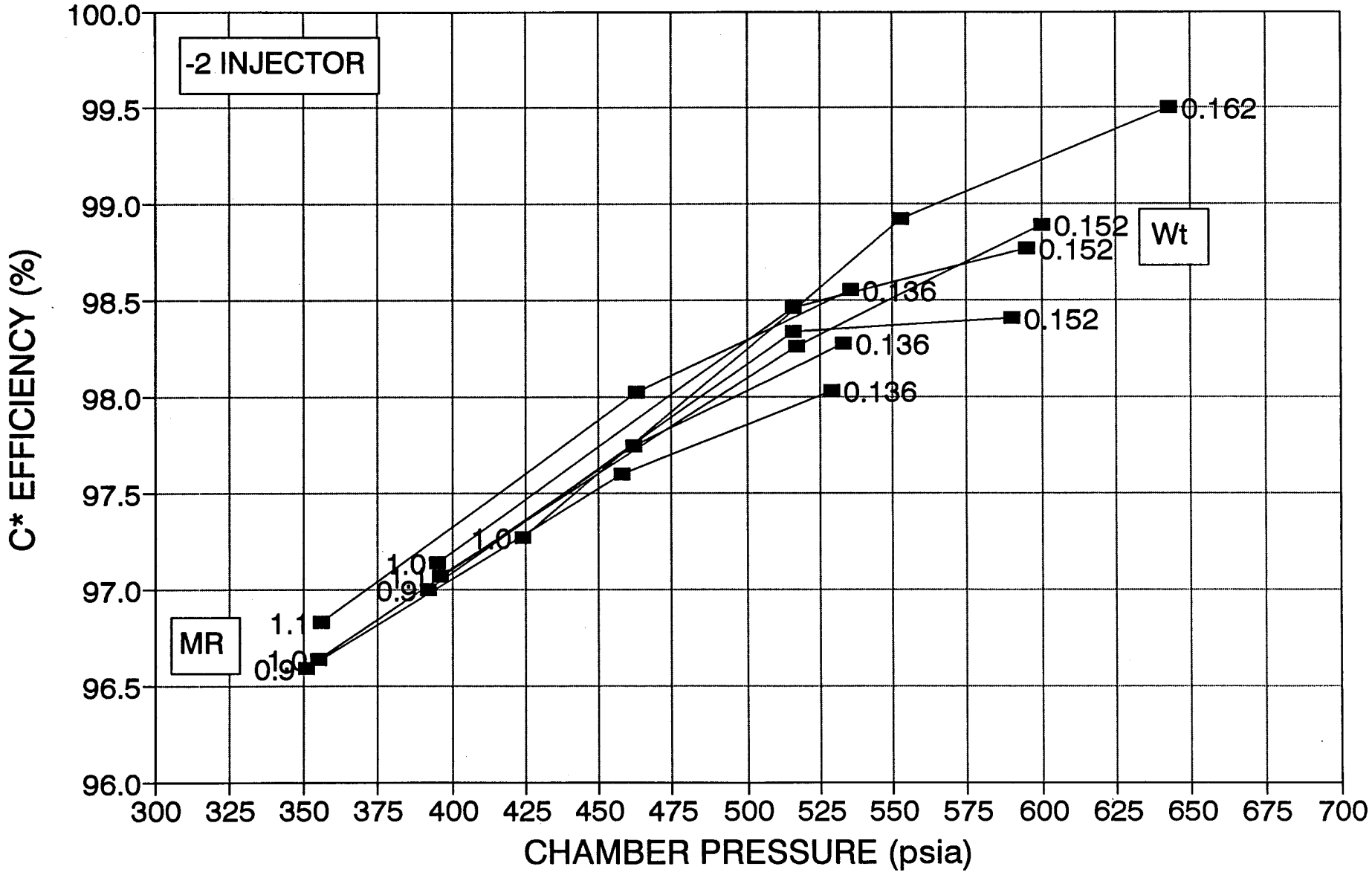

EFFECT OF PC ON PERFORMANCE

ISP BASED ON MEASURED C*

FIGURE 5.2.1-6

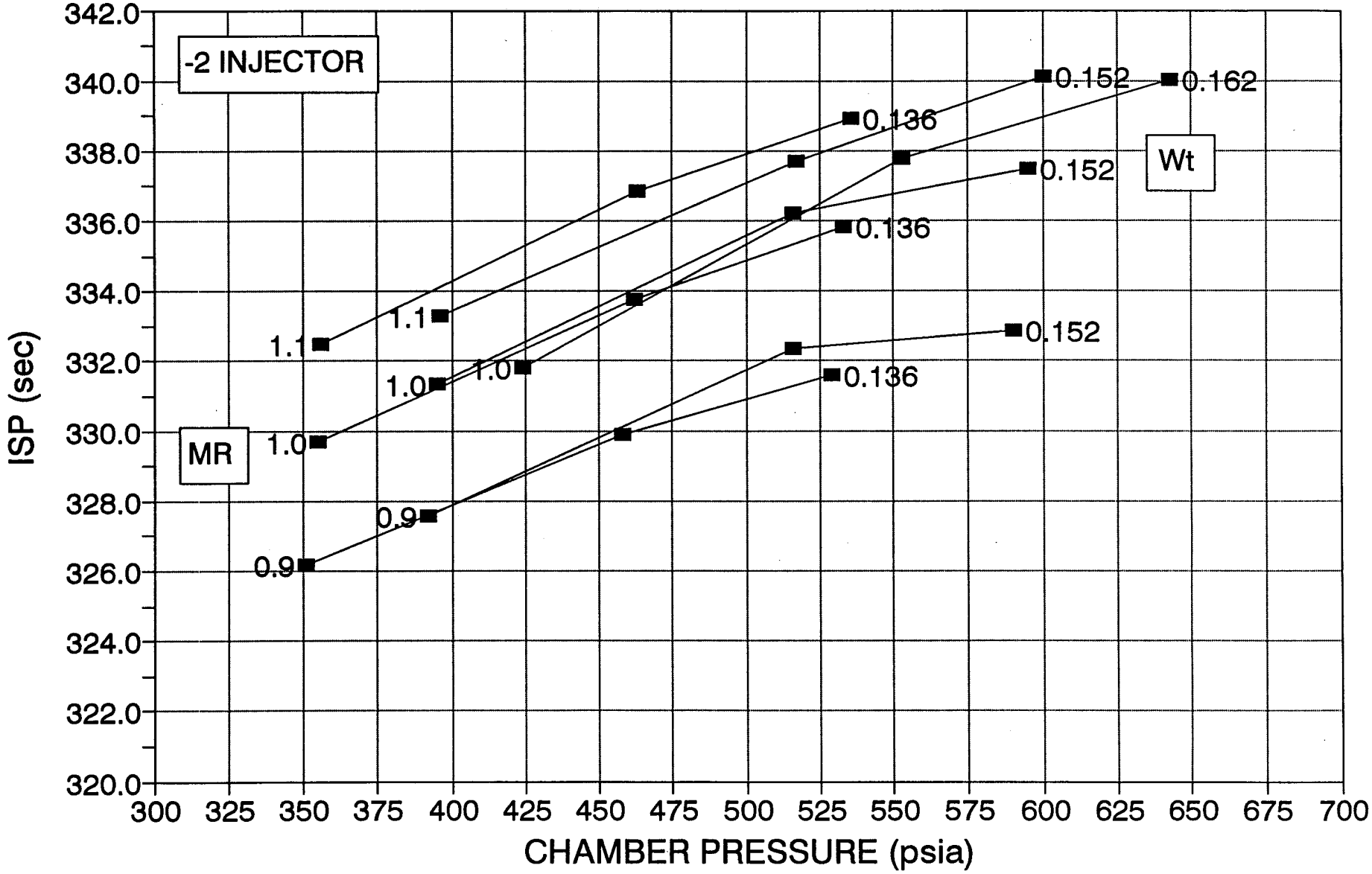

HIPES WATER-COOLED ENGINE

FIGURE 5.2.1-7

NOMINAL CONDITIONS

MR=1.0

Pc=515 PSIA

Wt=0.152 LBM/SEC

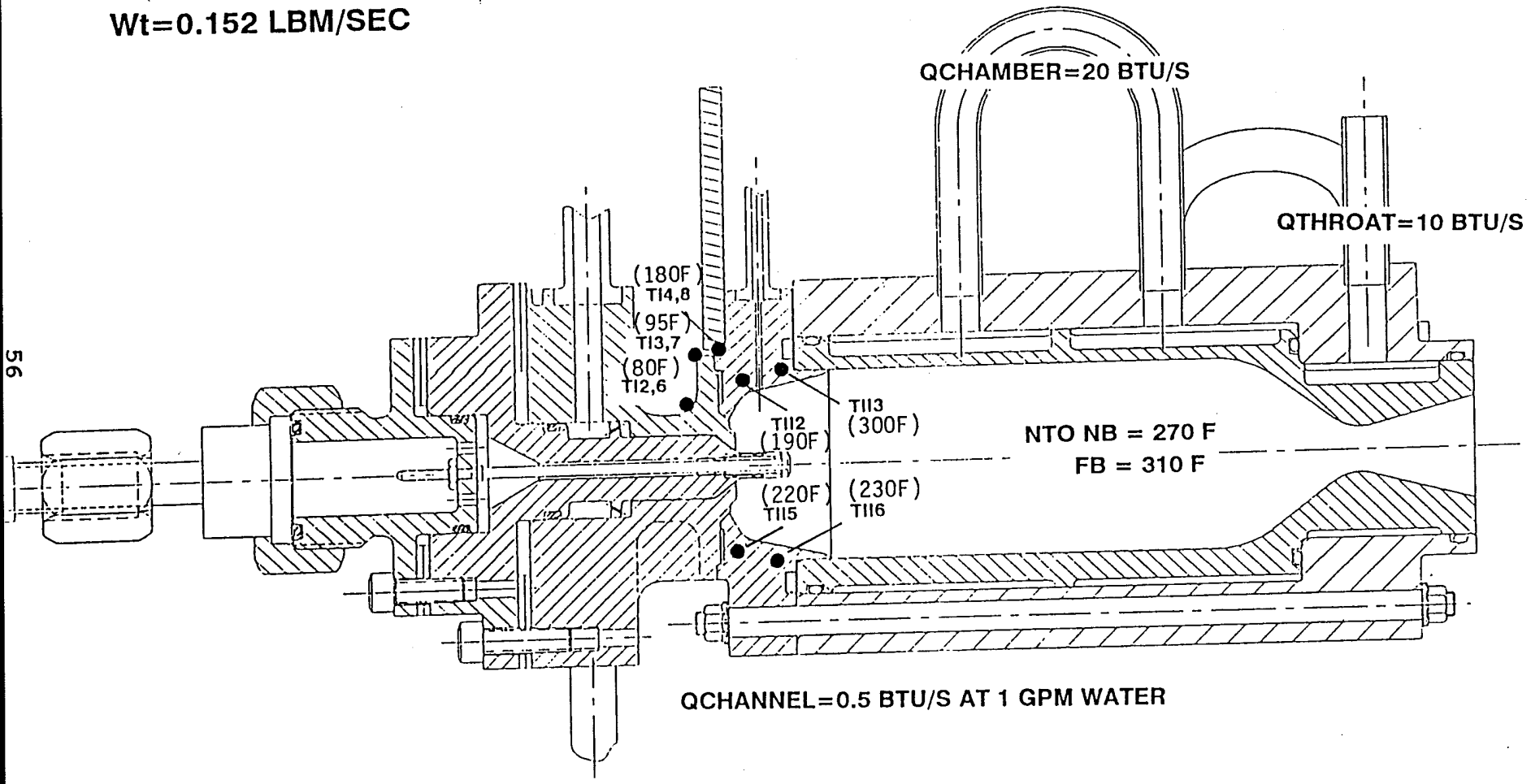

HIPES WATER COOLED ENGINE DOME TEMPERATURE SUMMARY

TRW

TABLE 5.2.1-2

HIPES WATER-COOLED ENGINE
N2O4-HYDRAZINE

							EXTERNAL DOME TEMPS						INTERNAL DOME TEMPS						
TEST NO. HA2A-	DUR SEC	T/S	INJ	Wt LBM/SEC	O/F	Pc PSIA	TI2 F	TI6 F	TI3 F	TI7 F	TI4 F	TI8 F	TII2 F	TII5 F	TII3 F	TII6 F	QCHAN BTU/S	QINJ GPM	TINJ F
4333	5	5.0	-2	0.1523	1.01	507.7	87	92	96	97	158	132	198	188	373	158			
4334	20	19.6	-2	0.1522	1.01	509.9	81	84	94	96	172	158	186	206	306	208			
4335	60	19.8	-2	0.1518	1.00	511.6	77	82	92	97	171	172	183	218	296	222			
		59.3	-2	0.1516	1.00	514.2	77	83	95	99	181	178	188	224	299	235			
4336	120	19.9	-2	0.1523	1.00	515.3	77	82	91	97	168	184	182	217	294	220	0.50	0.95	3.83
		59.9	-2	0.1521	1.00	515.8	77	83	94	99	178	189	187	222	296	232	0.53	0.94	4.07
		89.9	-2	0.1521	1.00	516.1	78	83	95	98	179	187	187	220	296	230	0.54	0.94	4.10
		117.9	-2	0.1519	1.00	516.0	78	83	95	98	179	185	187	217	295	228	0.53	0.94	4.05
4337	90	19.9	-2	0.1370	1.00	461.0	78	81	90	94	153	165	173	198	282	206	0.41	0.95	3.11
		59.9	-2	0.1370	1.00	462.0	78	81	93	96	163	170	176	202	282	217	0.43	0.95	3.23
		87.9	-2	0.1370	1.00	462.4	77	81	93	95	163	168	175	200	281	214	0.43	0.95	3.23
4338	90	19.9	-2	0.1363	0.90	456.2	78	80	88	90	143	147	165	177	259	182	0.39	0.95	2.97
		59.9	-2	0.1364	0.90	457.7	78	80	90	92	149	153	167	183	259	192	0.40	0.95	3.06
		87.9	-2	0.1364	0.90	458.2	77	79	90	92	149	153	167	182	259	192	0.41	0.95	3.11
4339	90	19.9	-2	0.1369	1.10	462.2	75	79	86	93	143	170	168	209	271		0.45	0.97	3.37
		59.9	-2	0.1367	1.10	463.1	75	79	87	95	149	174	168	214	267		0.46	0.97	3.45
		87.9	-2	0.1367	1.10	463.3	75	80	87	95	149	173	168	214	266		0.47	0.97	3.50
4340	90	19.9	-2	0.1524	0.91	513.4	75	78	85	89	143	153	167	182	268	186	0.42	0.96	3.18
		59.9	-2	0.1523	0.91	515.1	75	78	87	89	148	155	169	183	269	193	0.43	0.95	3.25
		87.8	-2	0.1523	0.91	515.5	75	78	87	89	148	154	169	182	269	192	0.44	0.95	3.31
4341	90	19.9	-2	0.1523	1.11	515.8	81	86	93	99	158	170	185	210	288	216	0.55	0.97	4.08
		59.9	-2	0.1523	1.11	517.4	81	85	94	99	162	171	183	209	279	220	0.55	0.97	4.10
		87.9	-2	0.1522	1.11	517.4	80	85	93	98	157	169	180	206	274	218	0.54	0.96	4.07
4342	90	19.9	-2	0.1617	1.00	550.6	81	86	93	99	157	158	191	212	276	218	0.56	0.96	4.19
		59.9	-2	0.1618	1.00	552.8	81	85	95	100	163	161	193	216	275	227	0.57	0.96	4.32
		87.9	-2	0.1618	1.00	553.4	81	85	95	100	163	159	193	214	275	225	0.58	0.96	4.35
4343	73	19.9	-2	0.1520	1.00	515.5	91	114	99	118	168	197	201	274	270	252	0.90	1.00	6.51
		59.9	-2	0.1520	1.00	517.6	90	109	105	120	187	208	212	290	311	269	0.89	1.00	6.37
		71.9	-2	0.1520	1.00	517.8	87	111	103	120	181	206	205	285	288	263	0.87	1.00	6.26
4345	20	19.6	-2	0.1511	1.00	513.9	95	96	107	107	181	182	238	209	345	227	0.61	1.00	4.41
4346	90	19.9	-2	0.1512	1.00	512.8	96	97	114	108	209	164	275	208	500	226	0.65	1.00	4.71
		59.9	-2	0.1514	1.00	515.0	95	96	116	110	216	170	272	215	476	237	0.67	1.00	4.84
		89.9	-2	0.1514	1.00	515.9	95	95	117	109	216	168	271	212	468	234	0.66	1.00	4.78
4347	90	19.9	-2	0.1513	1.11	513.1	101	102	123	114	219	165	288	214	491	226	0.71	0.97	5.24
		59.9	-2	0.1513	1.11	514.8	101	101	126	115	231	170	292	223	493	234	0.72	0.97	5.34
		89.9	-2	0.1513	1.11	515.5	100	100	126	115	232	168	293	220	491	231	0.72	0.97	5.36
4348	90	19.9	-2	0.1517	1.00	517.9	88	89	103	102	171	162	224	193	333	205	0.55	0.84	4.74
		59.9	-2	0.1515	1.00	519.4	89	90	107	103	182	166	228	200	333	213	0.58	0.84	4.96
		89.9	-2	0.1515	1.00	519.6	90	90	108	102	184	162	232	195	344	207	0.56	0.84	4.84
4349	90	19.9	-2	0.1515	1.00	517.7	92	92	108	106	174	162	227	196	343	207	0.51	0.61	6.04
		59.9	-2	0.1514	1.00	519.9	93	92	110	106	182	161	230	196	345	207	0.52	0.61	6.21
		89.9	-2	0.1513	1.00	520.0	93	92	110	106	183	159	229	194	346	205	0.52	0.60	6.21
4350	21	20.9	-2	0.1515	1.00	519.7	95	95	113	110	180	164	234	199	342	210	0.49	0.40	8.81

FIGURE 5.2.1-8

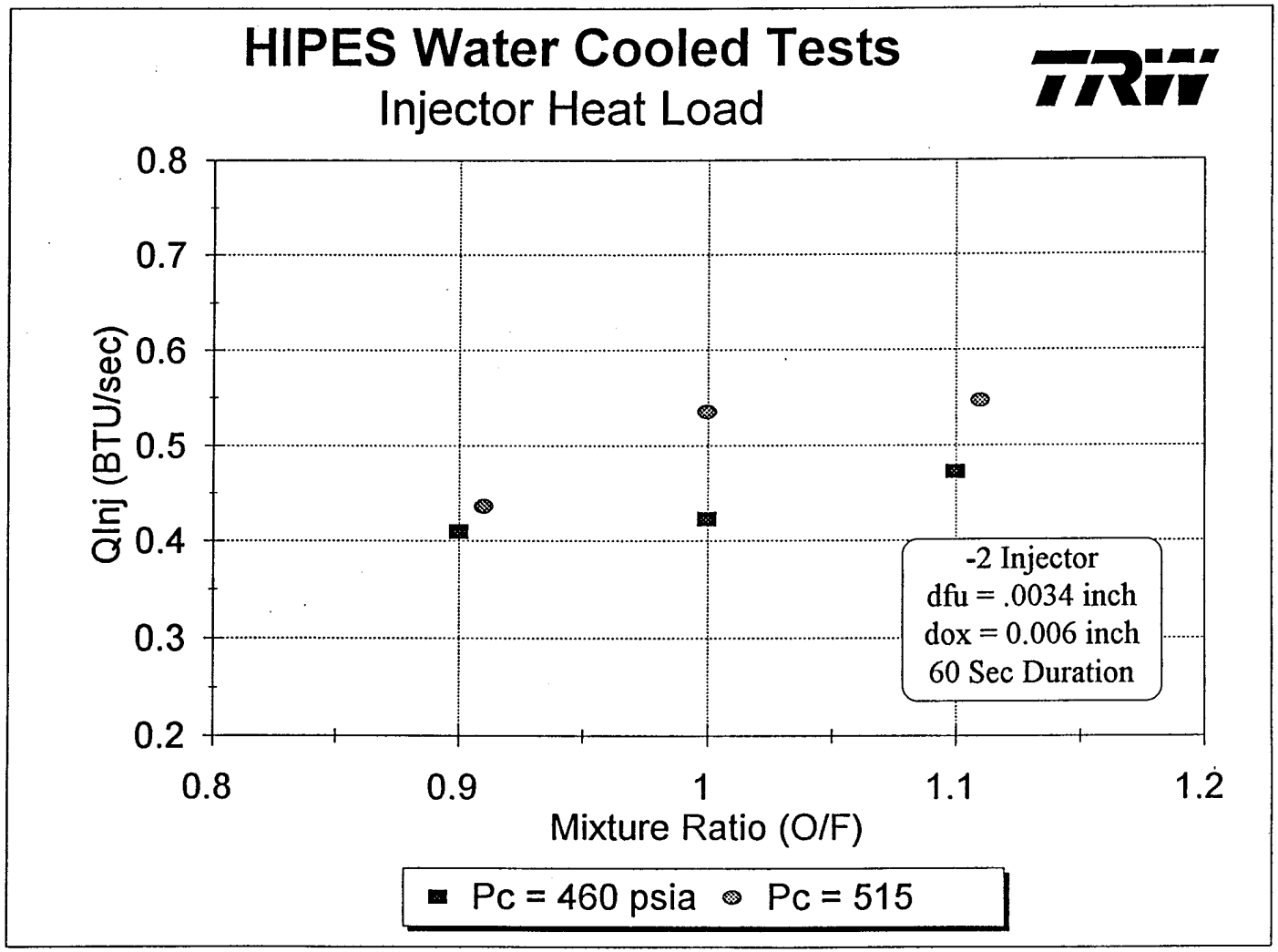
HIPES Water Cooled Tests
Injector Heat Load
TRW
0.8
0.7
0.6
0.5
0.4
0.3
0.2
QInj (BTU/sec)
0.8
0.9
1
1.1
1.2
Mixture Ratio (O/F)
-2 Injector
dfu = .0034 inch
dox = 0.006 inch
60 Sec Duration
Pc = 460 psia
Pc = 515

FIGURE 5.2.1-9

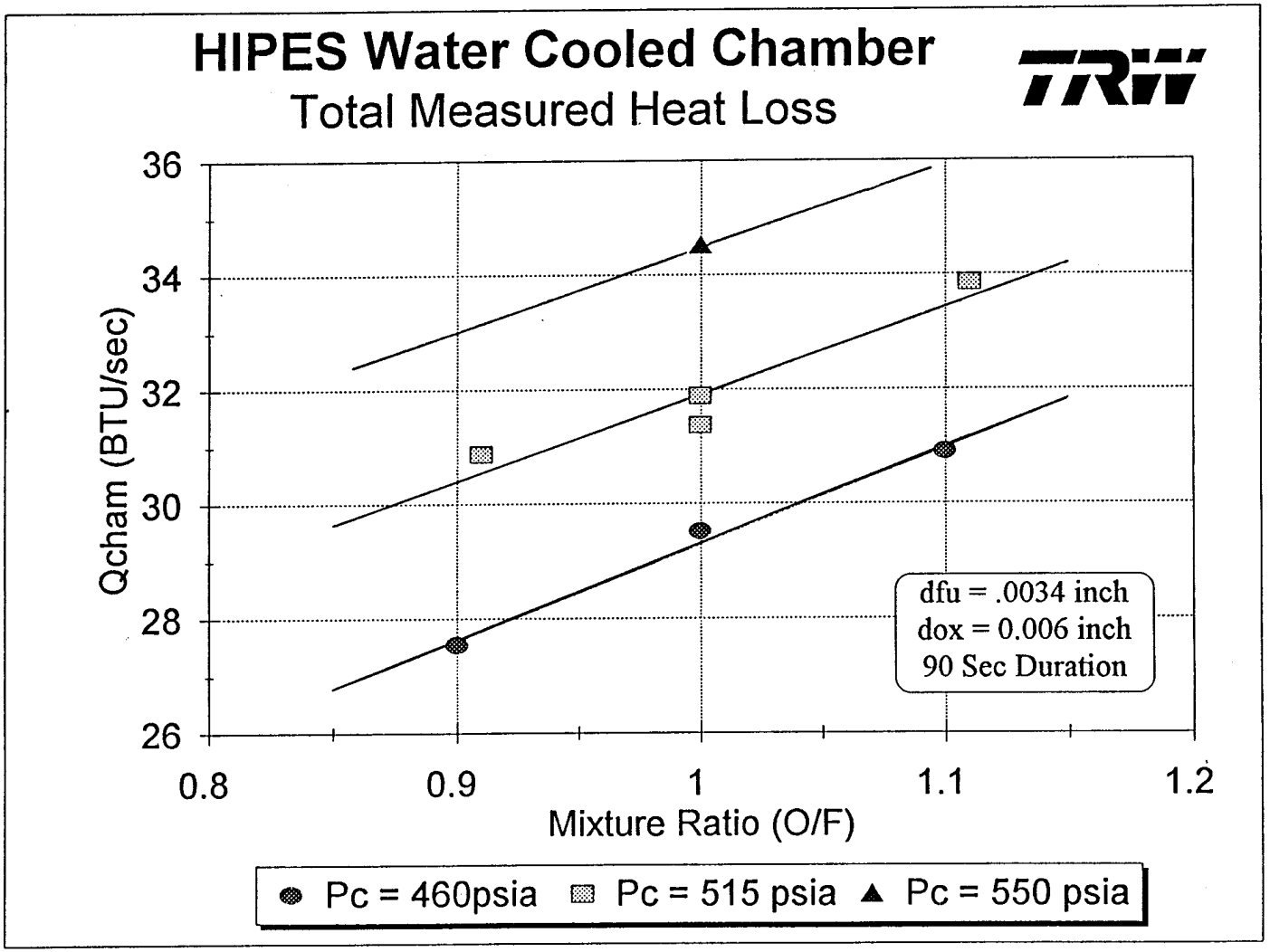
HIPES Water Cooled Chamber
Total Measured Heat Loss
TRW
Qcham (BTU/sec)
36
34
32
30
28
26
0.8
0.9
1
1.1
1.2
Mixture Ratio (O/F)
dfu = .0034 inch
dox = 0.006 inch
90 Sec Duration
Pc = 460psia
Pc = 515 psia
Pc = 550 psia

wall. Secondly, and probably more importantly, the higher chamber pressures yielded increased heat transfer coefficients, which naturally resulted in greater measured heat loads.

5.2.2 WATER-COOLED TESTS with MMH

A limited number of tests were conducted using MMH as an alternate fuel. Due to the differences in total flowrate, mixture ratio, and fuel density, the optimum injector gaps determined for hydrazine were not applicable for these tests. As a result, MMH testing began with a series of short duration tests to ascertain acceptable injector gap settings (velocities). These were found to be 0.0080" for oxidizer and 0.0026" for fuel. Following this, two longer duration tests were conducted to determine performance and steady-state heat transfer rates. The MMH tests conducted are summarized in Table 5.2.2-1.

Combustion performance with MMH was nearly identical to that observed for hydrazine (98.0- 98.7%), although as shown by Figure 5.2.2-1, delivered C* is approximately 120 ft/sec less than can be achieved with hydrazine due to theoretical differences in available performance. Like the hydrazine test results, performance was observed to increase with total propellant flowrate. Specific impulse of over 327.5-329 lbf-sec/lbm was achieved with the NTO/MMH propellant combination at a mixture ratio of 1.60.

Injector temperature data is presented in Table 5.2.2-2. The injector dome heat transfer rates that were measured for the MMH tests were equal to those measured for hydrazine, as shown in Figure 5.2.2-2. The chamber heat loss shown in Figure 5.2.2-3 was significantly greater for the MMH tests. This was due to the higher gas temperature in the chamber wall zone for the MMH tests.

5.3 RHENIUM CHAMBER TESTING

The final phase of testing was conducted with a PM (powder metallurgy) rhenium chamber with an electroplated iridium coating on both interior and exterior surfaces. In addition, the exterior surface was plasma sprayed with a hafnium oxide coating to increase the radiative emissive capability of the chamber. Blistering of the iridium coating was evident in two areas downstream of the throat prior to hot-fire testing. The iridium coating was known to have been defective in places due to contamination induced during the manufacturing process. This contamination caused the iridium coating to blister during the stress relief cycle imposed on the chamber prior to testing.

Three tests were conducted to demonstrate that the rhenium chamber and its coatings could withstand the thermal environment imposed by the combustion process, starting with a 3 sec checkout test, followed by a 10 sec test, and concluding with a 30 sec duration test. Post-test inspection after the 30-sec test revealed two interior surface gouges in the rhenium substrate that began just downstream of the throat plane where the original defects occurred, indicating the blisters had opened. New blistering of the iridium coating was also evident in areas farther downstream in the nozzle. The observed damage was considered severe enough to mandate termination of subsequent testing. Although the rhenium testing

TABLE 5.2.2-1 HIPES WATER-COOLED ENGINE TESTS

N2O4-MMH

TEST NO HA2A-	DUR SEC	INJ	Do INCH	Df INCH	Wt LBM/SEC	O/F	Pc PSIA	C* FT/SEC	Isp SEC
4352	5	-2	0.0085	0.0026	0.1545	1.59	516.2	5573	323.7
4353	10	-2	0.0085	0.003	0.1543	1.6	521.6	5647	328.0
4354	10	-2	0.008	0.0026	0.1543	1.6	522	5637	327.4
4355	10	-2	0.007	0.0026	0.1547	1.6	521.1	5601	325.3
4356	10	-2	0.0075	0.0026	0.1545	1.6	521.4	5583	324.3
4357	10	-2	0.0075	0.0022	0.1545	1.6	518.9	5523	320.8
4358	60	-2	0.008	0.0026	0.1545	1.6	528.4	5638	327.5
4359	60	-2	0.008	0.0026	0.1605	1.6	555.1	5668	329.2

HIPES MMH TEST RESULTS
WATER-COOLED COPPER CHAMBER

FIGURE 5.2.2-1

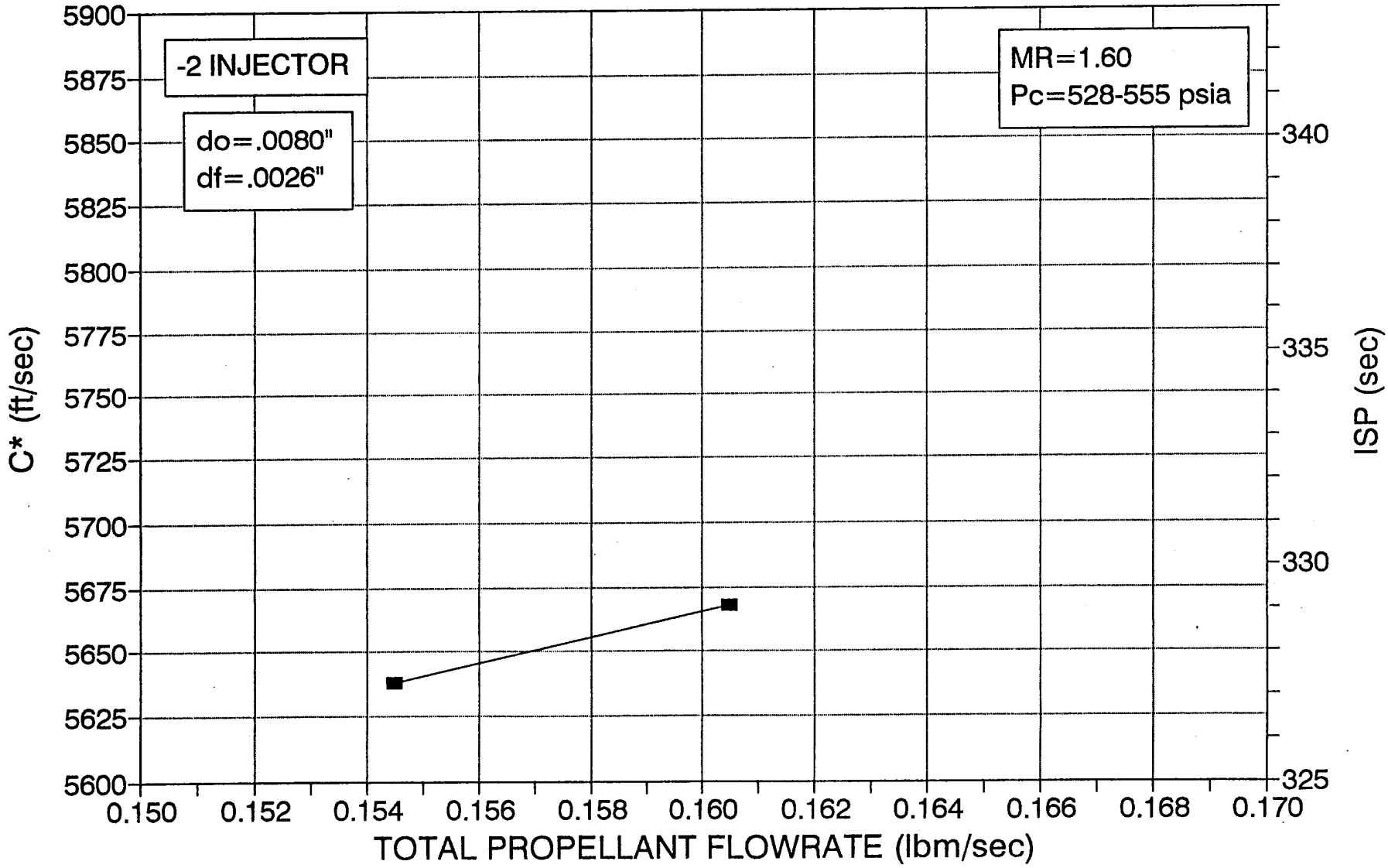

TABLE 5.2.2-2

HIPES WATER COOLED ENGINE DOME TEMPERATURE SUMMARY

HIPES WATER-COOLED ENGINE
N2O4-MMH

							EXTERNAL DOME TEMPS					INTERNAL DOME TEMPS							
TEST NO. HA2A-	DUR SEC	T/S	INJ	Wt LBM/SEC	O/F	Pc PSIA	TI2 F	TI6 F	TI3 F	TI7 F	TI4 F	TI8 F	TII2 F	TII5 F	TII3 F	TII6 F	QCHAN BTU/S	QINJ GPM	TINJ F
4352	5	5.0	-2	0.1593	1.47	516.8	81	84	82	83	120	123	155	161	272	129	0.38	1.01	2.74
4353	10	9.5	-2	0.1543	1.60	521.6	87	89	93	90	158	148	205	191	372	163	0.64	1.00	4.58
4354	10	9.5	-2	0.1543	1.60	522.0	82	86	89	89	142	143	174	182	281	158	0.51	1.01	3.63
4355	10	9.5	-2	0.1547	1.60	521.1	93	101	101	102	188	192	256	293	433	218	0.99	1.00	7.18
4356	10	9.5	-2	0.1545	1.60	521.4	89	96	96	93	173	163	236	240	407	183	0.73	0.99	5.37
4357	10	9.5	-2	0.1545	1.60	518.9	88	95	93	91	157	146	208	217	360	172	0.61	1.05	4.16
4358	60	10.0	-2	0.1544	1.60	521.5	90	97	94	94	160	151	209	221	333	180	0.66	1.05	4.51
		60.0	-2	0.1545	1.60	528.4	89	96	102	103	191	186	227	259	349	236	0.71	1.05	4.89
4359	60	10.0	-2	0.1603	1.60	548.6	90	93	93	91	157	139	206	205	335	178	0.60	1.05	4.12
		60.0	-2	0.1605	1.60	555.1	88	95	101	101	186	177	224	248	341	236	0.71	1.05	4.90

FIGURE 5.2.2-2

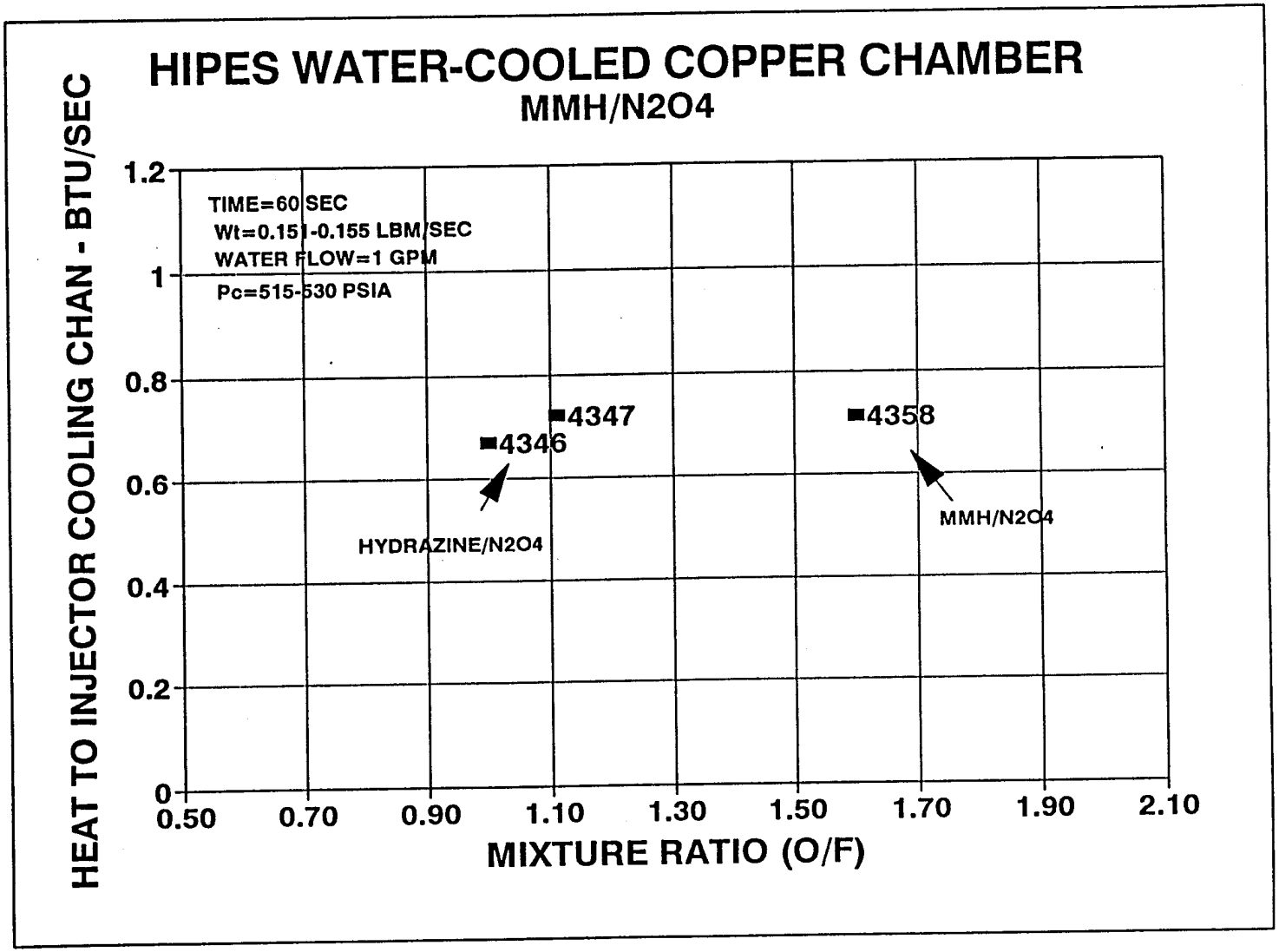
HIPES WATER-COOLED COPPER CHAMBER
MMH/N2O4
HEAT TO INJECTOR COOLING CHAN - BTU/SEC
TIME=60 SEC
Wt=0.151-0.155 LBM/SEC
WATER FLOW=1 GPM
Pc=515-530 PSIA
4346
4347
4358
HYDRAZINE/N2O4
MMH/N2O4
1.2
1
0.8
0.6
0.4
0.2
0
0.50
0.70
0.90
1.10
1.30
1.50
1.70
1.90
2.10
MIXTURE RATIO (O/F)

FIGURE 5.2.2-3

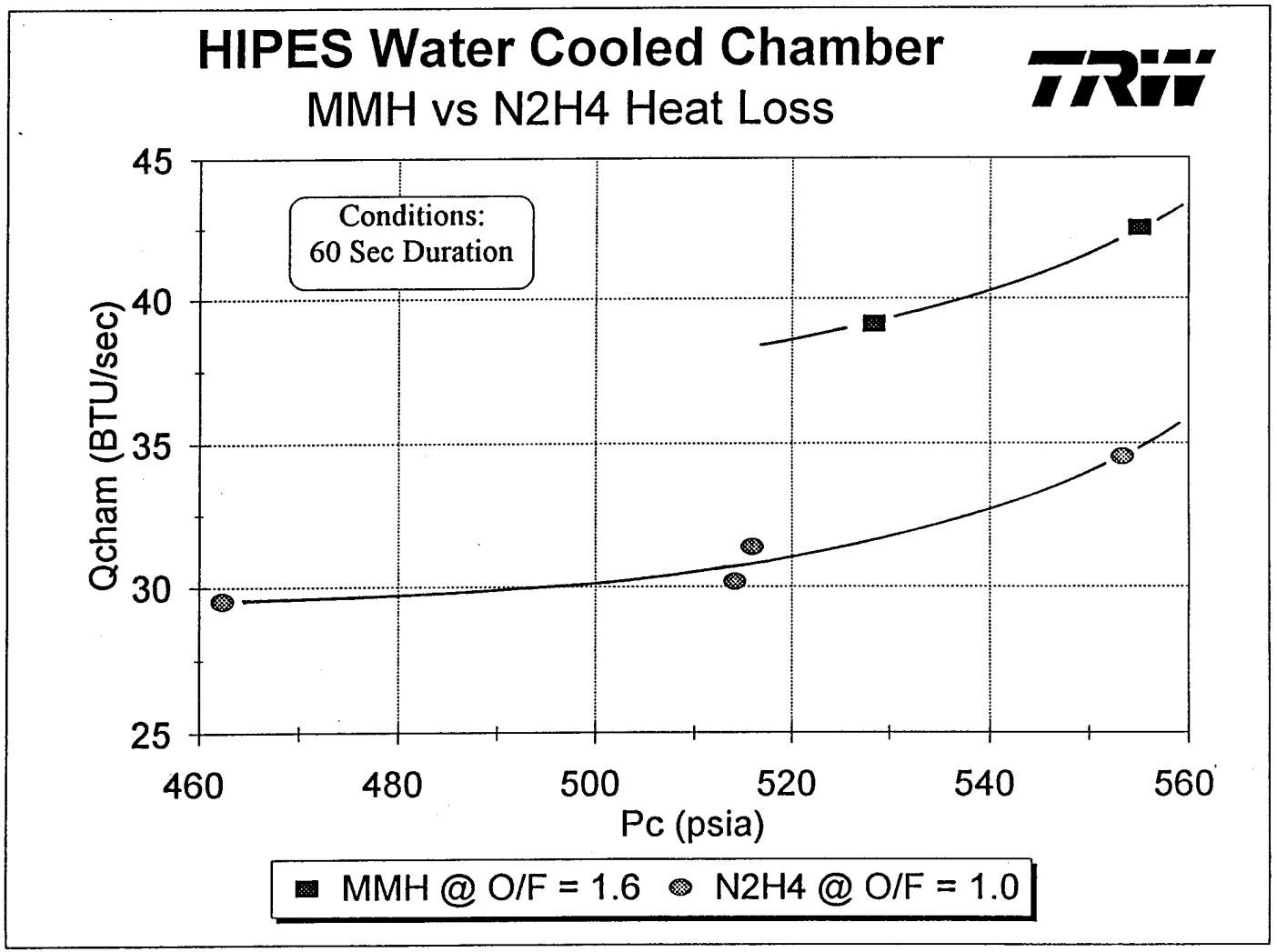
HIPES Water Cooled Chamber
MMH vs N2H4 Heat Loss
TRW
Conditions:
60 Sec Duration
Qcham (BTU/sec)
45
40
35
30
25
460
480
500
520
540
560
Pc (psia)
MMH @ O/F = 1.6
N2H4 @ O/F = 1.0

was abbreviated, the test series was considered successful in that the iridium coating in the region with the most severe thermal environment (the converging section) appeared to have survived completely intact. The PM rhenium thrust chamber and its accompanying coatings demonstrated viability as a combustion chamber that can withstand the thermal environment associated with a high- performance injector operating at high chamber pressures.

Performance data obtained on the last long duration test was in excellent agreement with the trends derived from the copper heatsink and water-cooled tests. Expected C* based on previous testing was 5755 ft/sec and the observed C* was actually 5755-5760 ft/sec. Figure 5.3-1 integrated the performance data obtained for the various configurations tested throughout the basic test program, and summarized the effects of both Pc and L*. The expected trend for C* versus L* as predicted by the film cooling model is shown for a constant chamber pressure of 500 psia. The actual performance values obtained for the water-cooled copper chamber and the rhenium chamber can be seen to be consistent with this trend. The trend also indicated that for an L* of 36", which was representative of the 500 psia heat-sink chamber, the expected C* was 5740 ft/sec. This value was graphically consistent with the performance levels measured with the 400 and 600 psia heat-sink chambers. Figure 5.3-1 indicated that the majority of C* increase observed while increasing chamber pressure from 400 to 600 psia was actually due to the accompanying increase in L*. The figure implied that of the 100 ft/sec C* rise obtained at the higher chamber pressure, only about 30 ft/sec was actually due to the increased Pc, while nearly 70 ft/sec can be attributed to the higher L*. Throat temperatures and chamber axial temperature profiles were determined with a combination of optical 2- color pyrometers and infrared imaging system. The axial temperature profile as measured by the infrared system and also the predicted profile generated by the film cooling model is presented in Figure 5.3-2. This figure showed that the measured temperature in the headend region of the chamber increased much more rapidly than predicted by the film cooling model. The model also did not predict the rather flat temperature profile that was observed along the first half of the chamber. This may have been due to the fact that the model assumed turbulent mixing throughout the chamber when in reality the gas flow was initially more laminar than expected.

Data from the 30 second test indicated that the injector had not quite reached thermal equilibrium. The heat load to the injector, shown in Figure 5.3-3, would have stabilized at approximately 1.5 Btu/sec. Analysis indicated that the oxidizer regen passage could remove 3 Btu/sec at the critical heat flux. These results, presented in Figure 5.3-4, indicate that the regen channel would be in the initial stages of nucleate boiling at the expected 1.5 Btu/sec heat load. External dome temperature predictions have shown that maximum steady-state injector temperatures would be approximately 500 °F.

PC & L* EFFECTS ON PERFORMANCE

NOMINAL MR & Wt

FIGURE 5.3-1

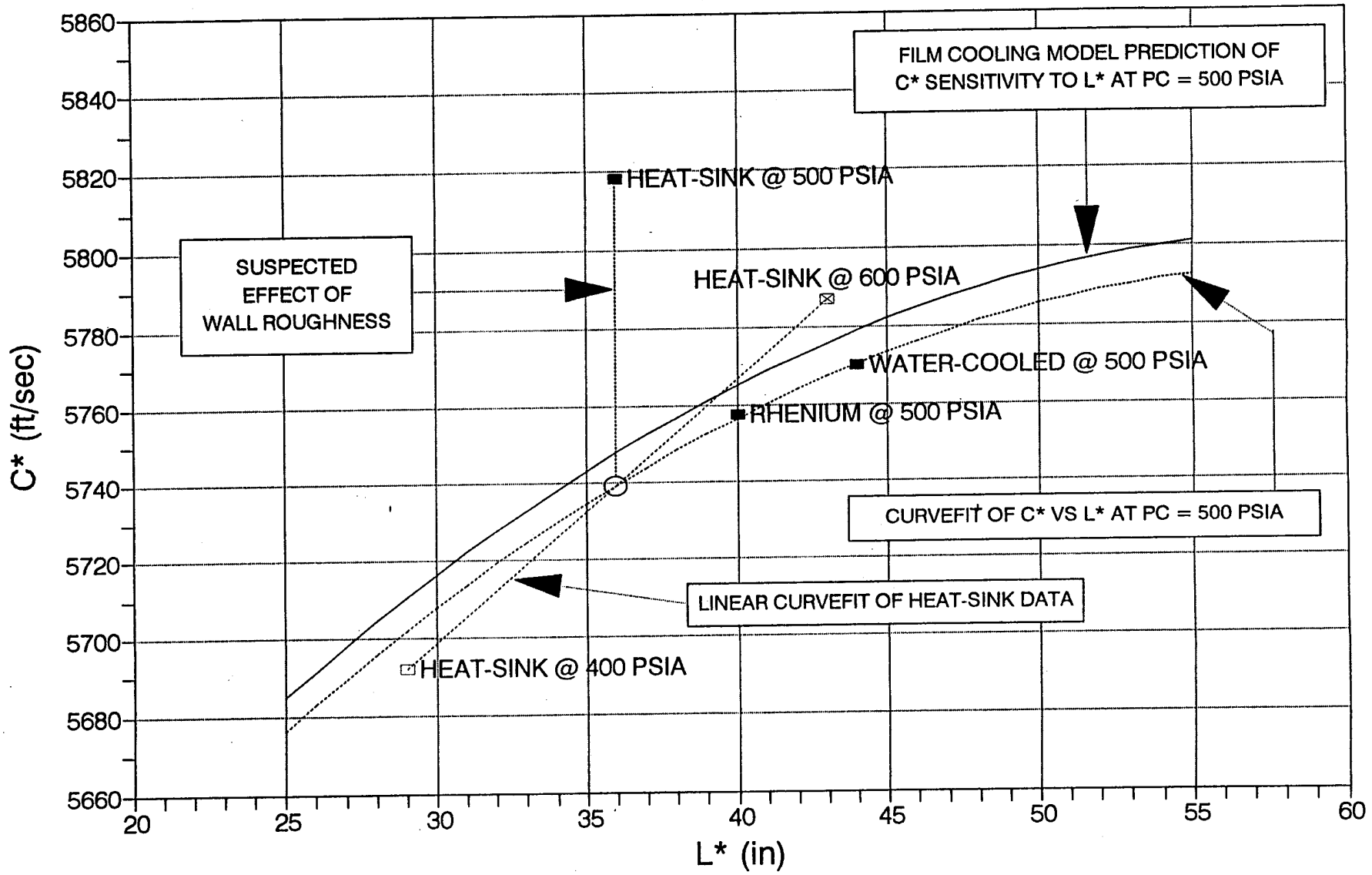

FIGURE 5.3-2

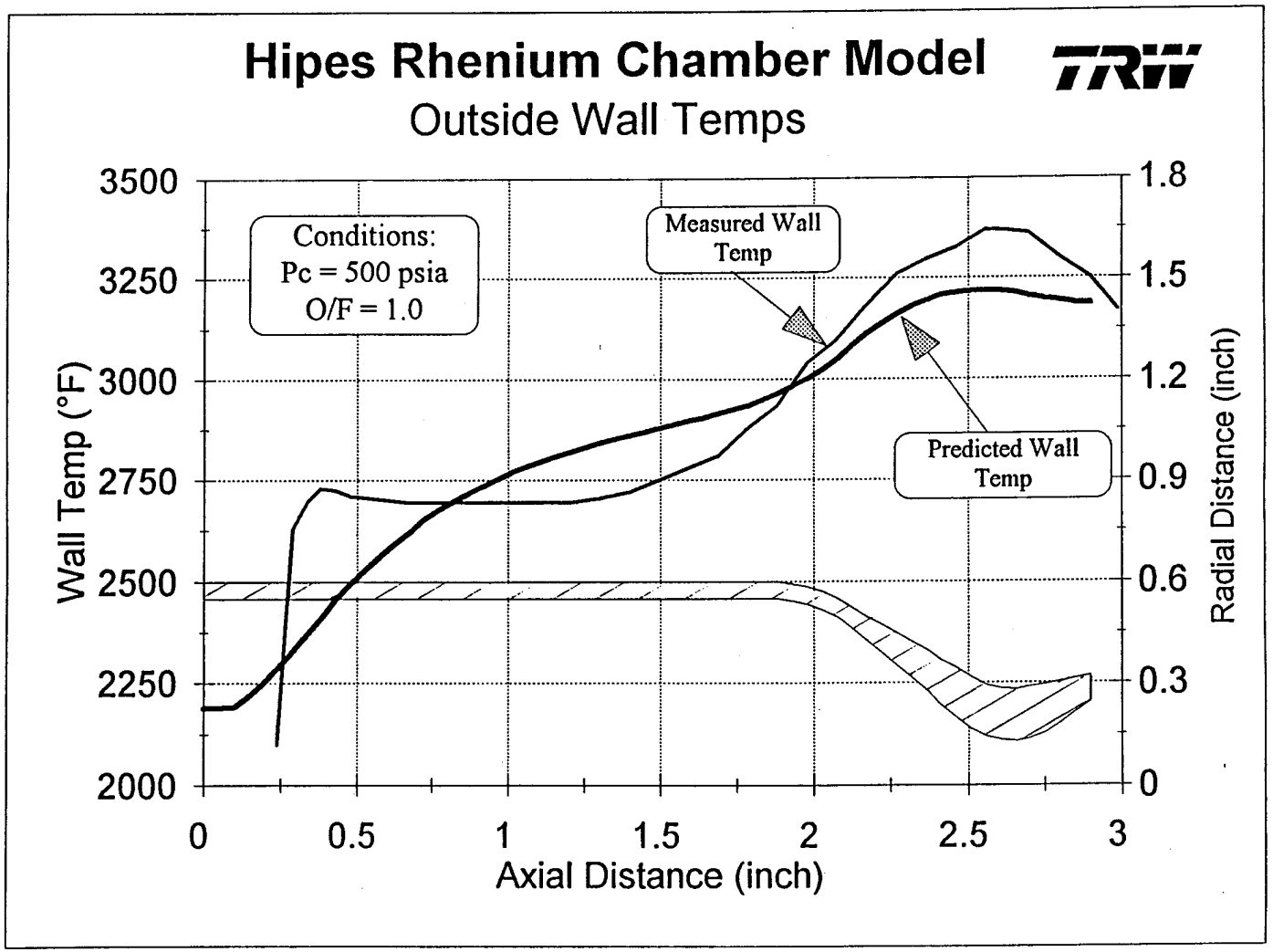
Hipes Rhenium Chamber Model
Outside Wall Temps
TRW
Conditions:
Pc = 500 psia
O/F = 1.0
Measured Wall Temp
Predicted Wall Temp
Wall Temp (°F)
3500
3250
3000
2750
2500
2250
2000
Radial Distance (inch)
1.8
1.5
1.2
0.9
0.6
0.3
0
0
0.5
1
1.5
2
2.5
3
Axial Distance (inch)

FIGURE 5.3-3

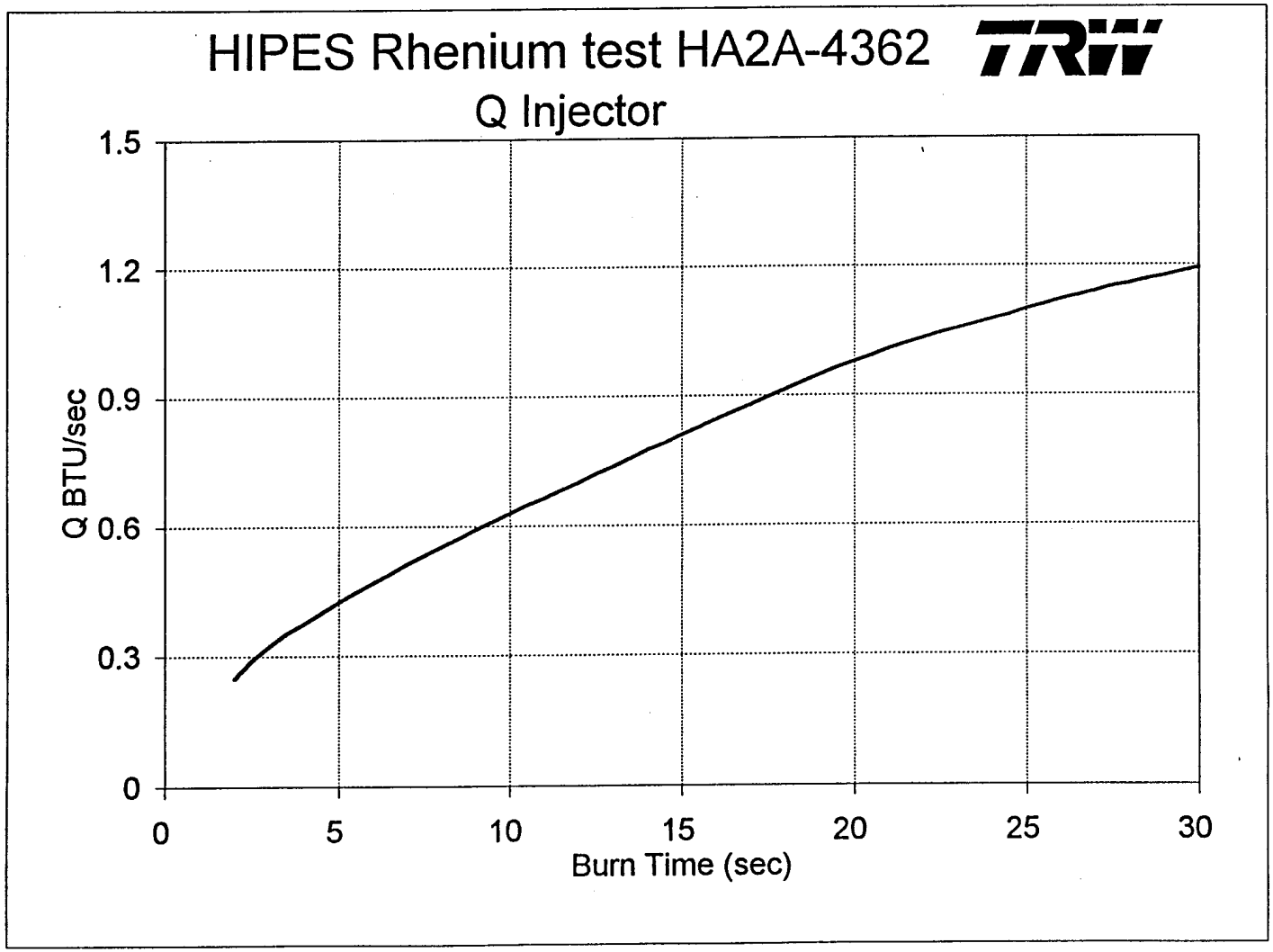
HIPES Rhenium test HA2A-4362
TRW
Q Injector
Q BTU/sec
1.5
1.2
0.9
0.6
0.3
0
0
5
10
15
20
25
30
Burn Time (sec)

FIGURE 5.3-4

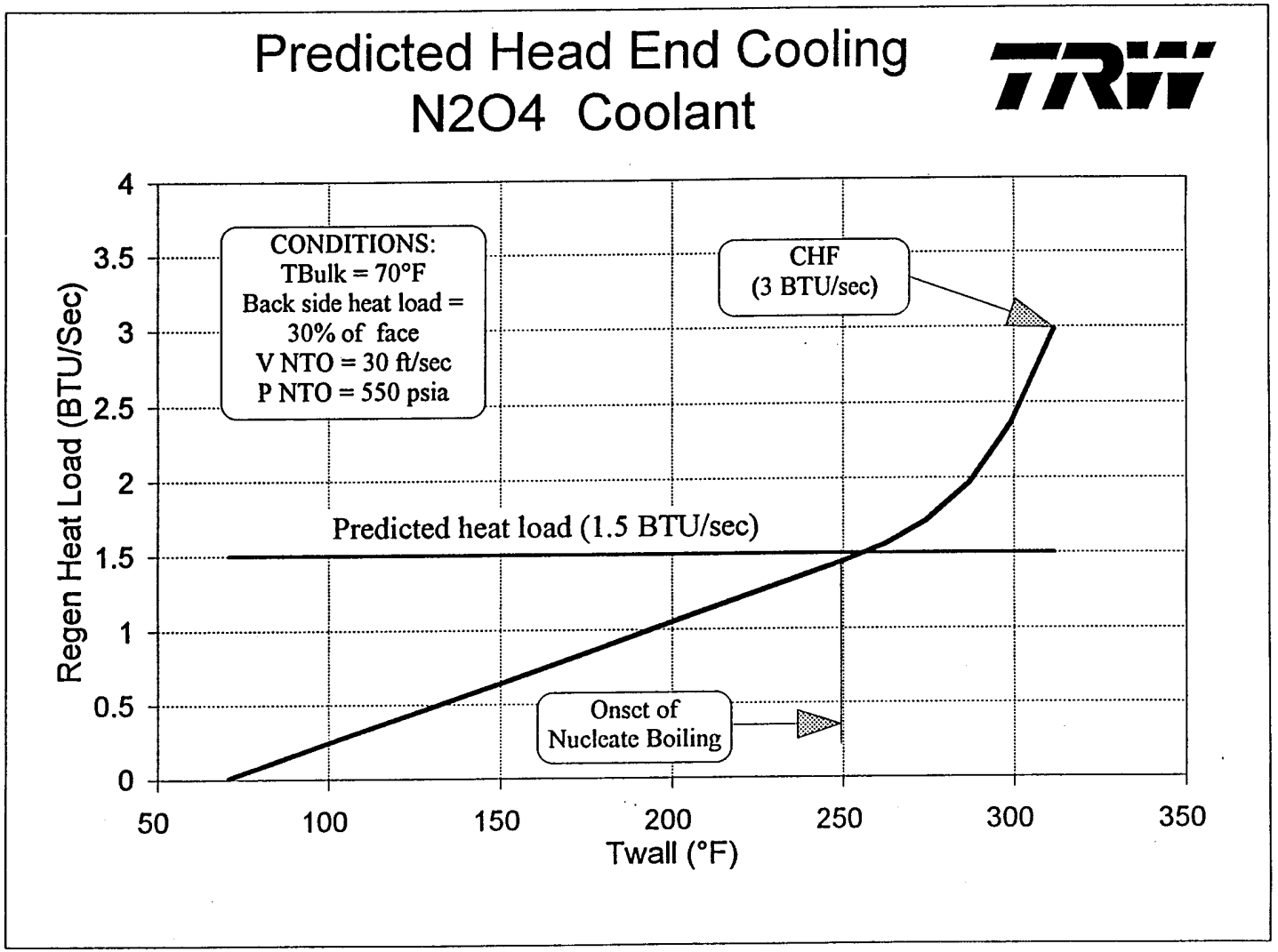
Predicted Head End Cooling
N2O4 Coolant
TRW
CONDITIONS:
TBulk = 70°F
Back side heat load =
30% of face
V NTO = 30 ft/sec
P NTO = 550 psia
CHF
(3 BTU/sec)
Predicted heat load (1.5 BTU/sec)
Onset of
Nucleate Boiling
Regen Heat Load (BTU/Sec)
Twall (°F)
0
0.5
1
1.5
2
2.5
3
3.5
4
50
100
150
200
250
300
350

5.4 TEST SUMMARY

The TRW HIPES basic program test series was extremely successful. Measured combustion efficiency was well above the original goal set at the beginning of the program. A significant amount of testing was conducted on several different hardware configurations. Data obtained from these tests produced consistent engineering trends that will prove valuable in the next design phase as the HIPES engine evolves. Preliminary results have indicated that in addition to high performance, the predicted maximum injector temperatures will be acceptable and the proposed chamber material will be compatible with the induced thermal environment.

6.0 CONCLUSIONS

The HIPES engine demonstrated high performance at high chamber pressure with both N_2O_4-N_2H_4 and N_2O_4-MMH yielding the following:

Isp_∞ = ~337 lbf-sec/lbm with N_2O_4-N_2H_4 at Pc =500 psia at F_∞ = 50 lbf

Isp_∞ = 327.5 lbf-sec/lbm with N_2O_4-MMH at Pc=500 psia at F_∞ =50 lbf

A powder metallurgy rhenium engine demonstrated operation with high performance at high chamber pressure (500 psia) which indicated the viability of this concept.

The HIPES engine upon development will provide major increases in lightsat payloads which provides major improvements in the spacecraft. TRW is a major lightsat producer and will use the HIPES engine upon completion of development.

REPORT DOCUMENTATION PAGE

Form Approved
OMB No. 0704-0188

1. AGENCY USE ONLY (*Leave blank*)	2. REPORT DATE	3. REPORT TYPE AND DATES COVERED
		Final Contractor Report

4. TITLE AND SUBTITLE

High Pressure Earth Storable Rocket Technology Program – Basic Program

5. FUNDING NUMBERS

WU–242–70–02
C–NAS3–27002

6. AUTHOR(S)

M.L. Chazen, D. Sicher, D. Huang, and T. Mueller

7. PERFORMING ORGANIZATION NAME(S) AND ADDRESS(ES)

TRW Space & Technology Division
Redondo Beach, California 90278

8. PERFORMING ORGANIZATION REPORT NUMBER

E–9514

9. SPONSORING/MONITORING AGENCY NAME(S) AND ADDRESS(ES)

National Aeronautics and Space Administration
Lewis Research Center
Cleveland, Ohio 44135–3191

10. SPONSORING/MONITORING AGENCY REPORT NUMBER

NASA CR–195449

11. SUPPLEMENTARY NOTES

Project Manager, James A. Biaglow, Space Propulsion Technology Division, NASA Lewis Research Center, organization code 5330, (216) 977–7480

12a. DISTRIBUTION/AVAILABILITY STATEMENT

Unclassified - Unlimited
Subject Category 20

This publication is available from the NASA Center for Aerospace Information, (301) 621–0390.

12b. DISTRIBUTION CODE

13. ABSTRACT ***(Maximum 200 words)***

The HIPES Program was conducted for NASA-LeRC by TRW. The Basic Program consisted of system studies, design of testbed engine, fabrication and testing of engine.Studies of both pressure-fed and pump-fed systems were investigated for N_2O_4 and both MMH and N_2H_4 fuels with the result that N_2H_4 provides the maximum payload for all satellites over MMH. The higher pressure engine offers improved performance with smaller envelope and associated weight savings. Pump-fed systems offer maximum payload for large and medium weight satellites while pressure-fed systems offer maximum payload for small light weight satellites. The major benefits of HIPES are high performance within a confined length maximizing payload for lightsats which are length(volume) constrained. Three types of thrust chambers were evaluated-Copper heatsink at 400, 500 and 600 psia chamber pressures for performance/thermal, water cooled to determine heat absorbed to predict rhenium engine operation and rhenium to validate the concept. The HIPES engine demonstrated very high performance at 50 lbf thrust(ε=150) and Pc=500 psia with both fuels:Isp=337 sec using N_2O_4-N_2H_4 and Isp=327.5 sec using N_2O_4-MMH indicating combustion efficiencies >98%. A powder metallurgy rhenium engine demonstrated operation with high performance at Pc=500 psia which indicated the viability of the concept.

14. SUBJECT TERMS

High pressure rocket; Earth storable

15. NUMBER OF PAGES

16. PRICE CODE

17. SECURITY CLASSIFICATION OF REPORT	18. SECURITY CLASSIFICATION OF THIS PAGE	19. SECURITY CLASSIFICATION OF ABSTRACT	20. LIMITATION OF ABSTRACT
Unclassified	Unclassified	Unclassified	